AD-A063 658 TENNESSEE UNIV KNOXVILLE ULTRASONICS LAB F/G 20/1
STUDIES OF LINEAR AND NONLINEAR ULTRASONIC PHENOMENA.(U)
NOV 78 M A BREAZEALE N00014-76-C-0177
UNCLASSIFIED TR-17 NL

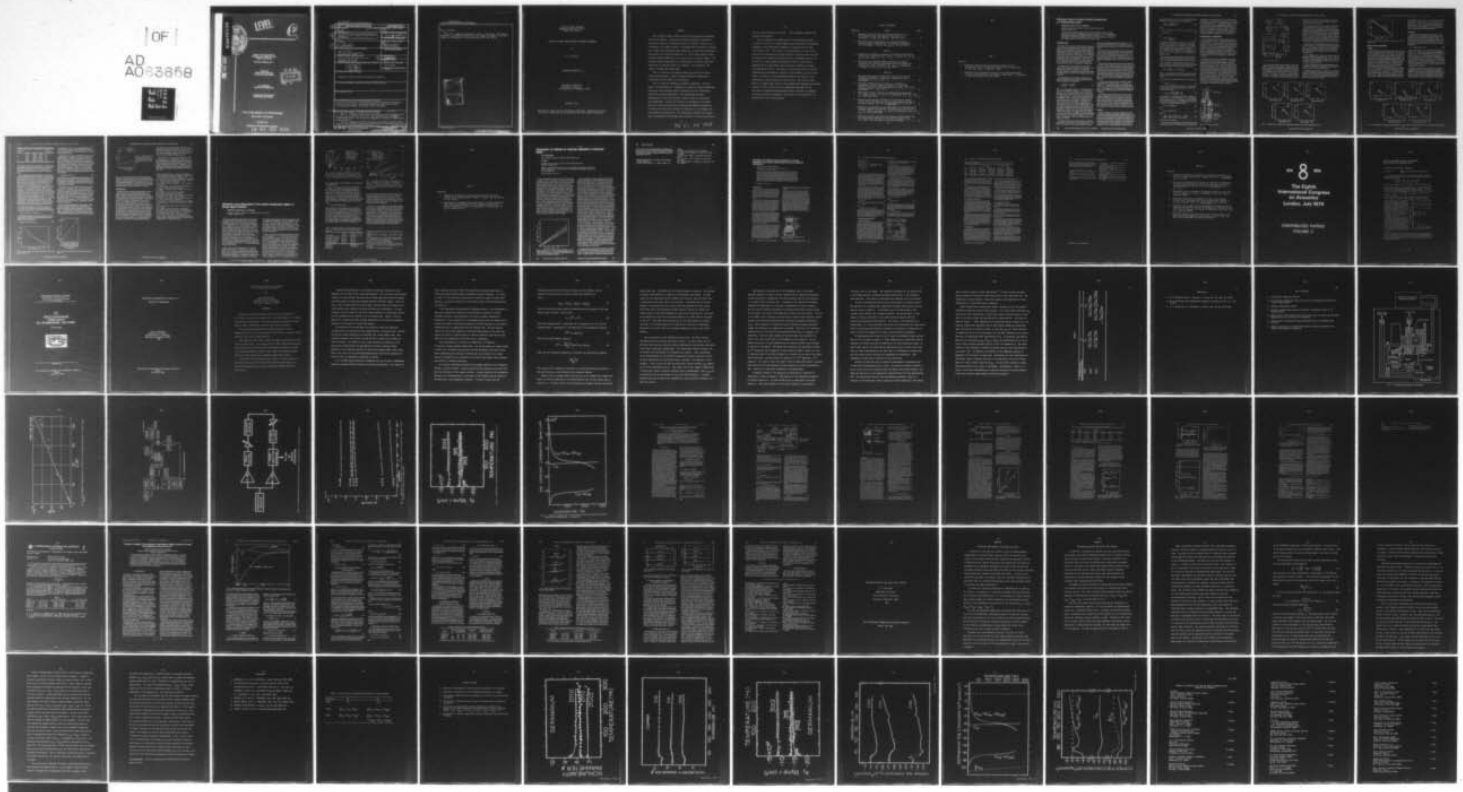

END
DATE FILMED
3-79
DDC

LEVEL II

(12) 55

OFFICE OF NAVAL RESEARCH
CONTRACT NO. N00014-76-C-0177
PROJECT NO. 384-306

TECHNICAL REPORT NO. 17

STUDIES OF LINEAR AND NONLINEAR ULTRASONIC PHENOMENA

M.A. BREAZEALE
PRINCIPAL INVESTIGATOR

ULTRASONICS LABORATORY
DEPARTMENT OF PHYSICS

THE UNIVERSITY OF TENNESSEE
Knoxville, Tennessee

JANUARY 1979

Unclassified

SECURITY CLASSIFICATION OF THIS PAGE (When Data Entered)

(14) TR- **REPORT DOCUMENTATION PAGE**

READ INSTRUCTIONS BEFORE COMPLETING FORM

1. REPORT NUMBER: 17 ✓
2. GOVT ACCESSION NO.
3. RECIPIENT'S CATALOG NUMBER: (9)

4. TITLE (and Subtitle): (6) STUDIES OF LINEAR AND NONLINEAR ULTRASONIC PHENOMENA
5. TYPE OF REPORT & PERIOD COVERED: Interim ≠ rept.
6. PERFORMING ORG. REPORT NUMBER

7. AUTHOR(s): (10) M. A. Breazeale
8. CONTRACT OR GRANT NUMBER(s): (15) N00014-76-C-0177

9. PERFORMING ORGANIZATION NAME AND ADDRESS
Dept. of Physics
The University of Tennessee
Knoxville, TN 37916

10. PROGRAM ELEMENT, PROJECT, TASK AREA & WORK UNIT NUMBERS

11. CONTROLLING OFFICE NAME AND ADDRESS
Office of Naval Research, Code 421
Department of the Navy
Arlington, VA 22217

(11)

12. REPORT DATE: November 1978
13. NUMBER OF PAGES: 80

14. MONITORING AGENCY NAME & ADDRESS (if different from Controlling Office)
(12) 84p.

15. SECURITY CLASS. (of this report): Unclassified
15a. DECLASSIFICATION/DOWNGRADING SCHEDULE

16. DISTRIBUTION STATEMENT (of this Report)

Approved for public release; distribution unlimited.

17. DISTRIBUTION STATEMENT (of the abstract entered in Block 20, if different from Report)

18. SUPPLEMENTARY NOTES

19. KEY WORDS (Continue on reverse side if necessary and identify by block number)
Binary liquid mixtures; critical mixing; pressure amplitude measurement; ultrasonic wave velocity measurement; nonlinear acoustics of solids; nonlinearity parameters; third-order elastic constants

20. ABSTRACT (Continue on reverse side if necessary and identify by block number)
beta, beta' -
The technical report is divided into three parts:

Part I. Ultrasonic wave velocity and attenuation are measured in the critical mixing region of the binary liquid mixture hexane and β,β'-dichloroethyl ether. The results are compared with results in other binary liquid mixtures.

Part II. Comparison of the measurement of ultrasonic pressure amplitudes by four different techniques and measurement of ultrasonic wave velocity in solids by use of capacitive transducers.
(see reverse)

DD FORM 1 JAN 73 1473 EDITION OF 1 NOV 65 IS OBSOLETE
S/N 0102-LF-014-6601

401 013

Unclassified
SECURITY CLASSIFICATION OF THIS PAGE (When Data Entered)

20. (continued)

Part III. Nonlinear acoustics of solids is discussed. Nonlinearity parameters of germanium, fused silica, and copper are measured, and their temperature dependence is determined between 3[illegible] K and 300[illegible] K.

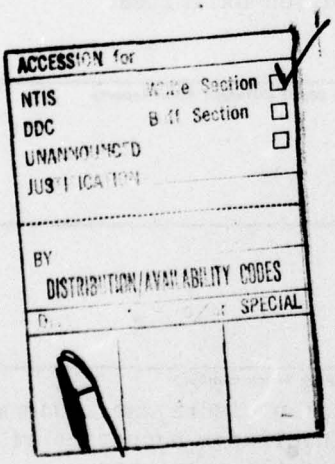

OFFICE OF NAVAL RESEARCH
CONTRACT NO. N00014-76-C-0177
PROJECT NO. 384-306

STUDIES OF LINEAR AND NONLINEAR ULTRASONIC PHENOMENA

by

M. A. Breazeale

TECHNICAL REPORT NO. 17

Ultrasonics Laboratory
Department of Physics
The University of Tennessee 37916

November 1978

PREFACE

This technical report comprises publications made between September 1974 and the present. During this period the program was expanded to include the study of the nonlinear acoustics of solids. Because of the broadening of the range of topics, in February 1978 we decided to separate out a single topic—Ultrasonic Wave Reflection at Liquid-Solid Interfaces—and present it as Technical Report No. 15. The current technical report overlaps Technical Report No. 15 in time, but not in subject matter. The current technical report gives our contributions to subjects other than reflection of ultrasonic waves at interfaces. For convenience, the report is divided into three parts.

Part I is made up of two papers dealing with critical mixing of binary liquid mixtures. These two papers essentially complete our contribution to this subject for the present.

Part II covers two different measurement techniques. The first paper is a presentation of a comparison of ultrasonic pressure amplitudes measured by three different optical techniques and by a thermocouple probe with calculated amplitudes. The measurements were made simultaneously in the same ultrasonic field in 1958, but previously were unpublished. A revival of interest in calibration at the Miami meeting of the Acoustical Society of America persuaded the author and Floyd Dunn that our results would be of interest to our colleagues and thus prompted the publication. The second paper describes the improvement in measurement of ultrasonic wave velocities in solids which results

from the use of capacitive transducer. This technique eliminates the perennial bond problem.

Part III comprises six contributions to the nonlinear acoustics of solids. The first is a short summary paper describing the temperature dependence of the nonlinearity parameters of germanium and of fused silica down to 77°K. The second is an invited paper, given at the 6th International Symposium on Nonlinear Acoustics in Moscow, which describes the measurement technique and present results on germanium down to 3°K. The third is a more extensive description of both the nonlinearity parameter and the third-order elastic constants of germanium between room temperature and 3°K. The fourth is a short paper given at the ICA in Madrid on the nonlinearity parameter of four different types of fused silica. The fifth is a more extensive account of the results of our experiments on the nonlinearity of fused silica. The sixth and final paper is a summary paper, given at the International Symposium on Nonlinear Acoustics in Paris, which gives the temperature dependence of the nonlinearity parameters and third-order elastic constants of germanium and copper and makes an attempt to relate them to other quantities of significance in solid state physics.

TABLE OF CONTENTS

PART I

Paper No.

1. "Ultrasonic Study of Critical Mixing of Hexane and β,β′-Dichloroethyl Ether" (Elizabeth M. Bains and M. A. Breazeale), J. Chem. Phys. 61 (3), 1238-1243 (1974).

2. "Ultrasonic Wave Attenuation in the Critical Temperature Region of Binary Liquid Mixtures" (Elizabeth M. Bains and M. A. Breazeale), J. Chem. Phys. 62 (2), 742-743 (1975).

Ultrasonic study of critical mixing of hexane and β, β'-dichloroethyl ether*

Elizabeth M. Bains and M. A. Breazeale

Department of Physics, The University of Tennessee, Knoxville, Tennessee 37916
(Received 8 February 1974)

The velocity and attenuation of ultrasonic waves in the critical temperature region of a binary mixture of hexane and β, β'-dichloroethyl ether have been measured at 1, 3, 5, 7, and 9 MHz. By assuming that the attenuation per wavelength is made up of two terms, $\alpha\lambda = Af^{-1/4} + Bf$, we obtain good agreement with the Fixman theory for both $\alpha\lambda$ and α/f^2. The magnitude of B, however, is only partially accounted for by our measured values of shear viscosity.

INTRODUCTION

Examination of the attenuation maximum for ultrasonic waves in the critical mixing region of binary liquids was begun by Lucas and Biquard,[1] who attempted to explain the observed maximum by analogy with the scattering of visible light from density fluctuations. This explanation had been successful for critical opalescence. Scattering of ultrasonic waves in the critical mixing region was investigated by Brown and Richardson.[2] Later Brown[3] reported that scattering accounts for the major part of the excess attenuation away from the critical point but a much smaller part as the critical point is approached.

A relaxation due to rearrangement of molecular clusters was proposed by Chynoweth and Schneider,[4] but Anantaraman, Walters, Edmonds, and Pings[5] and D'Arrigo, Mistura, and Tartaglia[6] reported that a single relaxation does not account for the frequency dependence of the data.

The attenuation of sound in fluids is classically assumed to depend upon two transport properties, shear viscosity and thermal conductivity:

$$\alpha\lambda = \frac{\pi\omega}{c^2\rho_0}\left(\frac{4}{3}\eta + \frac{(\gamma-1)K}{C_p}\right), \tag{1}$$

where ω is the angular frequency, c is the sound velocity, ρ_0 is the undisturbed density, η is the viscosity coefficient, γ is the ratio of specific heats, K is the thermal conductivity coefficient, and C_p is the specific heat at constant pressure. If the thermal conductivity term is negligible, then the attenuation per wavelength is directly proportional to the viscosity coefficient, and is also a linear function of frequency. Although an increase in viscosity at the critical mixing temperature was measured early in the study of binary liquids,[7] and a theoretical explanation of it has been offered,[8] the effect of this increase heretofore has been assumed to be negligible in explanations of the increase in attenuation in the critical region. The magnitude of this increase in viscosity is typically 5%–40%, whereas the magnitude of the increase in $\alpha\lambda$ is typically factors of 2–10. In the data to be presented, however, the effect of shear viscosity is noticeable.

In addition to this shear viscosity, there is evidently an increase in bulk viscosity in the critical region. The effect of the bulk viscosity on the attenuation of sound has been considered by Kawasaki and Tanaka,[9] who show that bulk viscosity gives an attenuation per wavelength which has the same form as that derived by Fixman.[10]

The theory derived by Fixman[10] using an excess heat capacity rather than bulk viscosity as the mechanism will be used in the interpretation of our results. This theory gives an $f^{-1/4}$ frequency dependence for $\alpha\lambda$, the temperature dependence of $\alpha\lambda$, and the temperature and frequency dependence of the velocity in the critical region.

Fixman derives the excess attenuation and dispersion of sound from the interaction between concentration fluctuations near the critical point and a sound wave passing through the region. The temperature variations associated with the adiabatic sound wave alter the concentration fluctuations, and these fluctuations decay toward the equilibrium distribution according to the diffusion equation. This decay distorts the temperature variation of the sound wave, and causes absorption of energy from the wave.

In recent years there have been a number of experimental tests of the Fixman theory. In a number of cases[5,6,11–13] it was observed that the frequency dependence of α/f^2 of the data followed that predicted by Fixman.[10] Anantaraman *et al.*[5] reported that although α/f^2 showed the frequency dependence predicted by Fixman, $\alpha\lambda$ did not.

The purpose of the present work is to show how the frequency dependence of both $\alpha\lambda$ and α/f^2 of critical mixture of hexane and β, β'-dichloroethyl ether (commonly called chlorex) can be brought into agreement with the Fixman theory. This is done by assuming an excess attenuation, whose frequency dependence is the same as that caused by viscosity, in addition to the excess attenuation resulting from the Fixman mechanism.

THEORY

Fixman calculates an excess heat capacity per unit volume due to variations in entropy, expressed in terms of Fourier components of the radial distribution function. The perturbation of the equilibrium components caused by temperature variations in the sound wave is evaluated by introducing into the diffusion equation a heat capacity that is dependent both on local temperature and on Fourier components of the radial distribution function that are

exponential functions of time. The excess heat capacity is obtained in terms of a complex integral and is

$$\Delta = \frac{k_B}{4\pi^2}\left(T_c \frac{\partial \kappa^2}{\partial T}\right)^2 \left(\frac{h}{\omega}\right)^{1/4} F(d)\,, \tag{2}$$

where

$$F(d) = d^{-1/2}\int_0^\infty w^4(w^2+1)^{-1}[-id^{-2}+w^2(w^2+1)]^{-1}dw\,, \tag{3}$$

$$d = \kappa^2(h/\omega)^{1/2}\,, \tag{4}$$

and

$$h = \frac{k_B T_c}{m_1}\,\frac{\phi_1 V_1^2(n_1+n_2)}{2\pi a\beta c_2}\,. \tag{5}$$

The integration variable in Eq. (2) is $w = k/\kappa$, and the parameters are Boltzmann's constant k_B, temperature T, critical temperature T_c, parameters of the radial distribution function κ and α, angular frequency ω, diffusion constant h, and molecular mass, molecular volume, volume fraction, number density, and mass fraction, m_1, V_1, ϕ_1, n_1, n_2 and c_1, c_2, respectively, for liquids 1 and 2.

The imaginary part of the integral in Eq. (3) determines the sound absorption and the real part of that integral determines the dispersion of the speed of sound.

The calculation of the attenuation and dispersion of sound is made by assuming that C_P and C_V are increased by the same amount by the composition fluctuations

$$C_P = C_P^0 + \frac{N_0\Delta}{n_1+n_2}\,, \quad C_V = C_V^0 + \frac{N_0\Delta}{n_1+n_2}\,, \tag{6}$$

where N_0 is Avogadro's number and C_P^0 and C_V^0 are heat capacities in the absence of critical composition fluctuations.

The sound wave propagating along the x axis is given by

$$\psi = \exp i(\omega x/c_c - \omega t)\,, \tag{7}$$

where c_c is the complex speed of sound. It is related to c_0, the speed of sound in the absence of critical composition fluctuations, by

$$c_c \approx c_0\left[1 - \frac{N_0\Delta}{2(n_1+n_2)C_P^0}\left(\frac{C_P^0}{C_V^0} - 1\right)\right]. \tag{8}$$

The real part of c_c is the speed of sound c. The imaginary part of ω/c_c is the attenuation α. The attenuation per wavelength is $2\pi c_0\alpha/\omega$. Using Eq. (2), the speed of sound and the attenuation per wavelength can be written in terms of the complex integral $F(d)$ as

$$c = c_0\{1 - \tfrac{1}{2}H\mathrm{Re}[F(d)]\} \tag{9}$$

and

$$\alpha\lambda_{\mathrm{Fixman}} = \pi H\mathrm{Im}[F(d)]\,, \tag{10}$$

where

$$H = \left(\frac{C_P^0}{C_V^0} - 1\right)\frac{R}{C_P^0}\left(T_c\frac{\partial\kappa^2}{\partial T}\right)^2 \frac{1}{4\pi^2(n_1+n_2)}\left(\frac{h}{\omega}\right)^{1/4} \tag{11}$$

and R is the gas constant.

The most direct comparison of the Fixman theory with experiment comes from a determination of the frequency dependence of the experimental $\alpha\lambda$. According to equations (10) and (11), the excess attenuation per wavelength $\alpha\lambda$ should depend on $f^{-1/4}$. As will be shown, the experimental data do show such a dependence; however, it is necessary first to remove the linear frequency dependence to be expected from shear viscosity. In order to do this, it is necessary to introduce a plot of α/f^2 as a function of frequency. This allows one to separate out the shear viscosity contribution as a constant term.

EXPERIMENTAL TECHNIQUES

A critical mixture of chlorex and hexane was sealed in a cylindrical glass tank. A drawing of the apparatus is shown in Fig. 1. Measurements of the ultrasonic attenuation and velocity were made by single crystal pulse techniques, with the pulses propagating between a piezoelectric quartz crystal in the transducer and the air-backed mica sheet in the reflector. The transducer could be translated through the liquids relative to the reflector, and the distance through which it moved could be measured with a 3-in. dial gauge to an accuracy of ± 0.001 in.

The electronic circuits used to generate and analyze the ultrasonic pulse are shown in Fig. 2. An rf pulse generated by an Arenberg Model PG650-G pulsed oscillator was fed into both an echo detecting circuit and a frequency measuring circuit. In the echo detecting circuit a diode switching circuit isolated the pulsed oscillator from the crystal and also protected the detector by clipping the initial pulse while minimizing attenuation of the low amplitude echoes. The 1 MHz signals were fed directly to an oscilloscope (Tektronix Type 555), but the higher frequency signals were detected by a Hewlett-Packard 855 Spectrum Analyzer before going to the oscilloscope. For the attenuation measurements the height of the first echo was measured with a voltage comparator unit (Type W) for different transducer positions.

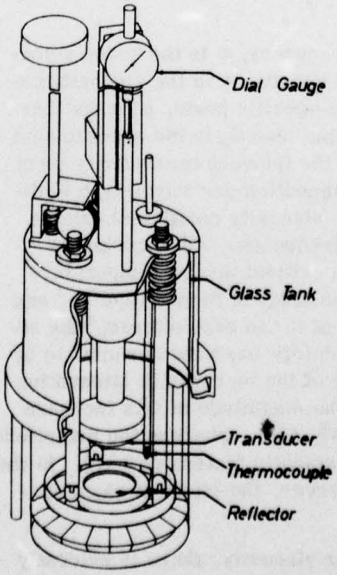

FIG. 1. Measurement chamber.

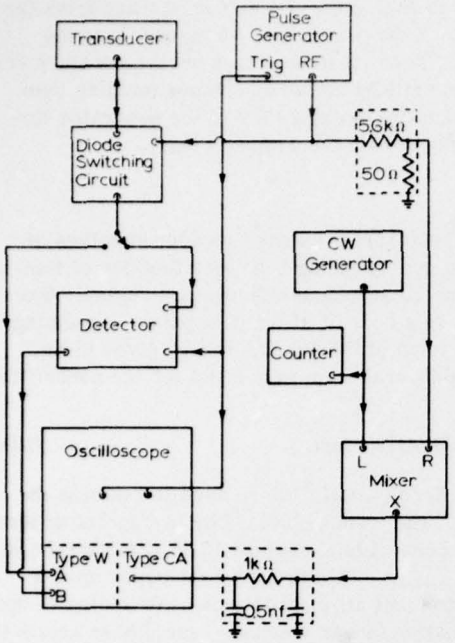

FIG. 2. Electronic system.

For the velocity measurements, echoes from double pulses generated by the Arenberg oscillator were overlapped to measure wavelength by a modified interferometer technique. The frequency counting circuit used a mixer (HP10504A/B) to mix the short (i.e., 20 μsec) rf pulses with a cw signal generated by an HP8601A Signal Generator. The difference frequency output signal from the mixer was displayed with the oscilloscope and the frequency of the generator was adjusted for zero beat. The frequency of the generator was then counted by a General Radio 1191-B Counter.

Temperature regulation was provided for the liquids under investigation through heat exchange liquids surrounding the tank. The temperature of the heat exchange liquids was regulated by a Haake Circulator. This regulation was $\pm 0.02\,^{\circ}C$ inside the circulator. The temperature stability of the binary liquids was much better than this because they were inside a carefully insulated container. The temperature of the binary liquids was measured by the glass-encapsulated iron-constantan thermocouple shown in Fig. 1 and displayed on a strip chart recorder.

After assembly, the apparatus was tested by making a measurement of α/f^2 for distilled water between 0 and $23.5\,^{\circ}C$. The measured values of α/f^2 fell within the experimental scatter of the data of Smith and Beyer.[14] They stated an average probable error of 5% for their measurements.

In the calibration data, as well as in the critical mixing data, a diffraction correction was made.[15] This correction was as large as 50% at 1 MHz, and was only 1% at 9 MHz. The intermediate frequencies had a correction between these extremes.

Velocity of ultrasonic waves in distilled water measured between 0 and $20\,^{\circ}C$ exhibited a mean deviation of 0.17% from the curve given by Wilson.[16]

Viscosity measurements were made using an Ostwald capillary viscometer in a bath whose temperature was controlled by an Artronix Model 5301 Temperature Controller. The viscometer was calibrated by using distilled water as a reference liquid.

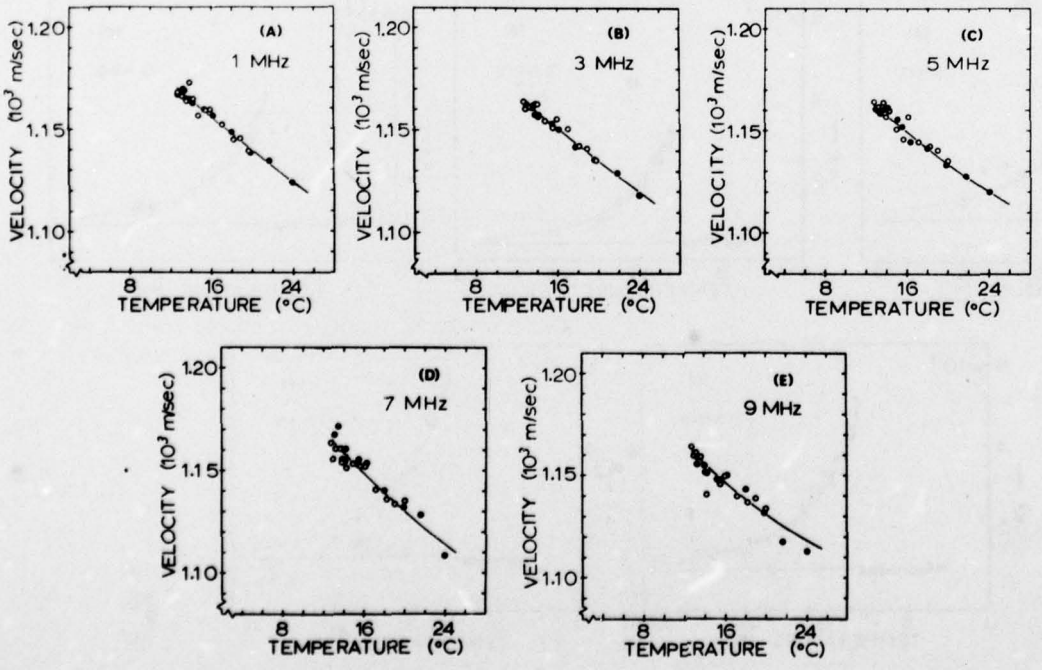

FIG. 3. Ultrasonic wave velocity in the single-phase region above the critical temperature $12.7\,^{\circ}C$.

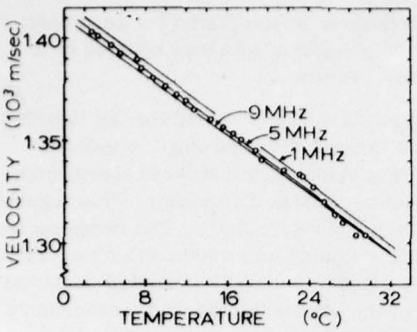

FIG. 4. Ultrasonic wave velocity in chlorex as a function of temperature.

RESULTS AND DISCUSSION

Velocity

Measured values of the ultrasonic wave velocity in the critical temperature region are shown in Figs. 3(a)–3(e) for the frequencies 1, 3, 5, 7, and 9 MHz. It is seen that the velocity in the single-phase temperature region increases as the critical temperature is approached. This behavior is the reverse of that predicted by the Fixman theory, but is reconcilable with it.[6] Both chlorex and hexane have a negative temperature coefficient larger than that for the mixture at the critical temperature. The temperature coefficient of hexane is[17] -4.4 m/sec °C. The velocity in chlorex as a function of temperature is given in Fig. 4, where the temperature coefficient is found to be -3.57 m/sec °C. (The data points for 5 MHz are shown in the figure; those for 1 and 9 MHz are not. The scatter at these frequencies was similar to that at 5 MHz.) The temperature coefficient of the velocities in Fig. 3 is ~ -4 m/sec °C away from the critical point. It decreases to ~ -5 m/sec °C at the critical point. Thus, it is seen that the temperature coefficient of the critical mixture becomes smaller than that of the noncritical mixture (or of the separated liquids) in agreement with the Fixman theory.

Attenuation

In Figs. 5(a)–5(e) are presented measured values of the attenuation per wavelength $\alpha\lambda$ as a function of temperature in the single-phase temperature region. The solid curves are a best fit of the data points, assuming the functional form of the Fixman theory given in Eq. (10) with an additional term to account for the noncritical attenuation:

$$\alpha\lambda = \pi H \,\mathrm{Im}[F(d)] + \text{const.} \tag{12}$$

The tables of Kendig *et al.*[18] were used to evaluate the integral $F(d)$. The values obtained by extrapolating these curves to the critical temperature 12.7 °C are shown in Table I as $\alpha\lambda_{\text{critical}}$. This procedure depends upon a tacit assumption that all mechanisms contributing to the critical attenuation (shear viscosity, etc.) have approximately the same temperature dependence. The fit of the experimental data is taken as an indication of the validity of this approximation; however, an improvement in the approximation is possible.

Measurement of the shear viscosity as a function of temperature allows one to introduce the temperature dependence of the noncritical attenuation through use of Eq. (1). (The temperature dependence of velocity is obtained from Fig. 3.) Both viscosity and velocity data were obtained from linear extrapolation of the asymp-

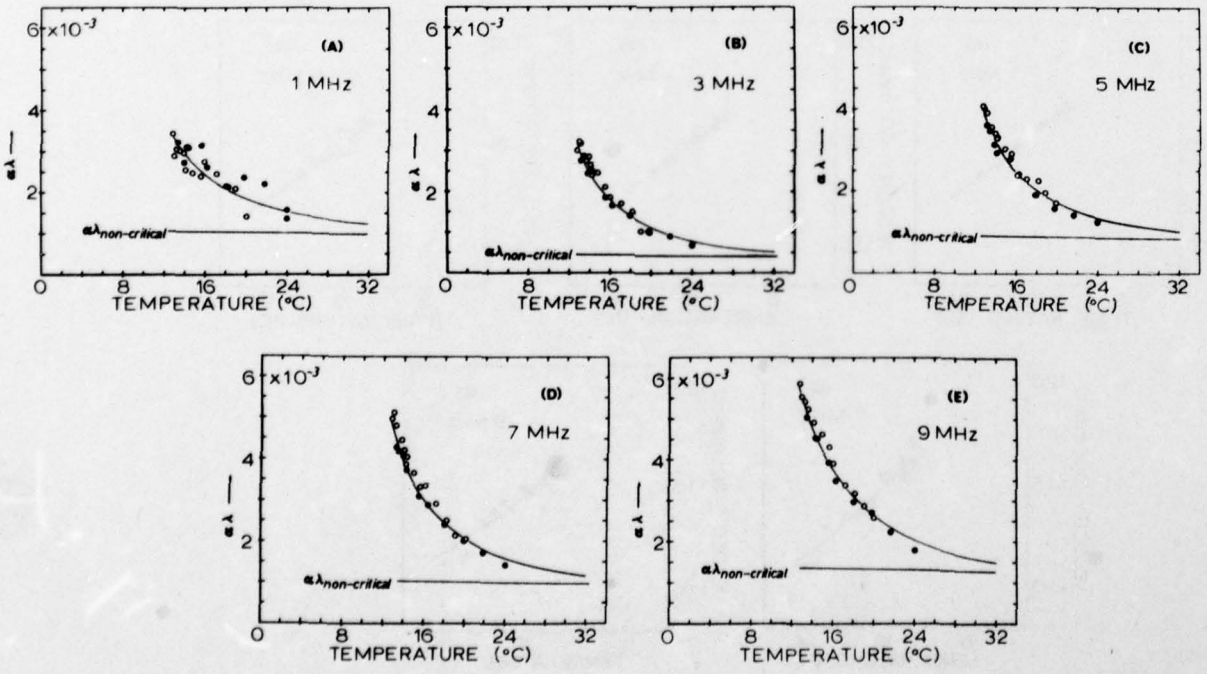

FIG. 5. Attenuation per wavelength in the single-phase region above the critical temperature 12.7 °C. Solid line is Fixman theory.

TABLE I. Parameters used in fitting data to the Fixman theory.

Frequency (MHz)	$\alpha\lambda_{critical}$	$\alpha\lambda_{excess}$	$\alpha\lambda_{Fixman}$	$(\alpha/f^2)_{excess}$ ($\times 10^{-16}$ sec^2/cm)
1	0.0034	0.00234	0.00199	200.0
3	0.0031	0.00265	0.00160	75.9
5	0.0040	0.00308	0.00134	53.0
7	0.0049	0.00387	0.00143	47.5
9	0.0057	0.00435	0.00121	41.6

totic values away from the critical point. For example, the assumed noncritical contribution to viscosity is indicated by a dotted line in Fig. 6, in which we have plotted experimental data for the chlorex–hexane mixture.

If one considers only shear viscosity, the attenuation per wavelength calculated from Eq. (1) is much smaller than that observed. Since we are unable to calculate the bulk viscosity contribution, we simply multiply by the factor required to bring the viscous attenuation to 80% of the attenuation calculated from Eq. (12) at 30 °C. (The trend of the data indicates that the noncritical contribution to $\alpha\lambda$ has approximately this value at that temperature. The use of 100% instead of 80% alters the magnitudes of calculated coefficients by a small amount, but does not alter the conclusion.) Using the extrapolated noncritical temperature dependence of η and c, the noncritical attenuation is extrapolated to 12.7 °C. The calculated curves are superimposed on Fig. 5. The critical contribution from shear viscosity and velocity would raise these curves by approximately 5% at the critical temperature. On the scale of Fig. 5, this difference is less than the width of the line labelled $\alpha\lambda$ noncritical.

The difference between the two curves in Fig. 5 at 12.7 °C has been defined as the excess attenuation per wavelength resulting from critical phenomena as follows:

$$\alpha\lambda_{excess} = \alpha\lambda_{critical} - \alpha\lambda_{noncritical}. \tag{13}$$

This excess attenuation, given in column 3 of Table I, is observed to be made up of two parts which have different frequency dependence:

$$\alpha\lambda_{excess} = \alpha\lambda_{Fixman} + \alpha\lambda_{viscelike}. \tag{14}$$

According to Eq. (10), $\alpha\lambda_{Fixman}$ is proportional to $f^{-1/4}$. The remaining attenuation per wavelength has been labeled "viscelike" because it is proportional to f, as is the viscosity contribution.

These values of $\alpha\lambda$ can be expressed in terms of α/f^2 by dividing by cf. Values of $(\alpha/f^2)_{excess}$ are given in Table I. Since viscosity contributions to α/f^2 are constant in frequency, one can plot α/f^2 as a function of frequency and identify the viscositylike contribution from an evaluation of the intercept. We chose to use the frequency dependence of $f^{-5/4}$ expected from the Fixman contribution as abscissa in Fig. 7. The fact that the data fall on a straight line with a nonzero intercept indicates that α/f^2_{excess} is adequately expressed by the sum of two terms:

$$(\alpha/f^2)_{excess} = A' f^{-5/4} + B'. \tag{15}$$

The coefficient A' is identified with the Fixman contribution; B' is viscositylike. Since the magnitude of B' is independent of frequency, this intercept value can be subtracted at each frequency to isolate the contribution of the Fixman mechanism.

The effect on $\alpha\lambda_{excess}$ of subtracting the viscositylike contribution is indicated in Fig. 8 in which we have plotted $\alpha\lambda_{excess}$ both before and after subtracting the viscositylike contribution obtained from Fig. 7. As can be seen, after correction the data follow a better straight-line behavior as a function of $f^{-1/4}$, in agreement with the Fixman theory. The uncorrected data show a curvature not seen in $\alpha\lambda_{Fixman}$. Use of any value of B' other than the intercept value of Fig. 7 introduces a similar curvature in $\alpha\lambda_{Fixman}$.

One can attempt to explain this viscositylike contribution by assuming that all viscous mechanisms increase in proportion to shear viscosity in the critical region. The viscosity increased by 6% in the critical region, as shown in Fig. 6. This would lead to an excess attenuation indicated by the cross-hatched region in

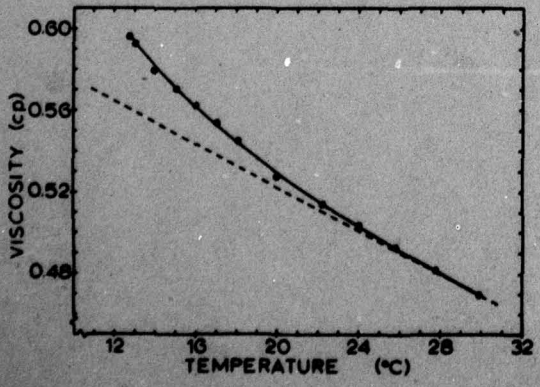

FIG. 6. Shear viscosity of the binary mixture above the critical temperature 12.7 °C.

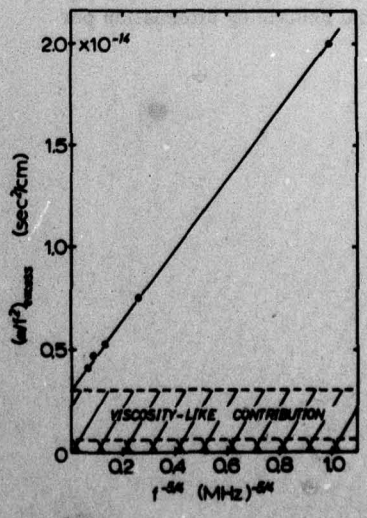

FIG. 7. Critical point values of the excess α/f^2 fitted to $f^{-5/4}$ dependence.

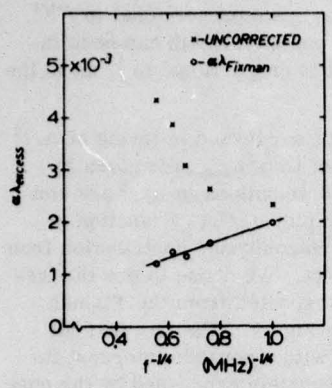

FIG. 8. Critical point values of the attenuation per wavelength fitted to the frequency dependence predicted by Fixman.

Fig. 7, which is less than 20% of the viscositylike contribution. We see, therefore, that simple assumptions about the viscous mechanisms do not allow us to account for the excess attenuation. But whatever its origin, the remaining excess attenuation appears to have a frequency dependence which is the same as that of viscosity.

CONCLUSION

Measured values of velocity and attenuation of ultrasonic waves in the critical temperature region of a chlorex–hexane mixture have been compared with the theory of Fixman. The velocity data show a trend which is consistent with the Fixman predictions. The attenuation data are found to be described by a sum of two terms. The frequency dependence of one term is in agreement with that predicted by the Fixman theory. The frequency dependence of the second term is that expected from shear viscosity; however, the magnitude of the viscositylike term is greater than can reasonably be expected from the critical increase in shear viscosity for this mixture. Although there should be a similar frequency dependence resulting from thermal conductivity, this contribution is expected to become vanishingly small in the critical region.[9] It would be tempting at this point to attribute the remaining attenuation per wavelength to bulk viscosity effects; however, such an assumption would be inconsistent with the results of Kawasaki and Tanaka,[9] who show that in the critical region the bulk viscosity produces an $\alpha\lambda$ which has the same form as the Fixman integral [Eq. (3)].

Note added in Proof: A recent publication by Peter H. Rogers and A. L. VanBuren [J. Acoust. Soc. Am. **55**, 724 (1974)] gives a simple closed-form expression which makes the correction of attenuation data for the effects of diffraction quite direct. In addition, this expression is valid over a wider range of distances than the graphical correction of Seki, Granato, and Truell (Ref. 15).

*Research supported by the U. S. Office of Naval Research. Based on experimental results of Elizabeth C. Miller (Bains), Ph.D. dissertation, University of Tennessee, 1972.

[1]R. Lucas and P. Biquard, Trans. Faraday Soc. 33, 130 (1937).
[2]A. E. Brown and E. G. Richardson, Phil. Mag. 4, 705 (1959).
[3]A. E. Brown, Acustica 18, 169 (1967).
[4]A. G. Chynoweth and W. G. Schneider, J. Chem. Phys. 19, 1566 (1951).
[5]A. V. Anantaraman, A. B. Walters, P.D. Edmonds, and C. J. Pings, J. Chem. Phys. 44, 2651 (1966).
[6]G. D'Arrigo, L. Mistura, and P. Tartaglia, Phys. Rev. A 1, 286 (1970).
[7]J. Friedländer, Z. Phys. Chem. 38, 385 (1901).
[8]M. Fixman, J. Chem. Phys. 36, 310 (1962).
[9]K. Kawasaki and M. Tanaka, Proc. Phys. Soc. 90, 791 (1967).
[10]M. Fixman, J. Chem. Phys. 36, 1961 (1962).
[11]G. D'Arrigo and D. Sette, J. Chem. Phys. 48, 691 (1968).
[12]S. S. Yun, J. Chem. Phys. 52, 5200 (1970).
[13]P. Kruus and T. A. Bak, Acta Chem. Scand. 20, 231 (1966).
[14]M. C. Smith and R. T. Beyer, J. Acoust. Soc. Am. 20, 608 (1948).
[15]H. Seki, A. Granato, and R. Truell, J. Acoust. Soc. Am. 28, 230 (1956).
[16]W. D. Wilson, J. Acoust. Soc. Am. 31, 1067 (1959).
[17]W. Schaaffs, "Molecular Acoustics," in *Landolt-Börnstein Numerical Data, New Series*, edited by K. H. Hellwege and A. M. Hellwege (Springer, Berlin, 1967), Vol. 5, p. 41.
[18]A. P. Kendig, R. H. Bigelow, P. D. Edmonds, and C. J. Pings, J. Chem. Phys. 40, 1451 (1964); ADI Auxiliary Publication Project, Photoduplication Service, Library of Congress, Washington, D.C., Document No. 8744.

Ultrasonic wave attenuation in the critical temperature region of binary liquid mixtures*

Elizabeth M. Bains and M. A. Breazeale

Department of Physics, The University of Tennessee, Knoxville, Tennessee 37916
(Received 13 September 1974)

Recently we published measurements of the attenuation and velocity of ultrasonic waves in the critical temperature region of the binary system hexane and β,β'-dichloroethyl ether.[1] By assuming a "viscosity-like" contribution to the critical attenuation in addition to the noncritical attenuation (which also has the frequency dependence expected for attenuation due to viscosity), we were able to obtain agreement with the theory of Fixman for the critical $\alpha\lambda$ as well as α/f^2. Previous authors, in fitting data to the Fixman theory, found agreement with α/f^2, but not with $\alpha\lambda$.[2-6] In this note we demonstrate that the assumption of a critical region "viscosity-like" contribution in the data for several other mixtures identifies a term in the critical $\alpha\lambda$ which agrees with the $f^{-1/4}$ frequency dependence of the Fixman[7] theory.

Figure 1 gives α/f^2 as a function of $f^{-5/4}$ for the binary mixtures listed. These data were taken from Refs. 1–6. In every case the agreement between data points and the straight line shown (the least squares fit of the data) is satisfactory, confirming the agreement of α/f^2 with the Fixman theory reported for these data. The nonzero intercept value isolates a part of α/f^2 that is independent of frequency, as is the attenuation due to viscosity. For all the data except that of Ref. 1, the intercepts include the noncritical attenuation as well as the critical region "viscosity-like" contributions. The noncritical attenuation was subtracted from each data point in Ref. 1 so that the intercept is only the "viscosity-like" contribution.

In Fig. 2 are given the same data plotted in the form $\alpha\lambda$ as a function of $f^{-1/4}$, which is the frequency dependence predicted by Fixman. The values of $\alpha\lambda$ were calculated by subtracting the intercept values shown in Fig. 1 from the appropriate experimental values of α/f^2 and multiplying by cf. As can be seen, the data points in Fig. 2 agree quite well with the straight lines, with the possible exception of the data of D'Arrigo, Mistura, and Tartaglia.[6] Several of their data points are also seen not to lie exactly on the line of Fig. 1. A smaller intercept on the α/f^2 curve would lead to a more linear $\alpha\lambda$ curve; however, for consistency we chose to define the intercept by the least squares fit of α/f^2 as a function of $f^{-5/4}$. The curvature of the $\alpha\lambda$

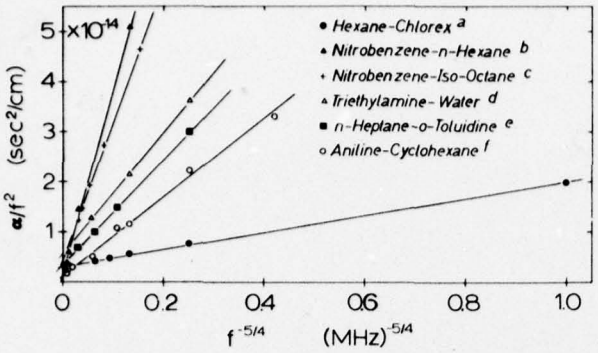

FIG. 1. Measured frequency dependence of α/f^2 for binary liquid mixtures. (a) Reference 1. (Chlorex is the common name for β, β'-dichloroethyl ether.) (b) Reference 2. (c) Reference 3. (d) Reference 4. (e) Reference 5. (f) Reference 6.

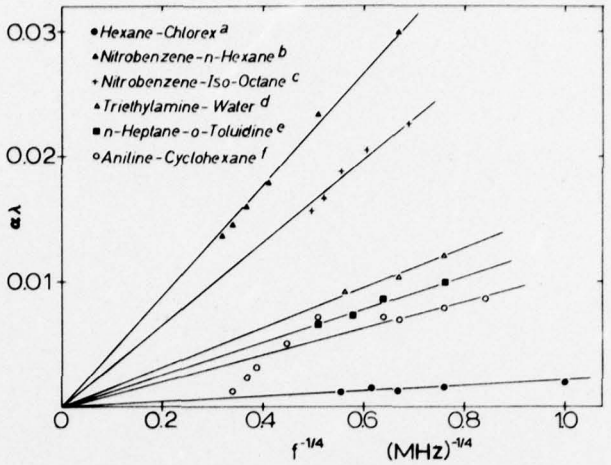

FIG. 2. Frequency dependence of $\alpha\lambda$ for binary liquid mixtures. (a) Reference 1. (b) Reference 2. (c) Reference 3. (d) Reference 4. (e) Reference 5. (Velocity was assumed to be 1250 m/sec. Another value would change the slope of the line slightly, but would make no change in the scatter of the data.) (f) Reference 6.

curves was found to be very sensitive to the magnitude of intercept used.

In Table I we compare the value of intercept found from Fig. 1 (for each set of data other than that of Ref. 1) with the value for noncritical attenuation obtained for those data by the experimenter. For the data of Ref. 1, as stated above, the figure shows values of excess α/f^2 with the noncritical contribution subtracted, so the existence of an intercept in that case clearly indicates a critical region "viscosity-like" term. Other experimenters expressed their total α/f^2 in the form

$$\alpha/f^2 = Af^{-5/4}\,\mathrm{Im}[F(d)] + B(T), \tag{1}$$

where $\mathrm{Im}[F(d)]$ is the imaginary part of the integral given by Fixman,[7] d depends on the temperature, and A and $B(T)$ are constants obtained by fit of the data to the temperature dependence predicted by Fixman. The term $B(T)$ is identified as the noncritical part of α/f^2. D'Arrigo, Mistura, and Tartaglia gave the value of $B(T)$ listed in Table I from their fit; the other values are average values for all frequencies calculated from experimental values of α/f^2 and the empirical A. In each case the intercept (which is the value required to isolate the Fixman term in $\alpha\lambda$) is larger than the previously calculated noncritical value of α/f^2. This would have remained true even if we had used a smaller intercept to bring the data of D'Arrigo, Mistura, and Tartaglia into better alignment.

In summary, the procedure we have outlined isolates that part of the critical attenuation that is accounted for by the theory of Fixman. For the cases given above, it also shows that a "viscosity-like" term exists in the critical region. For the hexane and β, β'-dichloroethyl ether system, it was found[1] that the critical region increase in shear viscosity was not sufficiently large to account for the magnitude of the "viscosity-like" term. Whether or not this is true for the other cases cannot be answered at present because of the lack of data on excess critical point viscosity for the other systems.

TABLE I. Comparison between intercept values of α/f^2 from Fig. 1 and the total noncritical α/f^2 obtained by the experimenter.

Binary mixture	Intercept ($\mathrm{sec}^2/\mathrm{cm}$)	$B(T)$ ($=\alpha/f^2$ noncritical) ($\mathrm{sec}^2/\mathrm{cm}$)
Nitrobenzene–n-hexane[a]	148×10^{-17}	126×10^{-17}
Nitrobenzene–iso-octane[b]	435×10^{-17}	315×10^{-17}
Triethylamine–water[c]	565×10^{-17}	343×10^{-17}
n-Heptane–o-toluidine[d]	348×10^{-17}	186×10^{-17}
Aniline–cyclohexane[e]	148×10^{-17}	100×10^{-17}

[a] Reference 2.
[b] Reference 3.
[c] Reference 4.
[d] Reference 5.
[e] Reference 6.

*Research supported in part by the U. S. Office of Naval Research.

[1] E. M. Bains and M. A. Breazeale, J. Chem. Phys. 61, 1238 (1974).
[2] G. D'Arrigo and D. Sette, J. Chem. Phys. 48, 691 (1968).
[3] A. V. Anantaraman, A. B. Walters, P. D. Edmonds, and C. J. Pings, J. Chem. Phys. 44, 2651 (1966).
[4] S. S. Yun, J. Chem. Phys. 52, 5200 (1970).
[5] S. N. Rao and K. S. Rao, J. Phys. Soc. Jpn. 33, 847 (1972).
[6] G. D'Arrigo, L. Mistura, and P. Tartaglia, Phys. Rev. A 1, 286 (1970).
[7] M. Fixman, J. Chem. Phys. 36, 1961 (1962).

PART II

Paper No.

1. "Comparison of Methods for Absolute Calibration of Ultrasonic Fields" (M. A. Breazeale and F. Dunn), J. Acoust. Soc. Am. 55 (3), 671-672 (1974).

2. "Elimination of Transducer Bond Corrections in Accurate Ultrasonic-Wave Velocity Measurements by Use of Capacitive Transducers" (John H. Cantrell, Jr., and M. A. Breazeale), J. Acoust. Soc. Am. 61 (2), 403-406 (1977).

Comparison of methods for absolute calibration of ultrasonic fields*

M. A. Breazeale

Physics Department, University of Tennessee, Knoxville, Tennessee 37916

F. Dunn

Bioacoustics Research Laboratory, University of Illinois, Urbana, Illinois 61801

(Received 10 December 1973)

Methods of determining the absolute ultrasonic pressure amplitude under identical circumstances are compared. Methods used are (1) radiation force on a small sphere, (2) thermoelectric probe, and (3) three optical techniques.

Subject Classification: 35.80; 80.30.

At the recent Society meeting in Miami (28 November–1 December 1972), the Technical Committee on Physical Acoustics sponsored three sessions on ultrasonic energy and power measurements. These sessions included state-of-the-art invited papers, tutorial papers, round table discussions, and contributed papers on current investigations. The attendance and discussion participation clearly showed that such measurements, and their interpretation, are of fundamental importance in a variety of ultrasonic research programs. During the round table discussions and discussions following formal presentations, a question was raised about the degree to which various absolute measurement procedures compare. Though considerable interest was exhibited in this point, no published works were recalled, extemporaneously, for citation. The present authors were reminded that they carried out such a comparison involving five different methods, at two laboratory sites, in 1958, but that the results had not been published. We report herein our findings in the hope that we may answer some of the questions raised in Miami.

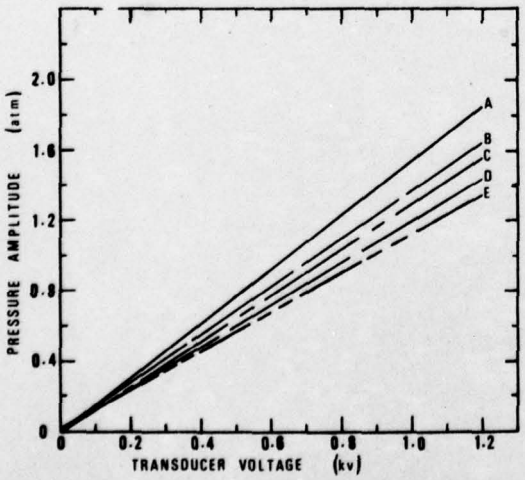

FIG. 1. Calibration of a 990-kHz quartz transducer: (A) calculated output with $e_{11}=4.77\times10^4$; (B) thermocouple probe; (C) optical image broadening (refraction); (D) light diffraction; (E) decrease of light intensity (refraction).

The circumstances of this comparison involved the research programs at Michigan State University under the direction of the late E. A. Hiedemann and at the University of Illinois under the direction of the late W. J. Fry. The former group had been concerned with three optical methods, viz., the refraction (image broadening) method,[1] the diffraction method,[2] and the refraction (decrease of light intensity) method,[3] while the latter group had been employing the method of radiation force on a small solid sphere[4] and the transient thermoelectric method.[5] While each group had found favorable comparison among the methods they embraced, more extensive treatment was considered desirable. The procedure involved the Illinois group calibrating one of its thermocouple probes against the radiation force detector (small solid sphere) and transporting it to the Michigan State campus where the former's experimental arrangement was duplicated. Thus the thermocouple probe was operated by the Michigan State group in the same way as in Illinois and its output compared with that detected by the three optical methods mentioned above. Figure 1 illustrates this comparison in water for the output from a 6-cm-diam quartz transducer, fundamental thickness resonant frequency 990 kHz. Curve A is the output calculated under the assumption that the transducer is a piston-like vibrator. The piezoelectric constant $e_{11}=4.77\times10^4$ was used in this calculation. Curve B is the average of values from the thermocouple probe, after correction for temperature variation of the output. Curve C is from the optical image broadening method.[1] Curve D is from the light diffraction method.[2] Curve E is from the decrease of light intensity method.[3] It is seen that the experimental results exhibit a total range of approximately ±10% about the mean, and that this mean is approximately 27% below that calculated from the voltage applied to the transducer. Because of the assumptions made in the calculation, one should consider this calculated value to be the maximum value possible under ideal conditions. The true value should be less than this, as the experimental results show.

Although further refinements of the optical methods[6] have reduced the scatter among the data, and the availability of lasers now makes the optical methods more direct, we present these results as a guide in estimat-

ing the accuracy to be expected when the research program requires such data, and the possibility of detailed investigation of pressure amplitude measurement techniques does not exist.

*Research supported by the U. S. Office of Naval Research, Acoustics Programs.

[1]T. Hueter and R. Pohlman, Z. F. Angew. Physik 1, 405 (1949).
[2]G. Willard, J. Acoust. Soc. Am. 21, 101 (1949).
[3]A. Loeber and E. A. Hiedeman, J. Acoust. Soc. Am. 28, 27 (1956).
[4]F. E. Fox and V. Griffing, J. Acoust. Soc. Am. 21, 352 (1949).
[5]W. J. Fry and F. J. Fry, J. Acoust. Soc. Am. 26, 294, 311 (1954).
[6]M. A. Breazeale and E. A. Hiedemann, J. Acoust. Soc. Am. 31, 24 (1959).

Elimination of transducer bond corrections in accurate ultrasonic-wave velocity measurements by use of capacitive transducers*

John H. Cantrell, Jr. and M. A. Breazeale

Department of Physics, The University of Tennessee, Knoxville, Tennessee 37916
(Received 4 May 1976; revised 5 October 1976)

A capacitive-driver–capacitive-detector system for generation and detection of ultrasonic waves has been developed. This eliminates the necessity of bonding piezoelectric transducers to solid samples. With the capacitive-driver–capacitive-detector system, free–free boundary conditions exist at the sample surfaces and longitudinal ultrasonic-wave velocities in solids can be measured accurately without correcting for ultrasonic-wave phase shifts due to sample-bonded transducer interfaces. The capacitive driver has a mica dielectric which increases the breakdown potential, but maintains the free–free boundary conditions at the solid specimen surfaces. This allows for a larger-amplitude ultrasonic signal to be generated in the sample than is possible with an air-gap capacitive driver. This improves the precision of the measurement. The accuracy of the method is comparable with that of bonded-transducer methods, after bond corrections are made.

PACS numbers: 43.35.Yb, 43.35.Cg

INTRODUCTION

Ultrasonic pulse-echo techniques are widely used in the measurement of elastic-wave velocities. Three fundamental pulse-echo methods for measuring phase velocities in solids have been reported. They are the gated double-pulse superposition method of Williams and Lamb,[1] the pulse-superposition method of McSkimin,[2] and the echo-overlap technique of May[3] and Papadakis.[4]

Until recently, it has been necessary to generate the ultrasonic pulses and to detect the resulting echoes by applying bursts of rf to a piezoelectric transducer bonded to the specimen surface. Such an arrangement necessitates making a correction in the velocity measurement due to ultrasonic-wave phase shifts at the specimen-transducer interface. In some situations, the effect of this coupling between specimen and transducer leads to considerable error if neglected.[5]

In order to eliminate the bond problem in compressional-wave measurements, the air-gap capacitive detector previously used to measure amplitudes of ultrasonic waves[6,7] was modified to function as an air-gap capacitive driver as well.[8] The air-gap capacitive-driver–capacitive-detector combination allowed the sample ends to vibrate with free–free boundary conditions exactly. No bond corrections were necessary because there were no bonds.

It is the purpose of this paper to report on the development of a dielectric capacitive driver to replace the air-gap capacitive driver. This new driver is capable of generating longitudinal ultrasonic pulses whose amplitudes are much larger than those in the previous system. We show that free–free boundary conditions still exist at the sample surface with this driver and that the error in the velocity measurements, without making any corrections, is comparable to the error in velocity measurements made with bonded transducers, after corrections for bond phase shifts.

I. THE CAPACITIVE-DRIVER–CAPACITIVE-DETECTOR SYSTEM

Figure 1 shows the mechanical parts of the dielectric-capacitive-driver–air-gap-capacitive-detector system with the sample in place. The sample rests on the grounded outer portion of the detector assembly. The grounded outer portion of the dielectric capacitive detector is recessed approximately 10 μm so that the electrode and sample face form a parallel-plate capacitor. The detector electrode is kept at a dc bias of the order of 150 V. The ultrasonic vibration of the sample face varies the gap spacing (and hence the capacitance), thereby generating an alternating electrical signal between the electrode and ground. This signal is amplified and displayed on the oscilloscope. The capacitive detector has been refined to the point that it is capable of giving absolute displacement amplitudes for 30-MHz ultrasonic waves having amplitudes as small as 10^{-4} A.[9]

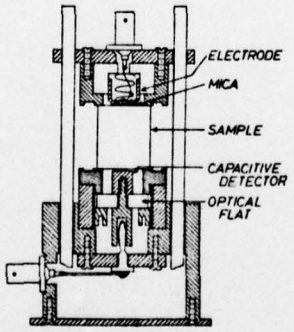

FIG. 1. Mechanical parts of the capacitive-driver–capacitive-detector system.

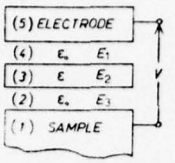

FIG. 2. Dielectric driver arrangement.

In the air-gap capacitive driver the inner electrode is also recessed approximately 10 μm to form a parallel plate capacitor with the sample surface, but in the dielectric capacitive driver a 7.5-μm-thick piece of mica (3) is sandwiched between the sample surface [outer electrode (1)] and the inner electrode (5) as shown in Fig. 2. Between the electrodes and the central mica dielectric (3) two air layers [(2) and (4)] are present because of slight irregularities of the contact surfaces.

The capacitive driver is not dc biased, but a pulsed sinusoidally varying rf voltage, $V = V_0 \sin\omega t$, applied between the electrodes [(1) and (5)], produces sinusoidally varying electric fields E_1, E_2, and E_3. It has been demonstrated[10] that the generation of ultrasonic waves in this situation is due to the effect of electrostatic forces acting directly on the ultrasonic-wave propagation medium. Hence, if E_3 is the electric field near the surface of the sample, the electrical force per unit area p at this surface is

$$p = \tfrac{1}{2}\epsilon_0 E_3^2 , \tag{1}$$

where ϵ_0 is the dielectric permittivity of air. Since

$$E_3 = E_{30} \sin\omega t , \tag{2}$$

then

$$p = \tfrac{1}{2}\epsilon_0 E_{30}^2 \sin^2\omega t = \tfrac{1}{4}\epsilon_0 E_{30}^2 (1 - \cos 2\omega t). \tag{3}$$

For present purposes, it is adequate to ignore the constant term in Eq. (3) and consider only the $\cos 2\omega t$ term. One sees that the pressure on the sample surface is applied at *twice* the frequency of the rf voltage. Thus, the ultrasonic wave generated in the sample has twice the frequency of the applied rf voltage.

II. THE EXPERIMENTAL SYSTEM

A. Method of measurement

The velocity measurements were made with the equipment arrangement as shown in Fig. 3. The gated double-pulse superposition method of Williams and Lamb[1] was employed. A pulsed ultrasonic signal is fed into the sample from the capacitive driver followed by another pulsed ultrasonic signal phase locked but delayed in time with respect to the first. The delay is adjusted such that superposition of the desired echoes from the two pulse trains is achieved. The resulting signal is received at the other end of the sample by the capacitive detector, passes through a wide-band i.f. amplifier whose center frequency is 20 MHz, and is displayed on an oscilloscope. Utilizing the fact that a continuous change in ultrasonic frequency results in a succession of superimposed echo maxima and minima, the ultrasonic velocity is calculated from

$$v = 2ml(\Delta f/\Delta n), \tag{4}$$

where Δf is the change in ultrasonic frequency corresponding to Δn minima, l is the sample length, and m is an integer (2 in our experiments) giving the relative position of the initial pulse train and the delayed pulse train. To enhance the sensitivity in detecting the superimposed echo minima, a boxcar integrator was incorporated into the system between the i. f. amplifier output and the oscilloscope.

B. A tuned transmission-line voltage transformer

The capacitive transducer is driven with a pulsed rf signal. The frequency is varied around 15 MHz to produce successive resonances. To obtain the voltages necessary for adequate ultrasonic amplitudes, a select length of transmission line was used to act as a tuned voltage transformer between the gated amplifier and the capacitive driver.

If S is the length of the transmission line, f is the rf drive frequency, V_s is the voltage across a purely reactive load of magnitude $|Z_L|$ (capacitive driver), V_0 is the voltage out of the gated amplifier, and Z_0 is the characteristic impedance of the transmission line, then for a lossless transmission line

$$V_s = V_0 \sin\phi \csc(\phi - \omega S/c), \tag{5}$$

where

$$\phi = -\tan^{-1}|Z_L|/Z_0 , \tag{6}$$

$$\omega = 2\pi f , \tag{7}$$

and c is the velocity of propagation of electromagnetic waves in the transmission line. Thus, for the proper length S, V_s/V_0 becomes very large. But the impedance looking out of the gated amplifier into the transmission line behaves as

$$Z_{in} = -jZ_0 \tan(\phi - \omega S/c). \tag{8}$$

Thus, for the condition that V_s/V_0 becomes large, Z_{in}, and consequently, V_0, become small. For this reason, the length of transmission line is chosen such that Z_{in}

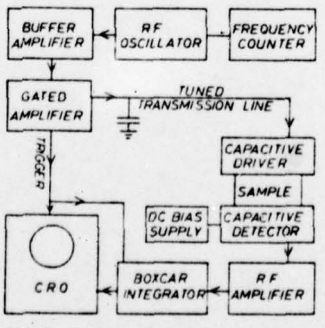

FIG. 3. Block diagram of experimental apparatus.

TABLE I. Sample lengths and comparative values of $\Delta f/\Delta n$ and velocity for air-gap driver measurements and dielectric driver measurements.

		Air gap driver		Dielectric driver	
Sample	Sample length (cm)	$\Delta f/\Delta n$ ($\times 10^{-2}$ MHz)	Velocity ($\times 10^5$ cm/sec)	$\Delta f/\Delta n$ ($\times 10^{-2}$ MHz)	Velocity ($\times 10^5$ cm/sec)
S-I	1.2593 ± 0.0002	5.8926 ± 0.0017	5.9364 ± 0.0020	5.8925 ± 0.0006	5.9363 ± 0.0012
S-II	1.2586 ± 0.0002	5.8957 ± 0.0013	5.9362 ± 0.0016	5.8958 ± 0.0005	5.9363 ± 0.0011
SW-I	1.2590 ± 0.0003	5.9099 ± 0.0017	5.9525 ± 0.0023	5.9100 ± 0.0005	5.9526 ± 0.0016
SW-II	1.2587 ± 0.0002	5.9121 ± 0.0013	5.9532 ± 0.0016	5.9122 ± 0.0004	5.9533 ± 0.0011
GE151	1.2721 ± 0.0001	5.8345 ± 0.0016	5.9378 ± 0.0017	5.8345 ± 0.0006	5.9378 ± 0.0008

looks inductive for our operation frequency. A variable capacitor is then placed in parallel with Z_{1a} to form a parallel resonant circuit. This arrangement increases the intensity of the generated ultrasonic signal by approximately 30 dB over that of the untuned transmission line.

The primary limitation on the generated ultrasonic-wave amplitude is set by dielectric breakdown in the capacitive transducer. However, this limitation is not as serious as one might assume. As the spacing of the electrodes in air is decreased, the breakdown potential goes up almost exponentially.[8] In the air-gap driver we were able to use fields as large as 200 kV/cm without breakdown. With the mica dielectric driver, we have been able to use fields larger than 1000 kV/cm.

III. EXPERIMENT AND RESULTS

In order to determine the effect of contact between the mica dielectric and the sample surface, velocity measurements were made on five fused silica samples at room temperature. Each sample was measured ten times with the dielectric capacitive driver and ten times with the air-gap capacitive driver. The results of the measurements are shown in Table I. The average values and standard deviations of $\Delta f/\Delta n$ and longitudinal velocities [Eq. (4)], as well as sample length l are given.

Previous work comparing velocity measurements with bonded transducers and air-gap transducers has confirmed experimentally that the air-gap capacitive-driver–capacitive-detector system eliminates the effects of transducer bonding.[8] The present agreement between the air-gap- and dielectric-driver measurements of $\Delta f/\Delta n$ for each sample confirms within experimental error that the dielectric driver also eliminates the effects of transducer bonding.

A. Analysis of error

The standard deviation in $\Delta f/\Delta n$ with the dielectric driver (approximately 0.008%) is significantly lower than with the air-gap driver (approximately 0.025%) because of the much larger ultrasonic signal generated by the dielectric driver. The null frequencies of the superimposed pulse trains were reproducible to within ±30 Hz, which is approximately two parts in 10^6. The relatively large standard deviations in the velocity calculations in Table I are due to lack of parallelism of the sample surfaces, which is reflected in the relatively large uncertainties in the sample lengths listed.

With electrically nonconducting samples, it is necessary to coat the end surfaces with a thin film of conducting material to function as the ground plates of the capacitive transducers. We found that approximately 1000 Å of copper is ideal for our purposes. According to our calculations, this coating introduces an error of no more than 0.003% in the velocity measurements.

Corrections in the velocity measurements due to diffraction were calculated[11–13] and serve to decrease the values listed in Table I by approximately 0.005%.

It is found that the total uncertainty in compressional-wave-velocity measurements with the dielectric capacitive-driver–capacitive-detector system is comparable to the uncertainty in velocity measurements with systems using bonded transducers.[1,2–4,14]

B. Advantages of the new system

The advantages of the previous capacitive-driver–capacitive-detector system have been enumerated.[8] They are:

(1) The tedious calculation of the effect of ultrasonic-wave phase shift at the bonded transducer-sample interface has been eliminated, with no sacrifice in experimental accuracy.

(2) The effect of the transducer resonance has been eliminated. Capacitive transducers have a flat frequency response.

(3) The effect of a variation in electronic loading and/or the change in thickness of the bonded transducer due to temperature changes in cryogenic velocity measurements have been eliminated. (These variations often force a change in rf drive frequency of the bonded transducer to maintain a given pulse shape.)

(4) Accuracy of attenuation measurements is improved. It is well known, especially in measurements at cryogenic temperatures, that the effect of transducer bonds often sets a limit on the accuracy of attenuation measurements by introducing temperature-dependent phase shifts in the received signals. Such effects are eliminated with the capacitive transducer.

In addition to these advantages, the introduction of a dielectric into the capacitive driver allows one to work with large-amplitude signals. As we have shown, this dielectric does not affect the free–free boundary con-

ditions if one is careful to keep it dry. Therefore, the accuracy of the previous capacitive driver is maintained, while the larger-amplitude signals allow one to improve the precision of the measurement.

*Research supported by the Office of Naval Research.

[1]J. Williams and J. Lamb, J. Acoust. Soc. Am. 30, 308–313 (1958).
[2]H. J. McSkimin, J. Acoust. Soc. Am. 33, 12–16 (1961).
[3]J. E. May, Jr., IRE Nat. Conv. Rec. 6, Pt. 2, 134–142 (1958).
[4]E. P. Papadakis, J. Acoust. Soc. Am. 42, 1045–1051 (1967).
[5]H. J. McSkimin and P. Andreatch, J. Acoust. Soc. Am. 34, 609–615 (1962).
[6]W. B. Gauster and M. A. Breazeale, Rev. Sci. Instrum. 37, 1544–1548 (1966).
[7]R. D. Peters, M. A. Breazeale, and B. K. Paré, Rev. Sci. Instrum. 39, 1505–1506 (1968).
[8]John H. Cantrell, Jr. and M. A. Breazeale, Proc. IEEE Ultrason. Symp. 537–539 (1974).
[9]R. D. Peters and M. A. Breazeale, Appl. Phys. Lett. 12, 106–108 (1968).
[10]D. Legros, J. Lewiner, and P. Biquard, J. Acoust. Soc. Am. 52, 196–198 (1972).
[11]H. Seki, A. Granato, and R. Truell, J. Acoust. Soc. Am. 28, 230–238 (1956).
[12]E. P. Papadakis, J. Acoust. Soc. Am. 40, 863–876 (1966).
[13]G. C. Benson and Osamu Kiyohara, J. Acoust. Soc. Am. 55, 184–185 (1974).
[14]E. P. Papadakis, J. Acoust. Soc. Am. 52, 843–846 (1972).

PART III

Paper No.

1. "Ultrasonic Nonlinearity Parameters" (presented at the 8th International Congress on Acoustics, London, July 1974). Proceedings, Vol. II, p. 518.

2. "Acoustical Nonlinearities of Solids as a Function of Temperature" (invited paper presented at the 6th International Symposium on Nonlinear Acoustics, Moscow, July 1975), Proceedings, Vol. 2, pp. 133-147.

3. "Third-Order Elastic Constants of Germanium between 300 and 3°K" (James A. Bains, Jr., and M. A. Breazeale), Phys. Rev. B 13 (8), 3623-3630 (1976).

4. "Ultrasonic Nonlinearity Parameters of Fused Silica between 3°K and 300°K" (presented at the 9th International Congress on Acoustics, Madrid, July 1977), Proceedings, Vol. II, p. 577.

5. "Ultrasonic Investigation of the Nonlinearity of Fused Silica for Different Hydroxyl-Ion Contents and Homogeneities between 300 and 3°K" (John H. Cantrell, Jr., and M. A. Breazeale), Phys. Rev. B 17 (12), 4864-4870 (1978).

6. "Nonlinear Acoustics and Solid State Physics" (presented at the 8th International Symposium on Nonlinear Acoustics, Paris, July 1978), to be published in Journal de Physique.

ICA 8 1974

The Eighth International Congress on Acoustics London, July 1974

CONTRIBUTED PAPERS
VOLUME II

EIGHTH INTERNATIONAL CONGRESS
ON ACOUSTICS, LONDON 1974

ULTRASONIC NONLINEARITY PARAMETERS

Breazeale M A — University of Tennessee, Knoxville, Tennessee, USA

A consistent definition of the nonlinearity parameters of gases, liquids, and solids can be made. By using an appropriate form of the nonlinear wave equation

$$\rho_0 \frac{\partial^2 u}{\partial x^2} = K_2 \frac{\partial^2 u}{\partial x^2} + (3K_2 + K_3) \frac{\partial u}{\partial x} \frac{\partial^2 u}{\partial x^2} ,$$

the nonlinearity parameter $\kappa = -(\frac{3K_2 + K_3}{K_2})$ can be recognized as the negative of the ratio of the coefficient of the nonlinear term to that of the linear term. The nonlinearity parameter has considerable significance for solids[1,2] as well as for liquids and gases. For isotropic solids and the [100] direction in single crystals, $K_2 = C_{11}$ and $K_3 = C_{111}$. Thus, $\kappa = -(3 + \frac{C_{111}}{C_{11}})$. For liquids $\kappa = 2 + B/A$. For gases $\kappa = 1 + C_p/C_v$.

For example, we calculate room temperature values: for air, $\kappa = 2.4$; for water $\kappa = 7.0$; for copper $\kappa_{[100]} = 5.25$; for germanium $\kappa_{[100]} = 2.78$. But for fused silica $\kappa = -9.2$. In our harmonic distortion experiments, the negative nonlinearity parameter implies that the waveform approaches a "backward sawtooth" as the wave progresses. In addition, the magnitudes of κ for fused silica[3] seem to be sensitive to small amounts of impurities. An OH content of 1200 ppm led to a measured $\kappa = -9.64$. The same fused silica with only 5 ppm OH had a measured $\kappa = -9.25$.

Figure 1 shows recently measured nonlinearity parameters of germanium[4] and fused silica plotted as a function of temperature. Consistent with other single crystals measured to date[5], germanium κ's are almost independent of temperature. That for the fused silica sample is not. [Research supported in part by the U.S. Office of Naval Research.]

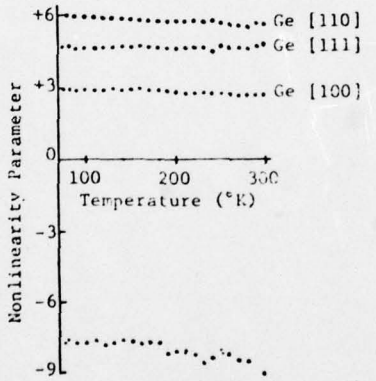

Fig. 1 Temperature Dependence of Nonlinearity Parameters

REFERENCES

(1) M.A. Breazeale and Joseph Ford, J. Appl. Phys. 36, 3486 (1965); (2) M.A. Breazeale, Int. J. Nondestructive Testing 4, 149 (1972); (3 & 4) W.T. Yost and M.A. Breazeale, J. Appl. Phys. 44, 1909 (1973); Phys. Rev. B 4 (1974); (5) R.D. Peters, M.A. Breazeale and V.K. Pare, Phys. Rev. B I, 3245 (1970).

МИНИСТЕРСТВО ВЫСШЕГО И СРЕДНЕГО
СПЕЦИАЛЬНОГО ОБРАЗОВАНИЯ СССР
МОСКОВСКИЙ ГОСУДАРСТВЕННЫЙ УНИВЕРСИТЕТ
им. М. В. ЛОМОНОСОВА

VI
МЕЖДУНАРОДНЫЙ СИМПОЗИУМ ПО НЕЛИНЕЙНОЙ АКУСТИКЕ

ПРОГРАММА

МОСКВА 1975

6th International Symposium on Nonlinear Acoustics
Moscow
July 8-10, 1975

[21]

ACOUSTICAL NONLINEARITIES OF SOLIDS AS A FUNCTION OF TEMPERATURE

M. A. Breazeale
Department of Physics
The University of Tennessee
Knoxville, Tennessee 37916
USA

International Symposium on Nonlinear Acoustics
Moscow
July 8-10, 1975

[22]

Acoustical Nonlinearities in Solids As a Function of Temperature

by

M. A. Breazeale
Department of Physics
The University of Tennessee
Knoxville, Tennessee 37919

ABSTRACT

Measurement of the fundamental and of the second harmonic of an initially sinusoidal ultrasonic wave in a solid allows one to compute its nonlinearity parameter. From this nonlinearity parameter one can isolate simple combinations of third order elastic constants.

We have developed apparatus for making measurement of the fundamental and of the second harmonic of an initially sinusoidal 30 MHz ultrasonic wave between 300°K and 3°K.

This apparatus and current results for copper, germanium and fused silica are discussed. It is shown that the finite amplitude distortion in fused silica is such that at the discontinuity distance one would have repeated rarefaction shocks. Both copper and germanium produce distortion which would lead to repeated compressional shocks.

In contrast to an assumption usually made in testing theories of the solid state, the third order elastic constants can change as a function of temperature--as much as 150% between 300°K and 3°K in one instance.

A detailed investigation of the subject of nonlinear acoustics is very important to the study of all acoustical phenomena. This is because technological progress has made possible the generation of large amplitude acoustical signals, and these signals of necessity propagate through a nonlinear medium. There are only a very few media which are truly linear, and even those which appear to be linear exhibit this behavior only under very special circumstances. An exact statement of what is meant by the words "linear medium" is surprisingly elusive, but this problem need not concern us at the present time. Rather, I want to discuss for a moment some very profound implications of the study of nonlinear acoustics to the subject of solid state physics.

The derivation of the nonlinear wave equation to describe acoustical nonlinearities in solids can be quite complicated for the general case. However, for special crystal symmetries the equations take a much simpler form. The nonlinear equations for isotropic solids and cubic crystals are as simple as that for fluids. As a matter of fact, these equations are identical to the equation for fluids within the approximation involved in making a Taylor expansion of the nonlinear equation for fluids and dropping higher-order terms. This is the reason one can speak meaningfully about nonlinearity parameters of solids as well as nonlinearity parameters of fluids.

It is through these nonlinearity parameters that one can make a fundamental connection between nonlinear acoustics and solid state physics. As a matter of

fact, nonlinear acoustics offers the possibility to measure quantities in solid state physics which cannot be measured by other techniques. Of course, in order for the acoustical quantities to be useful to people in solid state physics, a consistent definition of them must be made, and this has been done by Thurston.[1]

In my laboratory we have devoted considerable effort to the development of some new techniques for measuring the nonlinearity parameters of solids. Although initially it was sufficient to be able to measure nonlinearity parameters at room temperature, it soon became apparent that our results would be much more useful to solid state physics if we could measure as a function of temperature down to temperatures near the absolute zero. The most obvious reason for this is that theories of the solid state usually do not take into account the effect of thermal motion on elastic properties, and thus are made under the tacit assumption of absolute zero of temperature.

When one measures as a function of temperature, the apparatus of necessity becomes somewhat complicated. But the principles can remain simple. I should like to describe the apparatus we have developed in the past several years--emphasizing the principles involved--and to give some of our recent results on germanium as an indication of the solid state physics data available from studies of nonlinear acoustics.

An initially sinusoidal ultrasonic wave becomes distorted as it propagates through a nonlinear medium. Fourier analysis of this distorted wave shows that the second harmonic is the largest overtone. It grows linearly with propagation distance, and is proportional to the square of the frequency and the square of the amplitude of the fundamental component. In order to write down the

differential equation whose solution behaves in this fashion, one can specialize the equations to crystals having cubic symmetry and write

$$\rho_0 U_{tt} = K_2(U_{aa} + 3U_a U_{aa}) + K_3 U_a U_{aa} \tag{1}$$

where the subscripts denote partial differentiation with respect to the time and the space variable. The solution

$$U = U^{(0)} + U^{(1)}, \tag{2}$$

under the assumption that a sinusoidal wave is generated at a = 0, has the proper behavior. Measurement of the amplitude of the fundamental component

$$U^{(0)} = A \sin(ka-\omega t) \tag{3}$$

and of the second harmonic component

$$U^{(1)} = -\left(\frac{3K_2 + K_3}{8K_2}\right)(AK)^2 a \cos 2(ka-\omega t) \tag{4}$$

gives all the information necessary to calculate the nonlinearity parameter

$$\frac{3K_2 + K_3}{K_2}$$

for a solid if one confines his attention to the three principal directions in the cubic lattice, or any direction in an isotropic medium.

Before I go on to define what K_2 and K_3 are, let me digress for a moment and point out that the amplitude of the second harmonic (Eq. 4) has a minus sign in front of it. It turns out that for most media K_3 is negative and has a magnitude

greater than $3K_2$. This means that the second harmonic is positive. We reported in London last year[2] that an exception to this general rule exists. In fused silica at room temperature K_3 was assumed to be positive, with the result that in fused silica the minus sign is not concelled. This means that the second harmonic is generated 180° out of phase with that generated in other solids. Since that time we have developed a phase sensitive detector to measure the relative phase of the second harmonic in copper and in fused silica. The result is an unequivocal proof that the second harmonics are indeed 180° out of phase in the two.[3] This phase sensitive detector is now used routinely to monitor the phase of the second harmonic as we measure as a function of temperature. Therefore, in our data there is no possible ambiguity in sign of the second harmonic.

Let us now return to the definition of K_2 and K_3. For cubic crystals the expressions for K_2 and K_3 are given in Table I. As can be seen, for the principal directions K_2 and K_3 are linear combinations of second-order and third-order elastic constants, respectively. The second-order elastic constants can be obtained from measurement of ultrasonic wave velocity. Thus, measurement of the second harmonic of an initially sinusoidal ultrasonic wave gives values of these combinations of third-order elastic constants. For purposes of data analysis, I want to point out that the third-order elastic constant C_{111} appears in all of the expressions for K_3. Thus, these are not the simplest combinations of third-order elastic constants available from our measurements, since C_{111} can be subtracted from the expression for K_3 in the [110] direction. A similar simplification can be made in the expression for K_3 in the [111] direction, as I will show shortly.

Measurement of the amplitude of the fundamental and of the second harmonic component is made by use of a special form of capacitive microphone. We have measured the fundamental, the second harmonic and the third harmonic of a pulsed 30 MHz ultrasonic wave. A drawing of the capacitive microphone designed for measurement as a function of temperature is shown in Figure 1. An x-cut quartz transducer generates the ultrasonic wave which travels upward in the sample. The ends of the sample are optically flat and parallel. The end of the sample and the detector electrode form a parallel plate capacitor, whose spacing can be adjusted pneumatically by changing the pressure differential P_2-P_1. This adjustment is necessary because differential thermal expansion changes the spacing as the temperature is changed. Typically, this spacing is adjusted from 3 to 10 microns as the pressure differential is changed by one atmosphere. With such small spacing of the electrodes, and an applied d.c. bias of the order of 150 volts, the microphone is very sensitive. We can measure microvolts of signal generated as the pulsed ultrasonic wave impinges on the end of the sample. This means that ultrasonic wave amplitudes as small as 10^{-4} Angstroms can be measured, as can be seen in Figure 2, which is a plot of measured values of the third harmonic as a function of the cube of the fundamental amplitude. The data points are found at 0.1×10^{-3} Angstroms = 10^{-4} Angstroms. The slope of this curve gave a value of third-order elastic constants which agreed with values measured by other techniques to within approximately 10%. There were no adjustable parameters in the measurement.

A schematic diagram of the apparatus for measuring as a function of temperature is shown in Figure 3. The position of the capacitive microphone is labelled "detector." A pulsed 30 MHz signal is generated at the gated amplifier. This signal drives an x-cut quartz transducer to generate an

ultrasonic wave in the sample. The capacitive microphone on the opposite end of the sample produces an electrical signal proportional to the ultrasonic wave amplitude. This signal is amplified and is measured on an oscilloscope.

In order to measure the phase of the second harmonic we replaced the 60 MHz amplifier by a slightly more complicated frequency doubler phase sensitive detector shown in Figure 4. In the upper area the 30 MHz signal is fed through a phase shifter and a frequency doubler. The 60 MHz signal is then caused to interact coherently in the phase sensitive detector with the acoustically generated second harmonic. The output is then observed on an oscilloscope. As I have indicated, the results were unequivocal for fused silica and we are monitoring the phase as we measure as a function of temperature in order to detect any changes in the sign of the nonlinearity parameter.

We have measured the values of K_3 for copper and germanium single crystals down to 77°K, as shown in Figure 5. These combinations of third-order elastic constants are linear functions of temperature over this temperature range. As can be seen, some of the lines have an appreciable slope, so that even on the basis of these measurements we can state that it is inadequate to assume that the third-order elastic constants are independent of temperature. This assumption is often made in theories of the solid state.

Recently we have been able to extend the measurements in germanium down to much lower temperatures--down to 2.9°K. The results are shown in Figure 6. On our first run we were uncertain about the phase of the second harmonic, and hence the sign of K_3 in the temperature interval between 15°K and approximately 50°K. We had observed the fact that the Grüneisen parameter, which is a function of the third-order elastic constants, becomes negative in this region,

then is positive again at lower temperatures.[3] A second run with the phase sensitive detector produced the solid data points in the [110] direction. The uncertainty has been removed. These data represent our measurement of these combinations of third-order elastic constants.

These combinations of third-order elastic constants are not the simplest combinations available from our data, however. As I have already indicated, C_{111} and certain other combinations of third-order elastic constants appear in more than one of these curves, and can therefore be subtracted out. The result is shown in Figure 7. These combinations of third-order elastic constants are the simplest combinations available from our data without making any assumptions about the behavior of certain of them. We see that C_{111} is a linear function of temperature as far as we can measure, but the other combinations are strong functions of temperature below approximately 25°K. Of necessity, the behavior shown for the combination $C_{123} + 6C_{144} + 8C_{456}$ can be exhibited only if one or more of these constants becomes positive at very low temperatures. The implications of this statement to solid state physics are not truly appreciated at the present time. In addition, the behavior of the Grüneisen parameter of germanium is not mirrored in these data. Measurements of other combinations of third-order elastic constants will have to be made before one can be certain about any single constant other than C_{111}. The most direct method for making these measurements is not clear at the moment. Nevertheless, I think it is correct to say that investigations in nonlinear acoustics are making possible a much more detailed understanding of solid state physics.

TABLE I

Ultrasonic Wave Propagation Direction	K_2	K_3
[100]	C_{11}	C_{111}
[110]	$\frac{C_{11} + C_{12} + 2C_{44}}{2}$	$\frac{C_{111} + 3C_{112} + 12C_{166}}{4}$
[111]	$\frac{C_{11} + 2C_{12} + 4C_{44}}{3}$	$\frac{C_{111} + 6C_{112} + 12C_{144} + 24C_{166}}{9}$ $+ \frac{2C_{123} + 16C_{456}}{9}$

[30]

References

1. R. N. Thurston and M. J. Shapiro, J. Acoust. Soc. Am. 41, 1112 (1967).

2. M. A. Breazeale, 8th International Congress on Acoustics, Vol. 2, p. 518 (1974).

3. J. A. Bains and M. A. Breazeale, J. Acoust. Soc. Am. 57, 745 (1975).

List of Figures

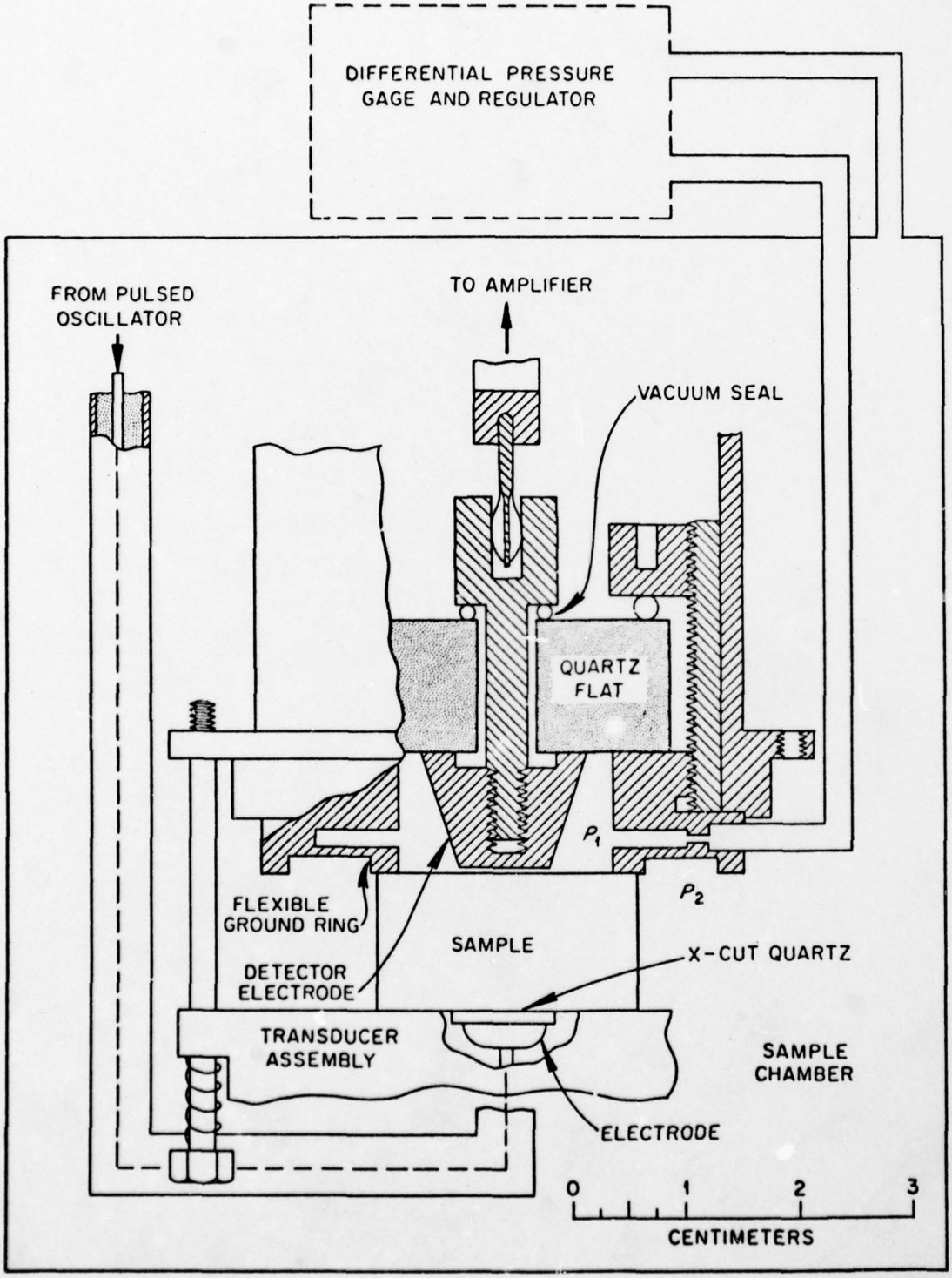

Fig. 1. Variable Gap Capacitive Detector

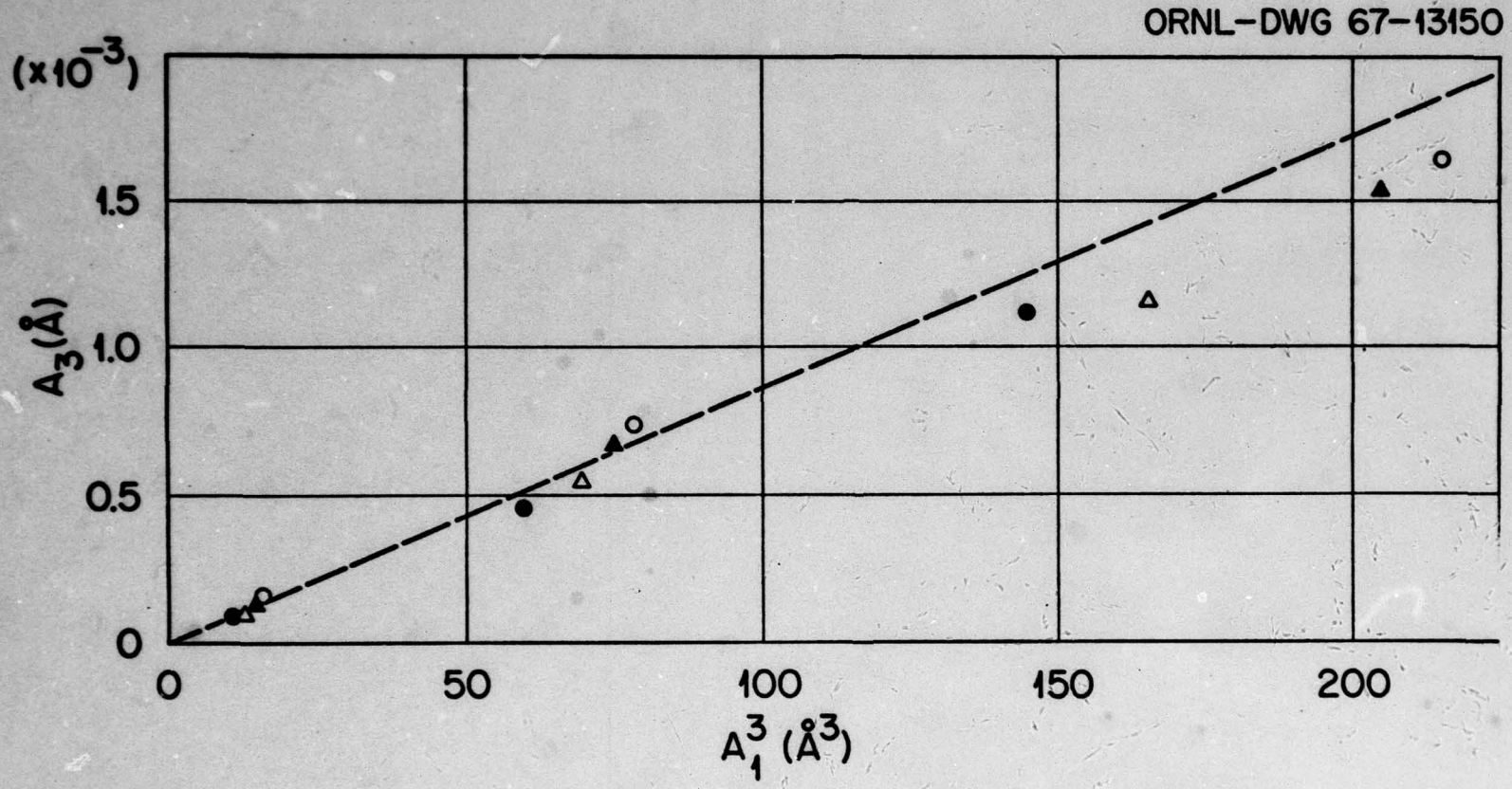

Fig. 2. Third Harmonic Amplitude versus the Cube of the Fundamental Amplitude in a [100] Copper Sample.

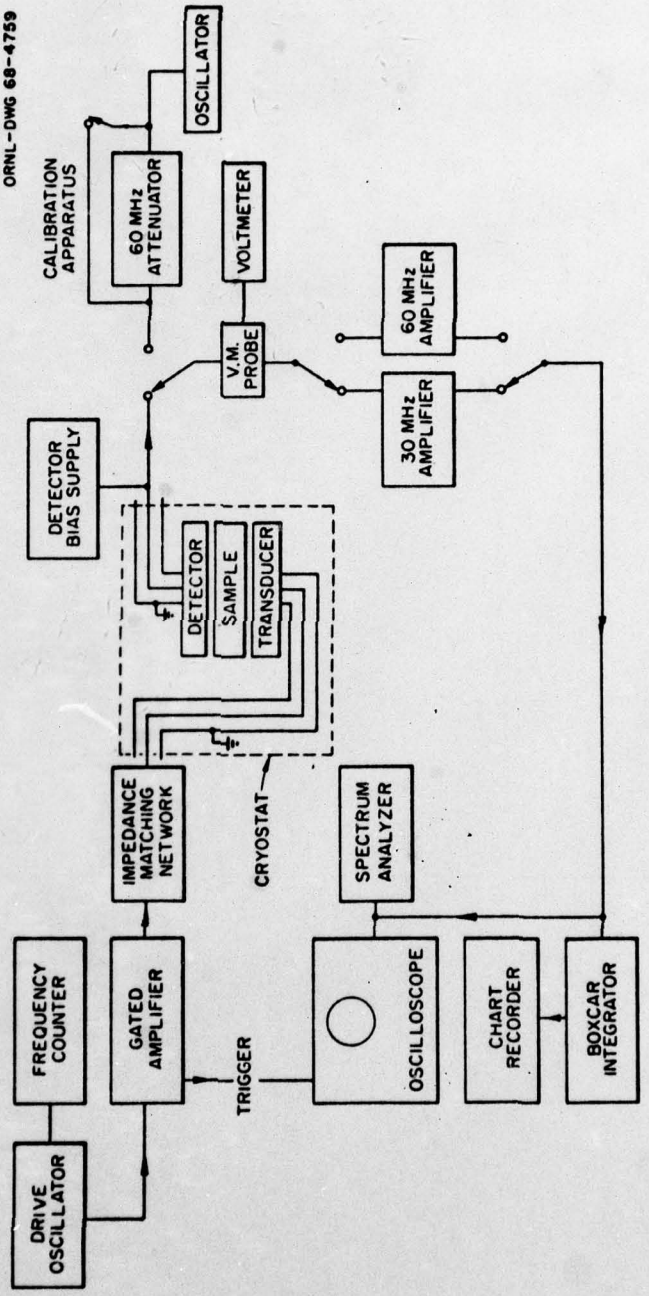

Fig. 3. Cryogenic Measurement System.

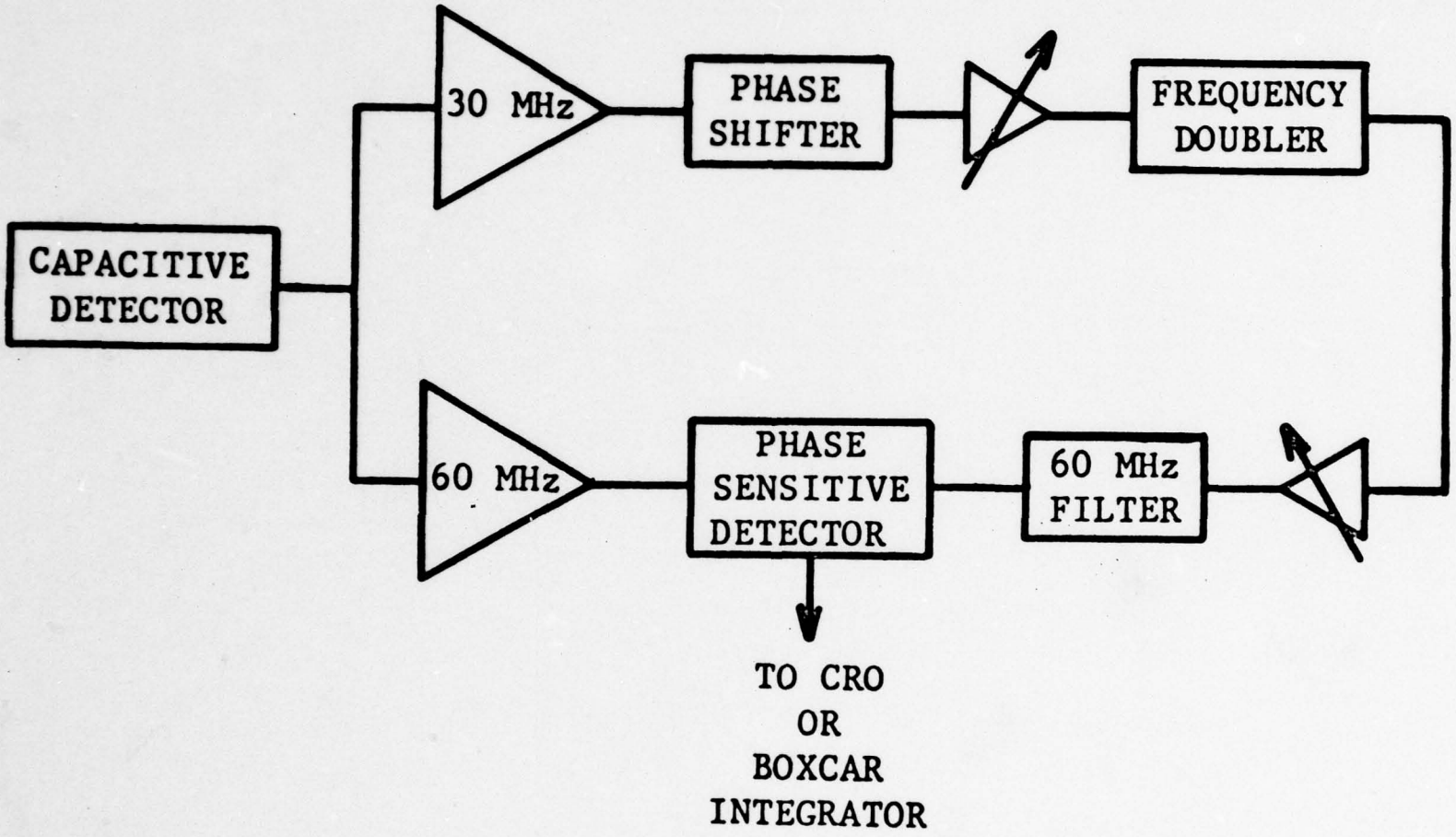

[36]

Fig. 4. Frequency Doubler Phase Sensitive Detector for Measuring Phase of the Second Harmonic.

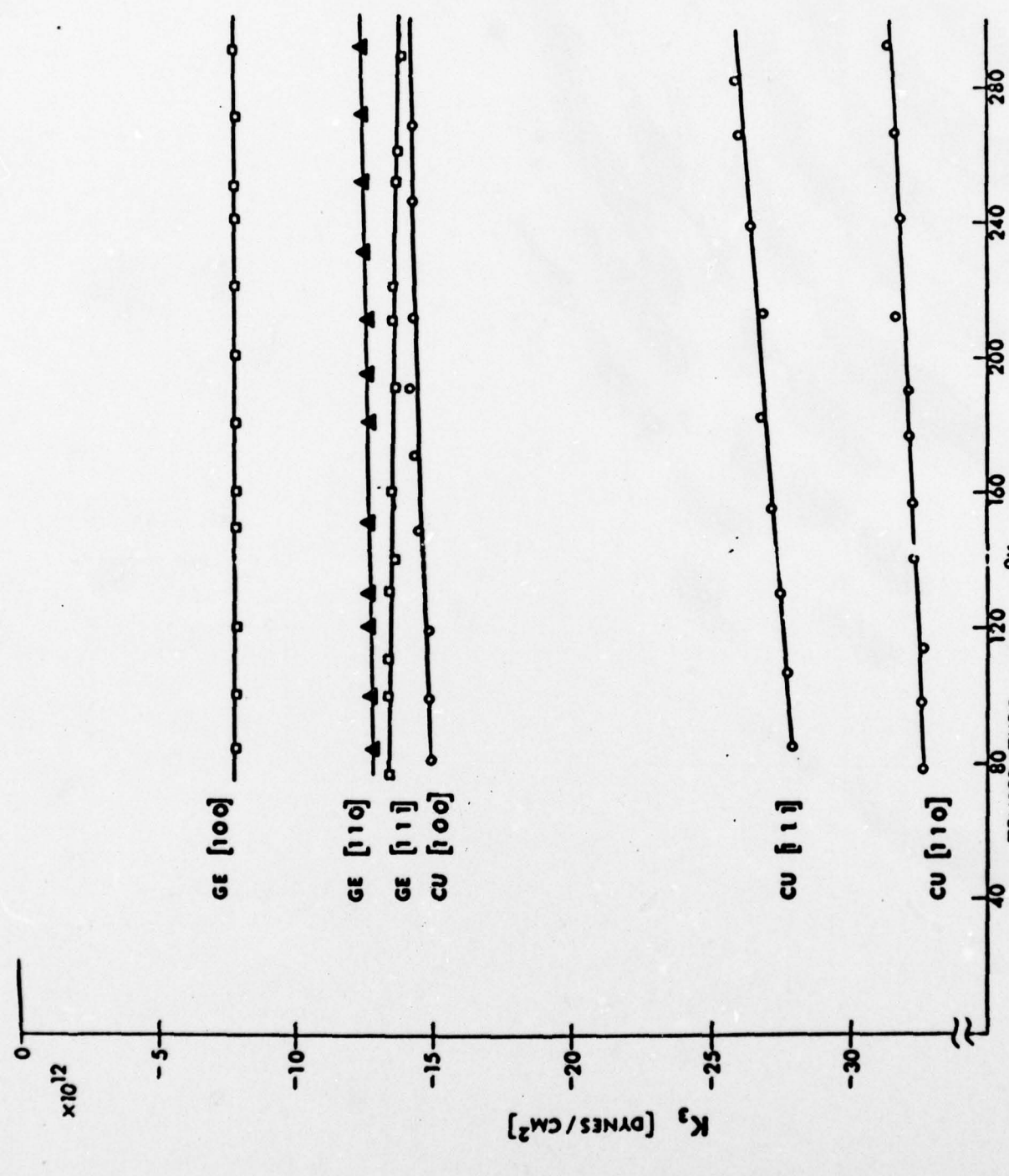

Fig. 5. Combinations of Third-Order Elastic Constants (K_3) for Copper and Germanium Single Crystals as a Function of Temperature.

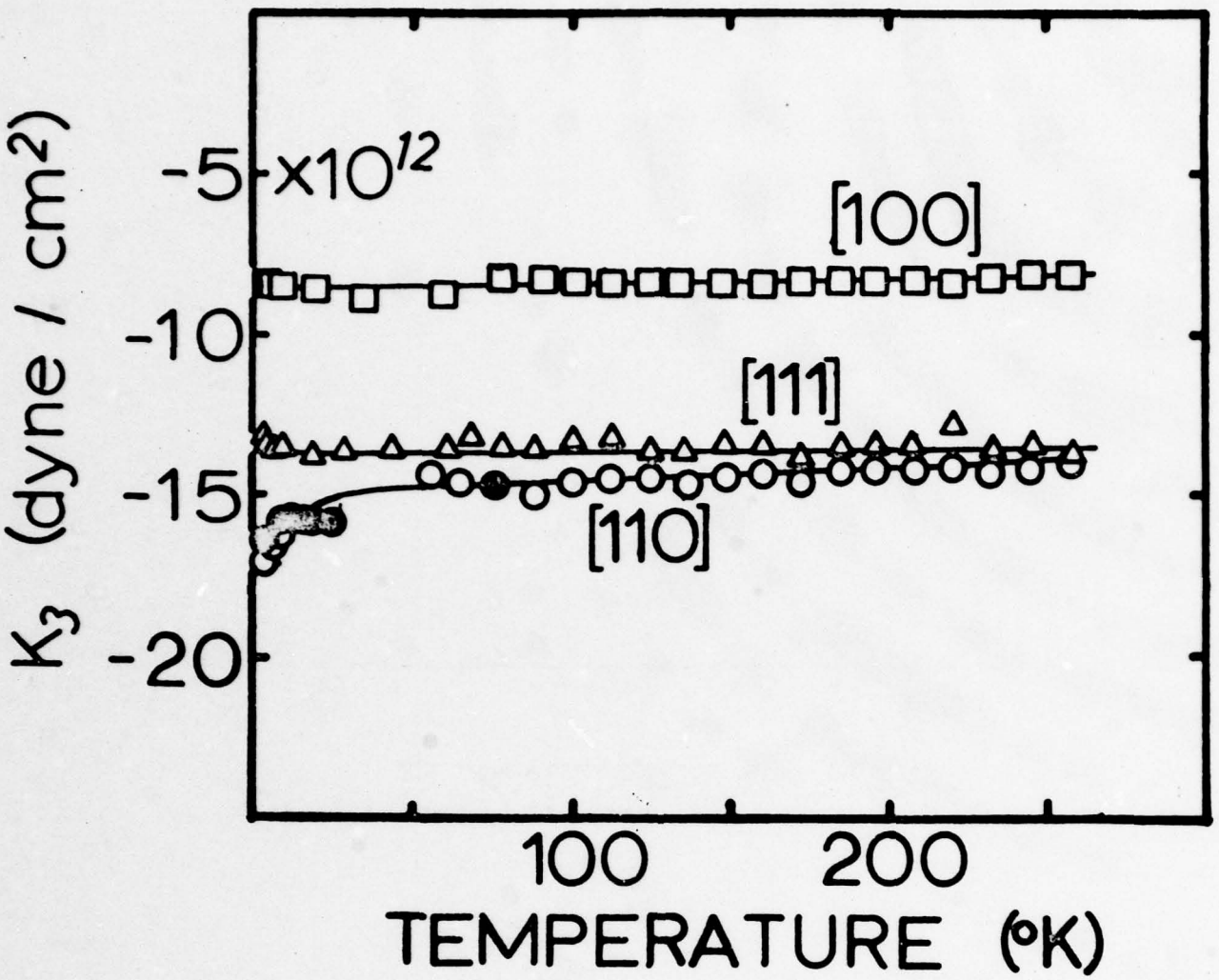

Fig. 6. Combinations of Third-Order Elastic Constants (K_3) for Germanium Down to 2.9°K.

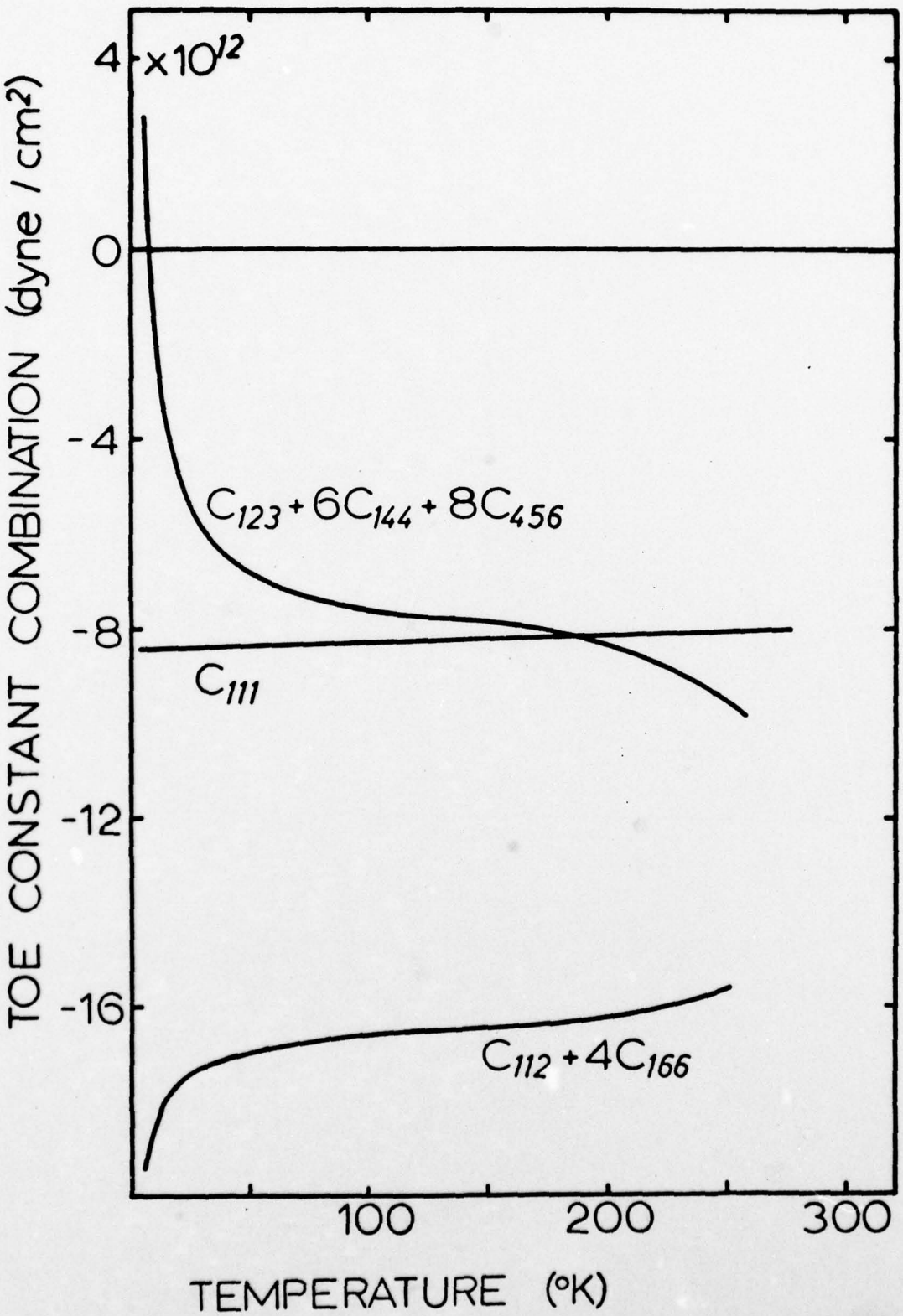

Fig. 7. Simplest Combinations of Third-Order Elastic Constants Available from Present Measurements on Germanium.

PHYSICAL REVIEW B VOLUME 13, NUMBER 8 15 APRIL 1976

Third-order elastic constants of germanium between 300 and 3°K†

James A. Bains, Jr. and M. A. Breazeale
Department of Physics, The University of Tennessee, Knoxville, Tennessee 37916
(Received 3 November 1975)

The ultrasonic harmonic-generation technique has been improved to the point that both amplitude and phase of the second harmonic of an initially sinusoidal ultrasonic wave in a solid can be measured between room temperature and 3°K. By measuring along the principal crystallographic directions, we have been able to determine temperature dependence of linear combinations of third-order elastic (TOE) constants of germanium. Between room temperature and 77°K the magnitude of the TOE constants does not vary greatly as a function of temperature. Between 77 and 3°K, C_{111} changes by +3%, $(C_{112}+4C_{166})$ changes by +16%, and $(6C_{144}+C_{123}+8C_{456})$ changes by −150%. All of these combinations of TOE constants are negative at 77°K, but below 7°K the combination $(6C_{144}+C_{123}+8C_{456})$ is positive. Temperature dependence of additional combinations is inferred by assuming that the "Anderson-Gruneisen parameter" is independent of temperature.

I. INTRODUCTION

The present work is an extension to very low temperatures of previously established techniques for measuring third-order elastic (TOE) constants. The technique involves the measurement of the distortion of an ultrasonic wave as it propagates through the solid. This distortion was observed in polycrystalline aluminum,[1] and in several single crystals[2] with quartz transducers. The measurement technique was refined with the development of a capacitive receiver.[3] This refinement, and subsequent ones,[4] allowed absolute amplitude measurements to be made at different temperatures. Such measurements have been used by a number of investigators[5] to calculate combinations of truly adiabatic TOE constants. Yost and Breazeale[6] combined results from using this technique with those of Dunham and Huntington[7] to obtain the first complete set of truly adiabatic TOE constants (of fused silica) at room temperature. TOE constants of copper[8] have been measured between room temperature and 80°K. More recently we reported[9] data on germanium between room temperature and 80°K. (This publication[9] *is hereinafter referred to as I.*) *The present* measurements were undertaken to extend the data on TOE constants on germanium to lower temperatures in an attempt to answer a fundamental question about the relationship between the elastic and the termal properties.

The thermal expansion of germanium is anomalous below 80°K.[10] A similar anomaly has been observed in all other diamond lattice materials measured to date.[11] At temperatures below approximately 0.2 θ_0 where θ_0 is the Debye temperature at 0°K, the thermal expansion changes from positive to negative and then becomes positive again at even lower temperatures. Calculations of the thermal expansion from the second-order elastic (SOE) constants and TOE constants[12,13,14] have not predicted the measured anomalous behavior at low temperatures. However, these calculations were based on the assumption that the TOE constants are not dependent on temperature (in lieu of actual data of TOE constant behavior at low temperature). We chose germanium for these low-temperature measurements to examine the validity of this assumption.

II. EXPERIMENTAL TECHNIQUE

Pure mode propagation is possible for a longitudinal ultrasonic wave in the three principal directions of a cupic crystal. In these special directions, the wave equation takes on the following form[15]:

$$\rho_0 \ddot{u} = K_2 \frac{\partial^2 u}{\partial a^2} + (3K_2 + K_3) \frac{\partial u}{\partial a} \frac{\partial^2 u}{\partial a^2} \tag{1}$$

where K_2 and K_3 are combinations of SOE and TOE constants, respectively, given in Table I.

If there is an initially sinusoidal disturbance at $a = 0$, this equation has the solution

$$u = A_1 \sin(ka - \omega t) - [(3K_2 + K_3)/8K_2] \times A_1^2 k^2 a \cos 2(ka - \omega t), \tag{2}$$

where k is the propagation constant $2\pi/\lambda$, a is the

TABLE I. K_2 and K_3 for principal directions of a cubic crystal.

Direction	K_2	K_3
[100]	C_{11}	C_{111}
[110]	$\frac{1}{2}(C_{11}+C_{12}+2C_{44})$	$\frac{1}{4}(C_{111}+3C_{112}+12C_{166})$
[111]	$\frac{1}{3}(C_{11}+2C_{12}+4C_{44})$	$\frac{1}{9}(C_{111}+6C_{112}+12C_{144}+24C_{166}+2C_{123}+16C_{456})$

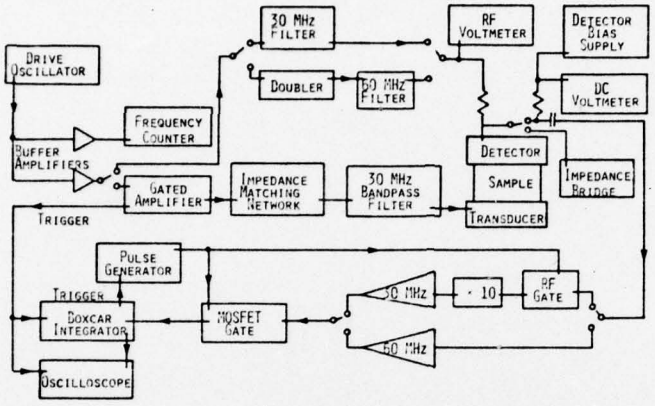

FIG. 1. Block diagran for room-temperature measurements.

propagation distance in the sample, and A_1 is the amplitude of the fundamental.

Thus the initially sinusoidal wave becomes distorted: a second harmonic is generated and grows linearly with propagation distance in the sample. The amplitude A_2 of this second harmonic is given by

$$A_2 = -[(3K_2 + K_3)/8K_2]\, A_1^2 k^2 a. \tag{3}$$

This harmonic distortion is the basis of the nonlinearity measurements in the present work. The parameter K_3 may be calculated by

$$K_3 = -3K_2(\beta + 1), \tag{4}$$

where

$$\beta = \tfrac{1}{2}(A_2/A_1^2)\,(1/k^2 a), \tag{5}$$

and the parameter K_2 may be found from the relation

$$K_2 = \rho_0 v^2, \tag{6}$$

where v is the velocity of sound in the appropriate direction in the medium.

A. Room-temperature measurements

A block diagram of the apparatus for making room-temperature measurements is shown in Fig. 1. A radio-frequency pulse of approximately 30 MHz is applied to an x-cut quartz transducer which is bonded to one end of the sample. The ultrasonic wave which propagates through the sample is detected at the other end by a capacitive receiver. In addition, provision is made to place a substitutional signal on the capacitive receiver so that accurate amplitude measurements can be made.

The air-gap capacitive receiver used is essentially the same as that described in detail by Gauster and Breazeale.[3] A 1.016-cm diam electrode is placed approximately 5 μm from the sample (both surfaces being optically flat), and a dc bias on the order of 150 V is applied across the gap through a large resistor (approximately 1 MΩ).

The method of introducing the substitutional signal differs somewhat from that previously used by Peters, Breazeale, and Pare[4] and in I. Previously the capacitive receiver itself had been removed from the circuit during the calibration procedures, and the calibrating signal was introduced through a substitutional capacitor, so that the equivalent circuit of the capacitive receiver (an ideal voltage generator in series with the capacitance of the receiver) was replaced by a real generator (whose voltage can be measured with a voltmeter) in series with the substitutional capacitor. (A second substitutional capacitor corrected for stray capacitance from the receiver to ground.)

In the present measurements, no circuit elements were substituted during the calibration. A substitutional signal which gave the same output as the ultrasonic signal was introduced across the capacitive receiver in such a way that the current of the substitutional signal could be measured. This current i can be related to the amplitude A of the ultrasonic wave by

$$i = 2AV_b\omega c/s, \tag{7}$$

where V_b is the dc bias on the receiver, ω is the angular frequency, c is the capacitance of the receiver, and s is the spacing of the capacitive re-

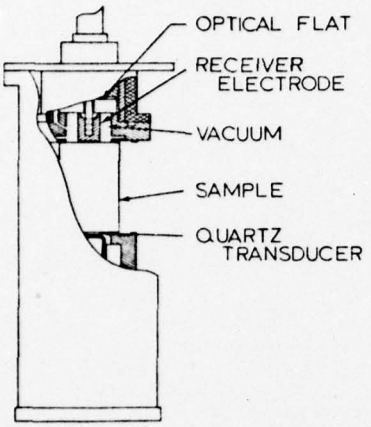

FIG. 2. Cutaway view of cryogenic apparatus.

ceiver plates.

The signal from the capacitive receiver is taken to either a 30- or 60-MHz bandpass amplifier. This amplified signal is detected and taken to a boxcar intergrator. The boxcar integrator selects a portion of the first echo and gives a signal out which is proportional to the time average of that portion of the echo. The germanium samples, being nonconductors, do not sufficiently shield the rf pulse at the transducer from the receiver, so that a 30 MHz pulse is received at the receiver (by radiation) before the ultrasonic wave reaches the receiver. This "feedthrough" pulse can be much larger than the echo of interest and, although it can be separated in time from the measured echo, it can overload the 30 MHz amplifier and the boxcar integrator. This problem was solved by gating the signal from the capacitive receiver so that only the echo of interest was passed.

After the fundamental and second-harmonic signals have been measured by the boxcar integrator, the continuous wave (cw) substitutional signal is introduced at the capacitive receiver. The 60 MHz substitutional signal is derived by doubling the 30 MHz signal with a ring bridge mixer. Both the 30 and 60 MHz substitutional signals are filtered to ensure spectral purity. These two signals are adjusted to give the same output from the boxcar integrator as the ultrasonic signals and are then measured with an rf voltmeter. From these measurements and a knowledge of the circuit impedances (which were obtained at each frequency used by measurements with a vector voltmeter), the current of the substitutional signal can be calculated.

B. Second-order elastic constants

The SOE constants were determined from room-temperature velocity measurements and the results were compared with the data of McSkimin and Adreatch[16] and McSkimin.[17] The agreement was within experimental error. The extensive tabulated data of McSkimin[17] were used in the calculations of the cryogenic data.

C. Cryogenic apparatus

The electonic apparatus for making measurements at low temperature is essentially the same as that for measuring at room temperature. Since relative measurements can be made, it is not necessary to calibrate at each temperature. Thus, a reference voltage is not necessary.

As shown in Fig. 2, the sample holder is enclosed in a stainless-steel can. This can shown is surrounded by another can. The space between the cans is evacuated to provide an insulating jacket around the inner can, and the cans are polished to reduce radiation losses. The cans are supported by three thin-walled cupro-nickel tubes. Two of the tubes have a smaller cupro-nickel tube centered inside to provide a 50-Ω coaxial transmission line and are also used as vacuum lines. The other tube houses the temperature sensor and heater leads, and also is used to supply a pressure to the inner can.

The capacitive receiver is similar to that in the room temperature apparatus, with the additional feature that the gap spacing can be controlled pneumatically.[4] The lapped ring against which the sample rests is undercut to make it a flexible diaphram approximately 0.038 cm thick. The space above the sample is evacuated and the capacitor gap spacing is adjusted by regulating the pressure in the inner can.

The entire apparatus is suspended inside a standard helium research dewar. The dewar can be sealed and temperatures below the room-pressure boiling point of the coolant may be obtained by pumping on the coolant (either liquid helium or nitrogen).

The temperature in the inner can is controlled by an electric resistance heater connected to a commercial temperature controller, and can be varied continuously from approximately 3 K to room temperature.

D. Cryogenic nonlinearity measurements

Only relative measurements need to be taken with the cryogenic apparatus. One firsts adjusts the driving signal to the quartz transducer so that

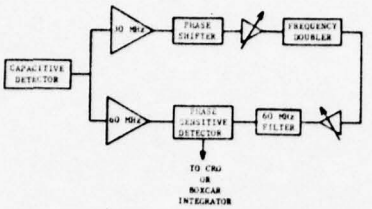

FIG. 3. Block diagram of phase-sensitive detector system.

the fundamental ultrasonic wave received at the capacitive receiver is the same at each temperature. The second harmonic is then measured by a slide-back technique: the dc bias voltage on the capacitive receiver is adjusted so that the electrical signal coming from the capacitive receiver is the same at all temperatures. The second-harmonic amplitude A_2 of the ultrasonic wave at two different temperatures (T_1 and T_2) are then related by

$$A_2(T_2) = A_2(T_1)\, V_b(T_1)/V_b(T_2). \tag{8}$$

The electrical feedthrough is worse in the cryogenic apparatus than it is in the room temperature apparatus. Therefore, a 60-MHz bandpass filter is used between the capacitive receiver and the amplifier to attenuate the 30-MHz feedthrough while passing the 60-MHz signal.

During the course of our measurements it became necessary to determine not only the magnitude of the second-harmonic amplitude, but also its sign. This resulted from the fact that K_3 were observed to change enough that they conceivably could have gone through zero. Such a condition would have been indicated by a phase shift of 180° in the second harmonic. For this reason we perfected a phase-sensitive detector to measure the sign of the second harmonic. (Phase-sensitive detectors which operate at 60 MHz are not commercially available to our knowledge.)

A block diagram of the phase sensitive detector system is shown in Fig. 3. A signal from the capacitive receiver is fed through a power splitter to a 30-MHz amplifier and a 60-MHz amplifier. The output of the 30-MHz amplifier is fed through a continuously variable phase shifter to a frequency doubler. This frequency doubled 30-MHz pulse echo train and the second-harmonic pulse echo train are fed into the phase-sensitive detector whose output is proportional to the cosine of the phase angle between the two 60-MHz signals. The phase shifter allows the phase angle between the two signals to be set to zero initially. If the sign of the second-harmonic amplitude changes as the temperature is changed, the output of the phase-sensitive detector is inverted.

Using this phase sensitive detector system, we were able to make an unequivocal assignment of the phase to the second-harmonic amplitude used in the calculations of the linear combinations of TOE constants we call K_3.

E. Samples

The samples used in this work, were the same ones used in I. These single crystals were 3.7803, 4.8242, and 3.4803 cm in the [100], [110], and [111] orientations, respectively. (The lengths are slightly changed since used in I because of lapping and recoating of the sample ends.) The sample ends were lapped and polished until optically flat and parallel to within 12 sec of arc. The ends were then made conductive by evaporating a copper coating approximation 1000 Å thick onto them.

III. RESULTS

A. Room-temperature nonlinearity measurements for Ge

The absolute amplitude measurements at room temperature are given in Fig. 4. The straight lines in the figures are least-squares fits to the data points. It can be seen that the data will fit very well with a straight line; however, this line does not pass through the origin because of residual noise. The slope of the line is (in the least-squares sense) the best fit to the value of the quan-

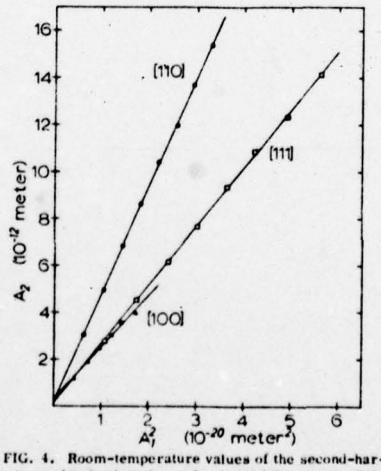

FIG. 4. Room-temperature values of the second-harmonic amplitude plotted as a function of the square of the fundamental amplitude.

TABLE II. Measured room-temperature values of β and K_3.

Sample orientation	Sample Length (cm)	β (Present value)	β (Extrapolated from data of I)[a]	β (average)	K_2[b] (10^{11} dyn/cm^2)	K_3 (10^{12} dyn/cm^2)
[110]	4.8242	2.08 ± 0.015	1.977 (1.928)	2.029	15.51925	−14.10
[111]	3.4803	1.71 ± 0.016	1.729 (1.633)	1.722	16.40807	−13.40
[100]	3.7803	1.05 ± 0.044	0.989 (0.923)	1.018	12.85280	−7.782

[a]W. T. Yost and M. A. Breazeale, Phys. Rev. B 9, 510 (1974).
[b]From the data of H. J. McSkimin and P. Andreatch, Jr., J. Appl. Phys. 34, 651 (1963).

tity

$$\tfrac{1}{8}\beta k_3^2 = k_2^2(3K_2 + K_3)/8K_2. \quad (9)$$

If the effect of the power lost from the fundamental to the second harmonic and by attenuation is considered, as was done in I, one finds that the present data satisfy the small amplitude assumption better than those in I. This can be seen in Fig. 5 in which we present values of the dimensionless parameter β calculated from both sets of data.

The data from I were corrected for the effect of residual noise in the equipment (which was not done previously). It is seen that the present data are best fit by a horizontal straight line and those of I are reasonably extrapolated in the manner described in that publication. The maximum difference between the sets of data is only 5.5%. In view of the fact that both measurements depend upon absolute measurements of displacement amplitudes on the order of 10^{-3} A, this agreement is quite satisfying.

Further comparisons between the present results and the data of I are given in Table II. In the third column is the value of β obtained by a least-squares fit to the present data and its standard deviation. In the fourth column is the value of β extrapolated from the data of I, after correction for residual noise. For reference, values originally listed in I are given in parentheses in this column. In the fifth column the average between the two values of β are given, and this is taken as the most probable value. In the last column is given the value of K_3 calculated from the most probable value of β and the value of K_2 listed in column 6.

The random error for the present measurement is somewhat higher than that of I. This is in large part because the present measurements were made at much lower amplitudes. The systematic errors are estimated to be within plus or minus 10%. This estimate is consistent with the differences between the present work and data in I.

The values of β in the [110] and the [100] directions are approximately 5% and 5.5% higher than those of I, while the value of β in the [111] direction is approximately 0.8% lower than that of I. The present measurements of the [111] sample were made at 29.5 MHz, and the measurements of the [110] and the [100] sample were made at 30.0 MHz. The impedances in the room-temperature apparatus were measured at each frequency, and it is presumably errors associated with these impedance measurements which are mainly responsible for the differences between the present values of β and those of I.

B. Temperature dependence of TOE constants

Figure 6 shows the data we obtained for the three different K_3's of germanium as a function

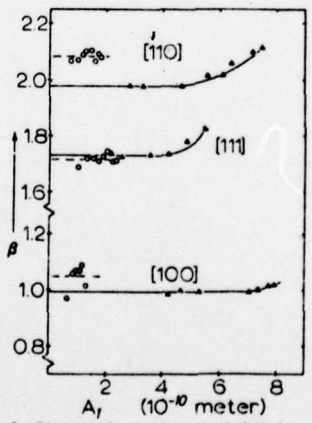

FIG. 5. Dimensionless parameter β plotted as a function of the fundamental amplitude. ○ present data; △ data from I [W. T. Yost and M. A. Breazeale, Phys. Rev. B 9, 510 (1974)].

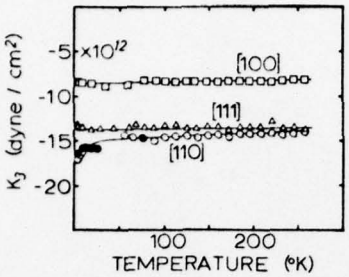

FIG. 6. Temperature dependence of the combinations of TOE constants K_3 for the three principal directions in Germanium.

of temperature. The first data runs, shown by the open symbols were taken without use of the phase-sensitive detector. The curves for the [100] and [111] directions are considered to be too smooth to admit a negative phase of the second harmonic from which the data were calculated. The data in the [110] direction were not

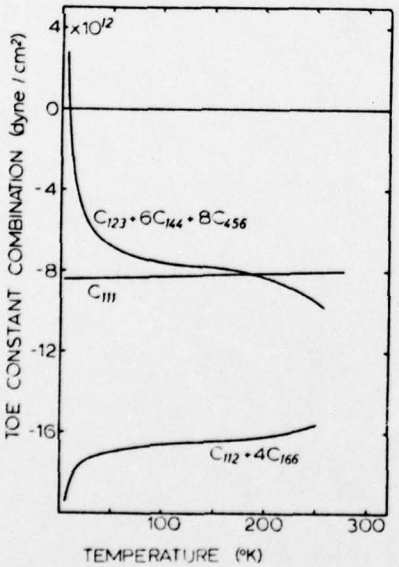

FIG. 7. Temperature dependence of the simplest combinations of TOE constants which can be calculated from the K_3 of Germanium.

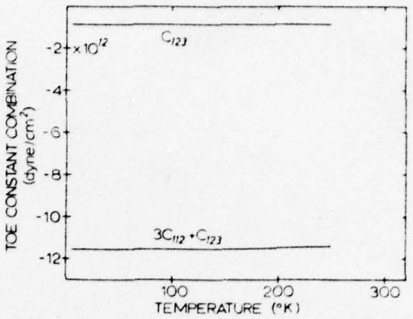

FIG. 8. Temperature dependence of certain TOE constants combinations calculated from our data under the assumption that the "Anderson-Grüneisen parameter" and C_{123} are temperature independent.

as smooth. The initial data between approximately 15 and 50 °K had shown a peak or dip depending on the interpretation of the phase. We also noted that a thermal gradient might have been responsible for this behavior. The apparatus was modified to eliminate thermal gradients and the phase-sensitive detector was added. The data shown as solid circles were taken with the modified apparatus. There is no ambiguity about the sign of the second-harmonic amplitude from which these data were calculated. The agreement between the two sets of data in the low-temperature range reassured us about the correctness of these data and allowed us to eliminate erroneous data points from this plot.

Down to liquid-nitrogen temperature, these data reproduce the results of I to well within 3%. The data for the [100] direction can be fit very well with a straight line down to 3 °K. The data for the [111] direction is essentially a straight line with a very slight upturn at very low temperatures. The data for the [110] direction are the only ones which show a marked deviation from a straight line. At low temperatures there is a definite downturn of the data.

These linear combinations of the TOE constants are not the simplest possible combinations available from our data. For example, C_{111} is contained in each of these curves, and therefore can be subtracted out. Proceeding in this fashion, we have evaluated the simplest combinations of TOE constants shown in Fig. 7.

As can be seen, there is not a great variation of these combinations of third-order elastic constants down to 77 °K. But between 77 and 3 °K there is a considerable variation in some of them. In particular, the combination $(C_{123}+6C_{144}+8C_{456})$

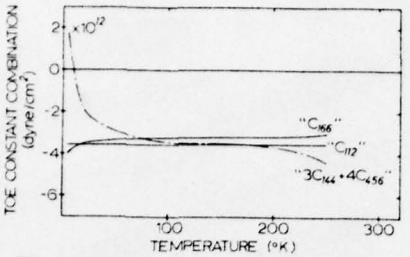

FIG. 9. Temperature dependence of certain TOE constant combinations calculated from our data assuming that both the "Anderson-Grüneisen parameter" and C_{123} are temperature independent.

crosses zero at 7 °K and becomes positive below that temperature. Since these are the TOE constants which would play a significant role in the transverse modes, we feel that the lack of agreement between theoretical calculation of thermal expansion from elastic data[12,13,14] and the measured thermal expansion might be attributed to the theoretical assumption that the TOE constants are independent of temperature.

III. ISOLATION OF ADDITIONAL TOE CONSTANTS

Further reduction of the data can be made if one makes the assumption that the "Anderson-Grüneisen parameter"[18] is not a function of temperature.[19] This assumption may be more valid than the assumption that the TOE constants are independent of temperature. Therefore, using it to isolate additional TOE constants from our data may prove to be instructive.

Using the data from our experiment, the data of McSkimin and Andreatch[16] (combination of TOE constants at room temperature), and the data of McSkimin[17] for the second-order constants C_{11} and C_{12} we can calculate the "Anderson-Grüneisen" parameter by Rao's formulation[20]:

$$\delta = -1 - (C_{111} + 6C_{112} + 2C_{123})/3(C_{11} + 2C_{12}). \quad (10)$$

If δ is indeed constant as a function of temperature, then the temperature dependence of the combination $3C_{112} + C_{123}$ can be obtained from our data. Under this assumption, this combination of TOE constants shows virtually no temperature dependence (see Fig. 8). If it is further assumed that C_{123} is not a function of temperature (and equal to the room temperature value obtained from the data of our experiment and McSkimin and Andreatch), additional TOE constants may be calculated. These calculated constants are given in Fig. 9 and are designated by enclosing the constants in quotation marks to specify that these calculations are based on the two assumptions given above.

In conclusion, the measurements indicate that there is a definite temperature dependence of some of the TOE constants. Since we cannot isolate all of the TOE constants, it is not feasible at present to determine the effect of this temperature dependence on the Grüneisen parameter calculation of Brugger and Fritz.[14] However, our assumption that the Anderson-Grüneisen parameter is independent of temperature has allowed us to plot most of the TOE constants as a function of temperature. The validity of this assumption, and hence of the curves drawn to Figs. 8 and 9, is open to question; however, one can observe that, to the extent these curves are valid, the greatest temperature dependence seems to be found in C_{166} and $3C_{144} + 4C_{456}$.

---

†Research supported in part by the U. S. Office of Naval Research. This paper is based in part on James A. Bains, Jr., doctoral dissertation, Dept. of Physics, The University of Tennessee, Knoxville, Tenn. 1974 (unpublished).

[1]M. A. Breazeale and D. O. Thompson, Appl. Phys. Lett. 3, 77 (1963).
[2]A. A. Gedroits and V. A. Krasilnikov, Zh. Eksp. Teor. Fiz. 43, 1592 (1962) [Sov. Phys.-JETP 16, 1122 (1963)].
[3]W. B. Gauster and M. A. Breazeale, Rev. Sci. Instrum. 37, 1544 (1966).
[4]R. D. Peters, M. A. Breazeale, and V. K. Paré, Rev. Sci. Instrum. 39, 1505 (1968).
[5]J. T. Mackey and R. T. Arnold, J. Appl. Phys. 40, 4806 (1969); A. L. Sanford and S. P. Zehner, Phys. Rev. 153, 1025 (1967); E. L. Meeks and R. T. Arnold, Phys. Rev. B 1, 982 (1970).
[6]W. T. Yost and M. A. Breazeale, J. Appl. Phys. 44, 1909 (1973).
[7]R. W. Dunham and H. B. Huntington, Phys. Rev. B 2, 1098 (1970).
[8]R. D. Peters, M. A. Breazeale, and V. K. Paré, Phys. Rev. B 1, 3215 (1970).
[9]W. T. Yost and M. A. Breazeale, Phys. Rev. B 9, 510 (1974).
[10]S. I. Novikova, Fiz. Tverd. Tela. 2, 43 (1960) [Sov. Phys.-Solid State 2, 37 (1960)]; R. D. McCammon and G. K. White, Phys. Rev. Lett. 10, 234 (1963).
[11]P. W. Sparks and C. A. Swenson, Phys. Rev. 163, 779 (1967); H. E. V. Erfling, Ann. Phys. (Leipz.) 41, 467 (1942); D. F. Gibbons, Phys. Rev. 112, 136 (1958).
[12]J. G. Collins, Philos. Mag. 8, 323 (1963).
[13]D. E. Schuele and C. S. Smith, J. Phys. Chem. Solids 25, 801 (1964).
[14]K. Brugger and T. C. Fritz, Phys. Rev. 157, 524

(1967).
[15]M. A. Breazeale and J. Ford, J. Appl. Phys. 36, 3486 (1965).
[16]H. J. McSkimin and P. Andreatch, Jr., J. Appl. Phys. 34, 651 (1963).
[17]H. J. McSkimin, J. Appl. Phys. 24, 988 (1953).
[18]O. L. Anderson, Phys. Rev. 144, 553 (1966).
[19]Y. A. Chang, J. Phys. Chem. Solids 28, 697 (1967).
[20]R. R. Rao, Phys. Rev. B 10, 4173 (1974).

9 INTERNATIONAL CONGRESS ON ACOUSTICS K
MADRID 4/9-VII-1977 25

ULTRASONIC NONLINEARITY PARAMETERS OF FUSED SILICA BETWEEN 3ºK and 300ºK

Breazeale, M. A.
Cantrell, J. H.

Department of Physics
The University of Tennessee
Knoxville, Tennessee 37916 USA

The nonlinearity parameters of fused silica have been measured between room temperature and 3° Kelvin by the harmonic generation technique (1).

A 30 MHz ultrasonic pulse is generated in samples of fused silica which differ in hydroxyl ion content and in homogeneity. As the ultrasonic wave propagates through the sample it generates harmonics of the 30 MHz fundamental. By use of a capacitive receiving transducer, amplitudes of both the fundamental and the second harmonic are measured. Typical values of the fundamental and second harmonic amplitudes are, respectively, 2.2 Angstroms and 9.3×10^{-3} Angstroms. These amplitudes are used to calculate the nonlinearity parameter (2)

$$\beta = -\left(\frac{3C_{11}+C_{111}}{3C_{11}}\right),$$

and hence the third-order elastic constant C_{111}. Room temperature values of these quantities for four different samples are given in Table I.

As the temperature is lowered to 3 °K, C_{111} changes by 16% for Suprasil W1, and less than this for the other samples. The variation of β is 7% for Suprasil 2, and less than this for the other samples. Since β can be related to the longitudinal mode strain Grüneisen parameter γ_{11}, this means that temperature dependence of the total Grüneisen parameter as great (3) as 800% must come from sources other than variations of the third-order elastic constant C_{111}. [Research sponsored by the Office of Naval Research.]

TABLE I

Sample	β	C_{11} (10^{11} dynes/cm^2)	C_{111} (10^{12} dynes/cm^2)
Suprasil W1	-3.86 ± 0.071	7.8059 ± 0.0029	6.70 ± 0.124
Suprasil W2	-3.93 ± 0.034	7.8078 ± 0.0020	6.85 ± 0.058
Suprasil 1	-4.14 ± 0.041	7.7633 ± 0.0016	7.31 ± 0.073
Suprasil 2	-3.90 ± 0.039	7.7633 ± 0.0014	6.75 ± 0.067

REFERENCES

1. R. D. Peters, M. A. Breazeale, and V. K. Paré, Phys. Rev. B 1, 3245-3250 (1970).
2. W. T. Yost and M. A. Breazeale, J. Appl. Phys. 44, 1909-1910 (1973).
3. W. Heinicke, G. Winterling, and K. Dransfeld, J. Acoust. Soc. Am. 49, 954-958 (1971).

PHYSICAL REVIEW B VOLUME 17, NUMBER 12 15 JUNE 1978

Ultrasonic investigation of the nonlinearity of fused silica for different hydroxyl-ion contents and homogeneities between 300 and 3°K

John H. Cantrell, Jr.* and M. A. Breazeale
Department of Physics, The University of Tennessee, Knoxville, Tennessee 37916
(Received 19 September 1977)

The harmonic-generation technique was used to measure the third-order elastic constants C_{111} of four types of fused silica. The samples differed in amount of OH content and directional homogeneity. The results indicate that a relatively large OH content in fused silica may give rise to a relatively greater value of C_{111} and that C_{111} is a weak function of temperature regardless of OH content. The relationship between the experimentally defined ultrasonic nonlinearity parameter $\beta = -(3C_{11} + C_{111})/3C_{11}$ and the Grüneisen parameter γ also has been determined. The measured temperature dependence of β indicates that in the Debye model elastic constants other than C_{11} and C_{111} must dominate the strong temperature dependence of the Grüneisen parameter for fused silica at low temperatures.

I. INTRODUCTION

A number of the physical properties of solids result from the fact that solids are inherently nonlinear. Among these properties are thermal expansion, attenuation of high-frequency sound waves, heat conduction, and wave-form distortion of ultrasonic waves passing through a solid. These nonlinear effects arise because of anharmonicity of the interatomic potential.

The earliest investigations of anharmonicity in solids were pursued from more purely thermodynamic experimentation. For example, Fizeau[1] was among the earliest investigators to measure thermal expansion.

Grüneisen[2] developed the relationship between the thermal-expansion coefficient and a parameter which was assumed to be temperature independent (the Grüneisen parameter γ). Barron[3,4] and Sheard[5] were among the first to make calculations relating the Grüneisen parameter to elastic data. They limited their calculations to the cases of high and low temperatures. Collins,[6] Schuele and Smith,[7] Brugger and Fritz,[8] and Gerlich[9] have made more extensive calculations to determine the temperature dependence of the Grüneisen parameter from elastic data using the quasiharmonic Debye model of solids. Thus, the Grüneisen constant is a convenient link between thermal-expansion data and elastic data.

The agreement of the calculated dependence of the Grüneisen parameter as a function of temperature with values measured from thermal expansion has been limited because of the lack of availability of elastic data [particularly third-order elastic (TOE) constants] as functions of temperature. For many materials such as Cu, Ag, Au, Al, and Na qualitative agreement exists, but some materials exhibit an anomalous behavior of the thermal-expansion coefficient as a function of temperature. One such material is fused silica. Fused silica has a positive thermal-expansion coefficient down to a temperature of approximately 0.3 of its Debye temperature. There the thermal-expansion coefficient becomes negative and continues to grow more negative as the temperature is lowered.[10] This gives rise to the anomalous behavior of the Grüneisen parameter γ shown in Fig. 1, where it is seen that γ also becomes negative around 0.3 of the Debye temperature and continues to become more negative as the temperature approaches zero. This is in contrast with germanium, for which γ levels off as the temperature approaches zero and with quartz which maintains a positive γ for all temperatures. Several investigations[3-6,11-15] indicate that at least part of the explanation for the behavior of fused silica may be due to the dominance of transverse-acoustical modes at these temperatures; however, this hypothesis can be tested only as information on the behavior of TOE constants as functions of temperature is collected. Since the TOE constants determine how a large amplitude ultrasonic wave distorts as it propagates through the solid, TOE constants can be calculated from ultrasonic wave distortion. We have chosen to measure this wave-form distortion in order to understand more fully the unusual behavior of fused silica.

Ultrasonic wave distortion was initially observed in polycrystalline aluminum[16] and in several single crystals[17] with quartz transducers. Absolute amplitude measurements became possible with the development of the capacitive receiver,[18] and measurements at different temperatures became possible with a later refinement.[19] Several investigators[20-22] have used this method to calculate combinations of truly adiabatic TOE constants. Yost and Breazeale[23] combined the results of this meth-

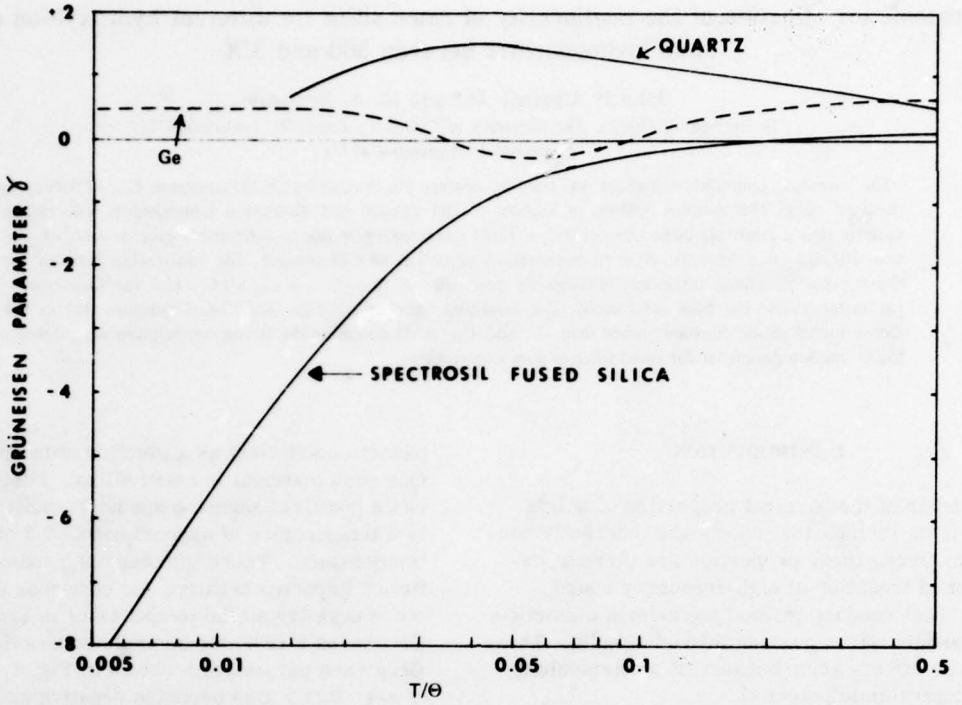

FIG. 1. Temperature dependence of the Grüneisen parameter for quartz, germanium, and spectrosil fused silica [from G. K. White, Cryogenic 4, 2 (1964)].

od with those of Dunham and Huntington[24] to obtain the first complete set of purely adiabatic TOE constants (of fused silica) at room temperature. Combinations of TOE constants of copper[25] and germanium[26] have been measured between room temperature and 77 °K. More recently, the measurements on germanium were extended to lower temperatures (3 °K).[27]

The purpose of the present investigation is to explore the results of anharmonicity more fully. To do this, we have measured the second harmonics of an initially sinusoidal ultrasonic wave in four different samples of fused silica between room temperature and 3 °K. From these data we have calculated the adiabatic TOE constant C_{111} as a function of temperature. Also, we have plotted the experimentally defined nonlinearity parameter $\beta = -(3C_{11} + C_{111}/3C_{11})$, because, as we show, there is a relationship between β and a Grüneisen parameter. The implications of the present results in light of the temperature dependence of the Grüneisen parameter are discussed.

II. THEORY

A. Ultrasonic nonlinearity in isotropic solids

For an isotropic solid pure mode propagation is possible for a longitudinal ultrasonic wave in any direction. In this special case the nonlinear wave equation takes the form[28]

$$\rho_0 \ddot{u} = C_{11} \frac{\partial^2 u}{\partial a^2} + (3C_{11} + C_{111}) \frac{\partial u}{\partial a} \frac{\partial^2 u}{\partial a^2}, \tag{1}$$

where ρ_0 is the mass density of the undisturbed medium, u is the particle displacement, a is the Lagrangian (laboratory) coordinate in any direction, and C_{11} and C_{111} are second- and third-order elastic constants, respectively.

Assuming an initially pure sinusoidal disturbance at $a = 0$, the solution to Eq. (1) may be written[28]

$$u = A_1 \sin(ka - \omega t) - [(3C_{11} + C_{111})/8C_{11}] A_1^2 k^2 \times a \cos 2(ka - \omega t), \tag{2}$$

where k is the propagation constant $2\pi/\lambda$, and ω is the angular frequency. Hence, an initial sinusoidal disturbance of amplitude A_1 distorts linearly with propagation distance a and generates a second harmonic of amplitude

$$A_2 = -[(3C_{11} + C_{111})/8C_{11}] A_1^2 k^2 a. \tag{3}$$

Solving Eq. (3) for C_{111} yields

$$C_{111} = -3C_{11}[\tfrac{8}{3}(A_2/A_1^2)(1/k^2 a) + 1]. \tag{4}$$

All quantities on the right-hand side of this equation can be measured and C_{111} can be determined.

The quantity

$$\tfrac{8}{3}(A_2/A_1^2)(1/k^2a)=\beta \tag{5}$$

in Eq. (4) is a significant quantity in this study. If β is zero, then A_2 is zero and no second harmonic is generated. Since the generation of a second harmonic is a direct measure of the nonlinearity of a solid then β may be referred to as the ultrasonic nonlinearity parameter. For isotropic solids β is expressed in terms of the elastic constants as

$$\beta=-(3C_{11}+C_{111})/3C_{11}. \tag{6}$$

B. Grüneisen parameters and their relationship to β

1. Grüneisen parameters

The anharmonicity of solids also can be investigated from thermodynamic measurements (e.g., volume expansivity, variations in isothermal compressibility as a function of temperature, etc.). Among those investigating anharmonicity from these techniques it has become common to express the results in terms of the Grüneisen parameter γ, defined by[2]

$$\gamma=\alpha/K_TC_V=\alpha/K_SC_P, \tag{7}$$

where α is the thermal volume expansivity, K_T and K_S are the isothermal and isentropic compressibilities, respectively, and C_V and C_P are the isochoric and isobaric heat capacities, respectively.

A relationship between γ and the elastic constants can be found from calculations based on the assumption that[5,7-9] (i) the material behaves like continuous anisotropic medium, (ii) the nondispersive Debye model of specific heats is valid, and (iii) the generalized Grüneisen parameters depend on temperature only through the lattice dimensions.

If one defines the volume generalized Grüneisen parameter for the mode $(p,\vec{q})$ by

$$\gamma(p,\vec{q})=-\frac{V}{\omega(p,\vec{q})}\left(\frac{\partial\omega(p,\vec{q})}{\partial V}\right)_T, \tag{8}$$

where p is the polarization index ($p=1,2,3$) corresponding to the three acoustical modes, $\vec{q}$ is the wave vector, V is the volume, T is the temperature, and $\omega(p,\vec{q})$ is the angular frequency of the mode. The Grüneisen parameter γ may then be expressed as[8]

$$\gamma=\sum_p\oint d\Omega\,\gamma(p,\hat{N})C(p,\hat{N})\Big/\sum_p\oint d\Omega\,C(p,\hat{N}), \tag{9}$$

where the integration is performed over the spatial direction $\hat{N}=\vec{q}/|\vec{q}|$ in the irreducible part of the Brillouin zone [in our case a sphere of radius $q_D=(6\pi^2/V_0)^{1/3}$, where V_0 is the volume per atom]. The specific heat of mode $(p,\hat{N})$ in Eq. (9) is given by

$$C(p,\hat{N})=\left(\frac{q_D}{2\pi}\right)^3\int_0^1 d\xi\,\frac{\xi^4[\theta(p,\hat{N})/T]^2}{\{\exp[\theta(p,\hat{N})/T]-1\}^2} \tag{10}$$

where $\theta(p,\hat{N})$ is the characteristic Debye temperature of mode $(p,\hat{N})$ given by

$$\theta(p,\hat{N})=(\hbar q_D/K)S(p,\hat{N}), \tag{11}$$

where K is the Boltzmann constant and

$$S(p,\hat{N})=\left(\frac{\partial\omega(p,\vec{q})}{\partial q}\right)_{q=0} \tag{12}$$

is the elastic wave speed of that mode.

It is convenient to introduce the *strain* generalized Grüneisen parameters $\gamma_{jk}(p,\vec{q})$ defined by

$$\gamma_{jk}(p,\vec{q})=-\left[\frac{1}{\omega(p,\vec{q})}\left(\frac{\partial\omega(p,\vec{q})}{\partial\eta_{jk}}\right)_T\right]_{\eta=0}, \tag{13}$$

where η is the Lagrangian strain tensor and the indices $j,k=1,2,3$. The *volume* generalized Grüneisen parameters can be expressed in terms of the *strain* generalized Grüneisen parameters by

$$\gamma(p,\vec{q})=\frac{1}{K_T}\sum_j\sum_{rs}S^T_{jjrs}\gamma_{rs}(p,\vec{q}), \tag{14}$$

where K_T is the isothermal compressibility and S^T_{jjrs} are the isothermal elastic compliance coefficients.

It has been shown[29] that $\gamma_{jk}(p,\vec{q})$ can be expressed in terms of the elastic constants by (Einstein notation)

$$\gamma_{jk}(p,\hat{N})=[1/2w(p,\hat{N})][2w(p,\hat{N})U_jU_k+(C_{jkmn}+C_{jkmnuv}U_uU_v)N_mN_n], \tag{15}$$

where

$$w(p,\hat{N})=C_{muv}N_mN_nU_uU_v. \tag{16}$$

$\hat{N}$ gives the direction of wave propagation, $\hat{U}$ is a unit vector along the direction of polarization appropriate to p, and the subscripted C's are the second- and third-order elastic constants in the equations.

2. Relationship to the ultrasonic nonlinearity parameter

For pure longitudinal acoustic modes in an isotropic solid, Eq. (15) reduces to the set of relations (using Voigt[30] notation)

$${}_1\gamma_{11}=-(3C_{11}+C_{111})/2C_{11}, \tag{17}$$

$${}_1\gamma_{22}={}_1\gamma_{33}=-(C_{12}+C_{112})/2C_{11}, \tag{18}$$

and

$$ {}_l\gamma_{ij}=0, \quad i\neq j, \tag{19}$$

where the prescript l indicates longitudinal-acoustical modes. From Eq. (6) and (17) it is seen that ${}_l\gamma_{11}$ is related directly to the ultrasonic nonlinearity parameter β by

$$ {}_l\gamma_{11}=\tfrac{3}{2}\beta . \tag{20}$$

Hence, one of the strain generalized Grüneisen parameters is measured directly by the present harmonic-generation technique.

For an isotropic solid Eq. (9) reduces to the form

$$ \gamma=(\gamma_l C_l+2\gamma_t C_t)/(C_l+2C_t), \tag{21}$$

where

$$ \gamma_l=+\tfrac{1}{2}\beta-(C_{12}+C_{112})/3C_{11} \tag{22}$$

is the longitudinal-mode *volume* generalized Grüneisen parameter obtained from Eq. (8), and C_l and C_t are the modal specific heats of Eq. (10). γ_t in Eq. (21) is the transverse-mode *volume* generalized Grüneisen parameter and is not easily expressed in terms of the ultrasonic nonlinearity parameter.

The significance of the relationship of the nonlinearity parameter β to the Grüneisen parameter γ is now established for the case of isotropic solids. It allows one to ascertain directly the contribution of the "longitudinal-mode" elastic constants C_{11} and C_{111} to the temperature dependence of the Grüneisen parameter when β is measured as a function of temperature.

III. EXPERIMENTAL TECHNIQUE

A. Apparatus and measurement techniques

The apparatus and measurement techniques for determining the amplitudes of fundamental and second-harmonic waves are described in detail elsewhere.[27] The amplitudes of the fundamental and the second-harmonic waves were measured absolutely in each sample at room temperature. These data were used in Eqs. (4) and (5) to determine room-temperature values of C_{111} and β. At all other temperatures the amplitudes were measured relative to the room-temperature values, and relative values of C_{111} and β were determined.

B. Second-order elastic constants

The second-order elastic (SOE) constant C_{11} appearing in Eq. (4) was determined from room-temperature longitudinal wave-velocity measurements, since

$$ C_{11}=\rho_0 V^2, \tag{23}$$

where ρ_0 is the mass density of the unstrained solid. The measurements were made with capacitive transducers[31] which eliminated the problem of bond corrections. The temperature dependence of C_{11} was calculated from the data of A. Zarembowitch[32] who measured the SOE constants of Purposil fused silica as a function of temperature. The SOE constants of the Suprasil fused-silica samples used in these experiments are assumed to have the same relative temperature dependence as that of Purposil.

C. Samples

The fused-silica samples used in this work were manufactured under the commercial designation Suprasil. All samples were cylindrical, approximately 2.54 cm in diameter, and were coated on each end with copper to a thickness of approximately 1000 Å. The length of each sample, impurity content, and the measured ultrasonic wave velocities at room temperature (27 °C) are given in Table I. The symbol W indicates that the sample has only 5 ppm of OH, while the unlettered samples have OH contents of 1200 ppm. The numerical designation 1 or 2 indicates the degree of homogeneity of the sample. The designation 1 indicates a guaranteed strong homogeneity in all directions, whereas the designation 2 implies a guaranteed strong homogeneity only in the direction perpendicular to the sample surfaces.

IV. RESULTS

A. Room-temperature measurements

Accurate room-temperature values of the nonlinearity parameter β and of C_{111} were determined by an extrapolation technique which minimized the effect of attenuation on the results.[26] The nonlinearity parameter β was measured for different

TABLE I. Samples used in this study and pertinent properties.

Sample	Impurity content (ppm) OH	Fluorine	Chlorine	Sample length (cm)	Longitudinal ultrasonic velocity (10^5 cm/sec)
Suprasil $W1$	5	260	260	1.2590 ± 0.0003	5.9526 ± 0.0016
Suprasil $W2$	5	260	260	1.2587 ± 0.0002	5.9533 ± 0.0011
Suprasil 1	1200	130	130	1.2593 ± 0.0002	5.9363 ± 0.0012
Suprasil 2	1200	130	130	1.2586 ± 0.0002	5.9363 ± 0.0011

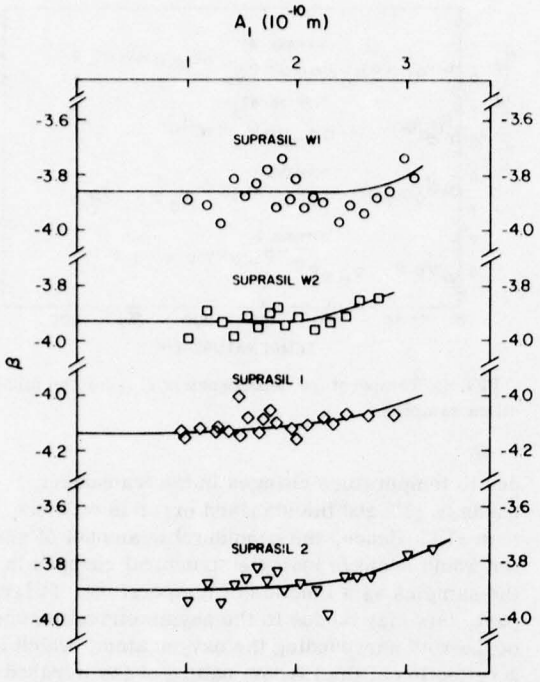

FIG. 2. Room-temperature plots of β as a function of the fundamental amplitude.

fundamental wave amplitudes A_1 for each sample. The resulting values of β were plotted as a function of A_1, as shown in Fig. 2. The solid curves are drawn through the data points in such a way that they approach $A_1 = 0$ with a horizontal tangent. Previous analysis[26] shows that this extrapolation corrects for the effect of attenuation. As can be seen the maximum magnitude of this correction is of the order of 5%.

The results of the extrapolated room-temperature measurements of β, C_{11}, and C_{111} are given in Table II. An examination of the table reveals that the SOE constants of the fused-silica samples with high OH content (Suprasil 1 and Suprasil 2) are lower than the samples with low OH content (Suprasil $W1$ and Suprasil $W2$). These results are consistent with those of Hetherington and Jack[33] who noted also that an increase in OH content caused an increase in mass density fluctuation as much as 3 parts in 10^3 in their experiments. Primak[34] suggested that in similar experiments by Fraser[35] in the ultrasonic range of frequencies the results reflect the effect of network cleavages induced by OH impurities.

Table II shows that β is negative for all fused-silica samples. This means that A_2 is also negative and that C_{111} is positive. Bains and Breazeale[36] have shown, using a phase-sensitive detector, that the harmonics of fused silica are generated out of phase with those generated by the same ultrasonic wave in copper. They conclude that the positive C_{111} of fused silica means that the solid becomes softer upon compression in contrast to copper which becomes stiffer upon compression.

According to Table II, Suprasil 1 has a substantially higher value of C_{111} than any of the other samples used in these experiments. It is tempting to infer that this is because of the high OH content of the sample (1200 ppm compared to 5 ppm for Suprasil $W1$ and Suprasil $W2$), but Suprasil 2 also has a high OH content (1200 ppm) and gives a value of C_{111} which lies between those of Suprasil $W1$ and Suprasil $W2$. The reason for this is not completely understood at this time. A check of all the samples with crossed polaroid sheets revealed that residual stresses were undetectable by this technique. Hence, residual stresses in a particular sample probably are not the cause of the difference.

A possible explanation may lie in the fact that even though Suprasil 2 is strongly homogeneous in the direction perpendicular to the sample faces, it may have inhomogeneities in other directions. If mass density variations existed parallel to the sample faces, then there would be an associated phase variation across the ultrasonic wave front. Such a situation leads to phase heterodyning which can cause significant changes in the amplitude of the electrical signal response.[37] Since this heterodyning is frequency dependent, fundamental and second-harmonic waves would be affected differently. The result could be a decrease in the measured value of C_{111} for Suprasil 2. If this were true, then one could consistently associate high C_{111} values with high OH content. Thus, the network cleavages introduced by the OH impurities

TABLE II. Measured room-temperature values of β, C_{11}, and C_{111}.[a]

Sample	β	C_{11} (10^{11} dyn/cm^2)	C_{111} (10^{12} dyn/cm^2)
Suprasil $W1$	-3.86 ± 0.071	7.8059 ± 0.0029	6.70 ± 0.124
Suprasil W_2	-3.93 ± 0.034	7.8078 ± 0.0020	6.85 ± 0.058
Suprasil 1	-4.14 ± 0.041	7.7633 ± 0.0016	7.31 ± 0.073
Suprasil 2	-3.90 ± 0.039	7.7633 ± 0.0014	6.75 ± 0.067

[a]The errors listed are the calculated standard deviations (random errors).

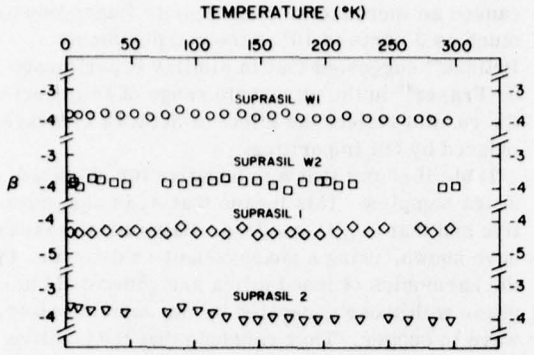

FIG. 3. Temperature dependence of β for the fused-silica samples.

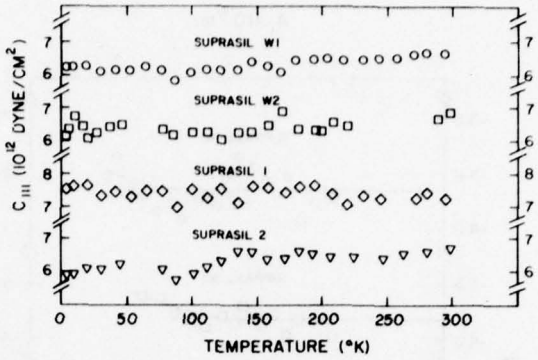

FIG. 4. Temperature dependence of C_{111} for the fused-silica samples.

which may be the cause of lower C_{11} values could also be the cause of higher C_{111} values.

B. Cryogenic measurements of β and its implications to the calculation of Grüneisen's γ

In making relative measurements with the cryogenic system, the quantity β is determined directly[27] [see Eq. (5)]. The resulting plots of β versus temperature in Fig. 3 indicate that β is virtually temperature independent. This means that the ${}_1\gamma_{11}$ component of the *strain* generalized Grüneisen parameter also is virtually temperature independent since ${}_1\gamma_{11} = \frac{3}{2}\beta$.

Therefore, the temperature variation of the experimentally determined Grüneisen parameter γ for fused silica shown in Fig. 1 must come from variations in the *volume* generalized Grüneisen parameter [see Eqs. (21) and (22)].

It is apparent from Eq. (21) that in order to obtain a negative value of the Grüneisen parameter at some temperature for fused silica, at least one of the *volume*-generalized Grüneisen parameters must be negative at that temperature since the model heat capacities C_t and C_ℓ are always positive. Barron[3,4] and Blackman[11] have suggested theoretical models which for some volume generalized Grüneisen parameters, associated with certain transverse-vibrational modes, do become negative. These transverse modes necessarily involve elastic constants other than C_{11} and C_{111}.

C. Cryogenic measurements of C_{111}

The behavior of C_{111} as a function of temperature can be determined directly from that of β. Figure 4 is the resulting plot of C_{111} versus temperature for the four samples. These curves show greater scatter in the data points than was experienced in previous experiments with copper[25] and germanium.[26,27] Further, the estimate of random error due to temperature changes in the transducer bonds is ±3% and the standard error is no more than ±1%. Hence, the considerable amount of scatter would seem to indicate structural changes in the samples as a function of temperature. In large part, this may be due to the asymmetrical nature of the void surrounding the oxygen atom, which is a reflection of the random nature of the tetrahedral network. As the temperature is lowered, evidence exists[34] that the Si–O–Si bond angle changes due to the asymmetrical vibrations of the oxygen atoms. Thus, the tetrahedral network of fused silica below the quenching temperature is in a state of stress. The resulting states of strain are more accentuated for the weak impurity bonds and this makes them more efficient electron traps than the strong Si–O bonds. This means that the effect of temperature changes is to cause variations, especially in anharmonic-dependent effects since it is these effects that are most sensitive to variation in structural symmetry and strain perturbations introduced by impurity sites.

Although scatter in the cryogenic measurements is too large to attach a great amount of significance to individual data points, trends in the C_{111}-versus-temperature data are apparent. The C_{111} values of Suprasil *W*1, Suprasil *W*2, and Suprasil 2 all show a slight general decrease of C_{111} with decreasing temperature. The C_{111} values of Suprasil 1 on the other hand do not decrease with decreasing temperature. As with the room-temperature measurements, Suprasil 1 (with high OH content) seems to be an anomaly. Again however, Suprasil 2 (also with high OH content) seems to show the general C_{111}-versus-temperature behavior as Suprasil *W*1 and Suprasil *W*2 (both with low OH content). Following the explanation given for the room-temperature measurements, it is conceivable that the lack of strong homogeneity in the Suprasil 2 sample gives rise to large density fluc-

tuations across the face of the ultrasonic beam. The change of temperature possibly may exaggerate these density fluctuations, thereby giving rise to the temperature dependence of C_{111} observed for Suprasil 2. The pronounced decrease of the C_{111} value of Suprasil 2 (Fig. 4) with decreasing temperature in the range 147–88 °K indicates that a strong structural change (and consequently density changes) may have taken place.

D. Conclusion

In conclusion, the present experimental determinations of β and C_{111} as functions of temperature allow an important inference to be made regarding the temperature dependence of the Grüneisen parameter for fused silica. If the quasiharmonic Debye model of a solid is assumed to hold for fused silica, then the relatively weak temperature dependence of β and C_{111} indicates that elastic constants, other than C_{11} and C_{111}, must dominate the strong temperature dependence of the experimentally determined Grüneisen parameter for fused silica at low temperatures. This is consistent with the suggestion of White and Birch[38] that transverse vibrations of fused silica are associated with the oxygen atoms of the tetrahedral network. The elastic constants associated with these transverse modes would be of the type C_{44}, C_{144}, and C_{456}, which do not enter into the measurements described here.

ACKNOWLEDGMENTS

This work was supported in part by the U. S. ONR. This paper is based in part on a doctoral dissertation submitted by one of us (J.H.C.) to the Dept. of Physics, University of Tennessee.

---

*Present address: NASA Langley Research Center, M/S 499, Hampton, Va. 23665.

[1]A. H. L. Fizeau, Poggendorf's Ann. Phys. 119, 87 (1863).
[2]E. Grüneisen, Hand. Phys. 10, 1 (1926).
[3]T. H. K. Barron, Philos. Mag. 46, 720 (1955).
[4]T. H. K. Barron, Ann. Phys. (N.Y.) 1, 77 (1957).
[5]F. W. Sheard, Philos. Mag. 3, 1381 (1958).
[6]J. G. Collins, Philos. Mag. 8, 323 (1963).
[7]D. E. Schuele and C. S. Smith, J. Phys. Chem. Solids 25, 801 (1964).
[8]K. Brugger and T. C. Fritz, Phys. Rev. 157, 524 (1967).
[9]D. Gerlich, Phys. Rev. B 11, 1365 (1975).
[10]G. K. White, Cryogenics 4, 2 (1964).
[11]M. Blackman, Philos. Mag. 3, 831 (1958).
[12]H. T. Smyth, J. Am. Ceram. Soc. 38, 140 (1955).
[13]H. T. Smyth, J. Am. Ceram. Soc. 36, 125 (1955).
[14]O. L. Anderson and G. J. Dienes, in *Noncrystalline Solids*, edited by Frechette (Wiley, New York, 1960), p. 449.
[15]O. L. Anderson and H. E. Bömmel, J. Am. Ceram. Soc. 38, 125 (1955).
[16]M. A. Breazeale and D. O. Thompson, Appl. Phys. Lett. 3, 77 (1963).
[17]A. A. Gedroits and V. A. Krasilnikov, Zh. Eksp. Teor. Fiz. 43, 1592 (1962); [Sov. Phys.-JETP 16, 1122 (1963)].
[18]W. B. Gauster and M. A. Breazeale, Rev. Sci. Instrum. 37, 1544 (1966).
[19]R. D. Peters, M. A. Breazeale, and V. K. Paré, Rev. Sci. Instrum. 39, 1505 (1968).
[20]J. T. Mackey and R. T. Arnold, J. Appl. Phys. 40, 4806 (1969).
[21]A. L. Sanford and S. P. Zehner, Phys. Rev. 153, 1025 (1967).
[22]E. L. Meeks and R. T. Arnold, Phys. Rev. B 1, 982 (1970).
[23]W. T. Yost and M. A. Breazeale, J. Appl. Phys. 44, 1909 (1973).
[24]R. W. Dunham and H. B. Huntington, Phys. Rev. B 2, 1098 (1970).
[25]R. D. Peters, M. A. Breazeale, and V. K. Paré, Phys. Rev. B 1, 3245 (1970).
[26]W. T. Yost and M. A. Breazeale, Phys. Rev. B 9, 510 (1974).
[27]James A. Bains, Jr. and M. A. Breazeale, Phys. Rev. B 13, 3623 (1976).
[28]M. A. Breazeale and J. Ford, J. Appl. Phys. 36, 3486 (1965).
[29]K. Brugger, Phys. Rev. 133, A1611 (1964).
[30]W. Voigt, *Lehrbuch der Kristallphysik* (Tuebner, Leipzig, 1928).
[31]John H. Cantrell, Jr. and M. A. Breazeale, J. Acoust. Soc. Am. 61, 403 (1977).
[32]A. Zarembowitch (private communication).
[33]G. Hetherington and K. H. Jack, Phys. Chem. Glasses 3, 129 (1962).
[34]W. Primak, *The Compacted States of Vitreous Silica* (Gordon and Breach, New York, 1975).
[35]D. B. Fraser, J. Appl. Phys. 39, 5868 (1968).
[36]James A. Bains, Jr. and M. A. Breazeale, J. Acoust. Soc. Am. 57, 745 (1975).
[37]Joseph S. Heyman and John H. Cantrell, Jr., Proc. IEEE Ultrasonics Symposium (1977), p. 124.
[38]G. K. White and J. A. Birch, Phys. Chem. Glasses 6, 85 (1965).

NONLINEAR ACOUSTICS AND SOLID STATE PHYSICS

M. A. Breazeale

Department of Physics

The University of Tennessee

Knoxville, Tennessee 37916

USA

8th International Symposium on Nonlinear Acoustics

Paris, July 1978

SOMMAIRE

ACOUSTIQUE NONLINÉAIRE ET PHYSIQUE DU SOLIDE

L'étude de l'acoustique non linéaire en plus de développements mathématiques et d'applications pratiques pleins de promesses nous conduit à des progrès essentiels dans l'étude de la physique du solide. La déformation non linéaire d'une onde ultra-sonore dans un solide est contrôlée par un paramètre nonlinéaire qui est à la fois fonction des constantes d'élasticité du troisième ordre [TOE] et fonction des constantes d'élasticité—plus connues—du deuxième ordre [SOE]. La mesure de la déformation des ondes ultrasonores rend alors possible l'évaluation des constantes TOE, les constantes SOE pouvant, elles, être évaluées d'après les vitesses des ondes ultrasonores.

Le nombre des constantes élastiques est dèterminé par la symètrie du cristal. La grandeur et le signe des constantes TOE sont determinés par les forces intermolèculaires. Si l'on considère un cristal cubique dans lequel existent les forces centrales et les interactions les plus proches, à des températures voisines de 0 °K on trouve que $C_{111} = 2C_{112} = 2C_{166}$ et $C_{123} = C_{456} = C_{144} = 0$.

Au cours des dernières années nous avons mesuré les constantes TOE en fonction de température, descendant jusqu'à 3 °K dans des cristaux tels que le germanium et le cuivre et dans de la silice amorphe fusible. Nous présentons un résumé des résultats accesibles à l'heure actuelle et nous faisons une comparaison du comportement des forces intermoléculaires pour des cristaux de types différents.

Récemment nous avons découvert que dans le cuivre les forces centrales et les interactions les plus proches semblent prévaloir pour déterminer les constantes TOE pour les températures de 40 °K et de 190 °K. Toutefois il n'en est rien à 0 °K contrairement ce a quoi l'on pourrait s'attendre.

ABSTRACT

NONLINEAR ACOUSTICS AND SOLID STATE PHYSICS

In addition to mathematical advances and very promising practical applications, the study of Nonlinear Acoustics now is leading to fundamental advances in Solid State Physics. Nonlinear distortion of an ultrasonic wave in a solid is controlled by a nonlinearity parameter which is a function of the third-order elastic (TOE) constants as well as the second-order elastic (SOE) (the usual) elastic constants. Measurement of the waveform distortion, then, makes possible the evaluation of the TOE constants, because the SOE constants can be evaluated from ultrasonic wave velocities.

The number of elastic constants is determined by the crystal symmetry. The magnitude and sign of the TOE constants are determined by intermolecular forces. In a cubic crystal in which central forces and nearest-neighbor interactions exist one would find $C_{111} = 2C_{112} = 2C_{166}$ and $C_{123} = C_{456} = C_{144} = 0$ in the limit of 0 °K.

Over the past several years we have measured TOE constants as a function of temperature down to 3 °K in such crystals as germanium and copper and in amorphous fused silica. A summary of presently available data is presented, and a comparison of the behavior of the intermolecular forces for different types of crystals is made. Recently we have found that in copper central forces and nearest-neighbor interactions seem to predominate in determining TOE constants, but this does not happen near 0 °K as expected. It seems to happen near 40 °K and again at 190 °K.

When a sinusoidal ultrasonic wave of finite amplitude propagates through a nonlinear medium it undergoes waveform distortion, as we all know. The amount of this distortion and its dependence upon frequency and propagation distance are determined by the nonlinearity parameter of the propagating medium. For gases this nonlinearity parameter is simply $\gamma + 1$ where γ is the ratio of specific heats. For liquids it is $B/A + 2$, where B/A is the ratio of two terms in the equation of state. For solids the situation is somewhat more complicated. Not only are there both longitudinal and transverse waves to consider, but also the fact that solids can be anisotropic means that the longitudinal and transverse waves in general are coupled, so that one cannot define a nonlinearity parameter for every possible direction in a crystalline solid. Our solution to this problem has been to consider the propagation of finite amplitude ultrasonic waves only along the principal crystallographic directions, and to restrict our attention for the present to crystals of cubic symmetry. In the principal directions pure mode propagation exists for the longitudinal wave, even though the transverse wave is always coupled to a longitudinal wave. The pure-mode longitudinal wave is coupled to its own second harmonic in exactly the same way a longitudinal wave in a fluid is. For these waves a nonlinearity parameter can be defined, and it is found that the nonlinearity parameter is a function of the second-order elastic (SOE) constants and third-order elastic (TOE) constants. The study of nonlinear distortion of ultrasonic waves in solids, then, has produced a means of measuring the TOE constants (the SOE constants can be determined from the velocity of ultrasonic waves in the sample). Furthermore, the technique can be adapted to measurements as a function of temperature, which produces results which

are of fundamental importance to solid state physics. At present this is the only technique which is consistently producing such results. Some of our recent results are quite exciting; however, first let me remind you of the technique.

In the principal directions in a cubic crystal longitudinal waves of finite amplitude are described by[1]

$$\rho_0 \ddot{u} = K_2 \frac{\partial^2 u}{\partial a^2} + (3K_2 + K_3) \frac{\partial u}{\partial a} \frac{\partial^2 u}{\partial a^2} \tag{1}$$

where K_2 and K_3 are linear combinations, respectively, of the SOE and TOE constants, as shown in Table I. The nonlinearity parameter[2] is the negative of the ratio of the nonlinear term to the linear term in Eq. 1, namely,

$$- \frac{3K_2 + K_3}{K_2} = \beta \ . \tag{2}$$

For an initially sinusoidal disturbance at a = 0, the solution takes the form

$$u = A_1 \sin(ka-\omega t) + \frac{A_1^2 k^2 a\beta}{8} \cos 2(ka-\omega t) + \ldots \tag{3}$$

in which the second harmonic amplitude

$$A_2 = \frac{A_1^2 k^2 a\beta}{8} \tag{4}$$

contains the nonlinearity parameter β. Our measurements, then, consist of absolute measurement of the second harmonic amplitude, the fundamental amplitude, the frequency, and the sample length. The only real problem in these measurements is the fact that the second harmonic amplitude is so low (of the order of 10^{-2} Å at 60 MHz) that care must be exercised in getting an accurate value. A capacitive detector has worked well for us, so that we have been able to determine β for several samples—not only at room temperature,[3] but also at low temperatures—down to 3 °K.[4] The behavior of β as a function of temperature and the behavior of the TOE constants as a function of temperature are

of most interest at present. Let us contrast their behavior in germanium, in which covalent bonding among the atoms exists, with that in copper, in which exchange energy resulting from overlapping of closed electronic shells seems to predominate in determining the elastic constants.

Nonlinearity parameters measured as a function of temperature for germanium are shown in Fig. 1; those for copper are shown in Fig. 2. In each case a smooth curve is drawn connecting the data points. As can be seen, the nonlinearity parameter is different in the three principal directions in both cases, but the difference in the magnitudes between germanium and copper is not great. Furthermore, the magnitude increases in the order [100], [111], and [110] in both cases. The variation with temperature is not great, the greatest variation being only 20% for the [110] direction in germanium. One can conclude, therefore, that the nonlinearity parameter of solids, like the Grüneisen parameter, should be nominally independent of temperature.

There is much more information to be obtained from these data, however. Even though we cannot isolate all six of the TOE constants, we can isolate certain combinations of them. These are the quantities listed in Table I as K_3. Using Eq. (2), and known values of $K_2 = \rho V^2$, we can determine the combinations K_3 plotted in Figs. 3 and 4. The value of K_3 for the [100] direction is the single TOE constant C_{111}. The values of K_3 in the other directions are the more complicated linear combinations in Table I. Upon examination it is clear that the curves in Figs. 3 and 4 still are not the simplest combinations of TOE constants available from the data. C_{111} appears in each expression for K_3, so it can be subtracted out. In this manner one can obtain the curves shown in Figs. 5 and 6, which are the simplest combinations of TOE constants available from our data on the nonlinearity parameters.

Further interpretation of these curves is facilitated by comparison with a model. We will use the simplest model available: a model in which we assume that the atoms interact by central forces, and in which there are only nearest-neighbor interactions. Such a model has proved to be inadequate to explain the magnitude of SOE constants, as we know. It predicts that $C_{11} = 2C_{12} = 2C_{44}$, which is not satisfied by any of the cubic crystals. On the other hand, we are concerned with the TOE constants which are determined by the nonlinear interactions. For the TOE constants the central forces, nearest-neighbor interaction model predicts that $C_{111} = 2C_{112} = 2C_{166}$ and $C_{123} = C_{456} = C_{144} = 0$. We can use these expressions to see how well those quantities we can measure actually follow the predictions of the model. In Figs. 5 and 6 the combination $C_{123} + 6C_{144} + 8C_{456}$ should vanish. Fig. 5 shows that this actually happens at approximately 15 °K for germanium. The fact that this combination becomes positive below this temperature cannot be explained at the moment. Another test of the agreement between the data and the central forces, nearest-neighbor model comes from the fact that, according to the model the combination $C_{112} + 4C_{166} = 5/2\ C_{111}$. On Figs. 5 and 6 the value $5/2\ C_{111}$ is indicated by a dotted line. For germanium the combination $C_{112} + 4C_{166}$ indeed is approaching $5/2\ C_{111}$ near 0 °K. This means that near 0 °K the central forces, nearest-neighbor model can be used to predict quite well the relationship among the TOE constants of germanium. This is consistent, because the model is expected to be most accurate at 0 °K, and less accurate as the temperature is increased.

Let us now turn to the data for copper. The same combinations of TOE constants are shown in Fig. 6. C_{111} has more or less the same behavior for copper as for germanium, with only a slightly larger

variation with temperature. Likewise, there is reasonable agreement between $C_{112} + 4C_{166}$ and $5/2\ C_{111}$, except that for copper the agreement remains essentially the same, a difference of approximately 6%, for all temperatures. For copper the combination $C_{123} + 6C_{144} + 8C_{456}$ is more nearly zero for the entire temperature range. In fact, it vanishes completely at two temperatures: 40 °K and again at 200 °K.

Let us assume for the moment that the TOE constants of copper actually do follow the predictions of the central forces, nearest-neighbor model. In that case we would be left with the necessity of explaining the dips in the data in Fig. 6 which occur between 40 and 200 °K. If we examine known physical mechanisms we find that dislocation interaction, first reported by Bordoni,[5] can produce in copper a peak in attenuation which has a similar temperature behavior. Seeger and Mann[6] have pointed out that nonlinearity is very large near a dislocation. Therefore, we are led to speculate that we are viewing for the first time the effect of Bordoni relaxation on the measured value of the TOE constants of copper. The samples we used for these measurements were neutron irradiated to reduce dislocation interactions. Thus, if this is the correct interpretation of the data, we can say immediately that our measurements are especially sensitive to the presence of dislocations. Additional measurements after further neutron irradiation or after annealing will be required to confirm whether this is the correct interpretation of the temperature dependence of the TOE constants of copper.

Acknowledgment: Research supported by the United States Office of Naval Research.

References

1. BREAZEALE, M. A. and JOSEPH FORD, J. Appl. Phys. 36 (1965) 3486.
2. The nonlinearity parameter β is three times as large as the dimensionless parameter B previously used by W. T. YOST and M. A. BREAZEALE in Phys. Rev. B 9 (1974 510 and by JAMES A. BAINS and M. A. BREAZEALE in Phys. Rev. B 13 (1976) 3623.
3. GAUSTER, W. B. and M. A. BREAZEALE, Phys. Rev. 168 (1968) 655.
4. BAINS, JAMES A. and M. A. BREAZEALE, Phys. Rev. B 13 (1976) 3623.
5. BORDONI, PIERO GIORGIO, J. Acoust. Soc. Am. 26 (1954) 495.
6. SEEGAR, A. and E. MANN, Z. Naturforschung 14a (1959) 154.

Table 1. K_2 and K_3 for principal directions of a cubic crystal

Direction	K_2	K_3
[100]	C_{11}	C_{111}
[110]	$\frac{1}{2}(C_{11} + C_{12} + 2C_{44})$	$\frac{1}{4}(C_{111} + 3C_{112} + 12C_{166})$
[111]	$\frac{1}{3}(C_{11} + 2C_{12} + 4C_{44})$	$\frac{1}{9}(C_{111} + 6C_{112} + 12C_{144} + 24C_{166} + 2C_{123} + 16C_{456})$

FIGURE CAPTIONS

1. Temperature dependence of the nonlinearity parameters of germanium.

2. Temperature dependence of the nonlinearity parameters of copper.

3. TOE constant combination K_3 for germanium calculated from nonlinearity parameters.

4. TOE constant combination K_3 for copper calculated from nonlinearity parameters.

5. Comparison of simplest TOE constant combination available from germanium data with predictions of central forces, nearest-neighbor model: $C_{112} + 4C_{166} = 5/2\ C_{111}$ and $C_{123} + 6C_{144} + 8C_{456} = 0$.

6. Comparison of simplest copper TOE constant combination and predictions of model.

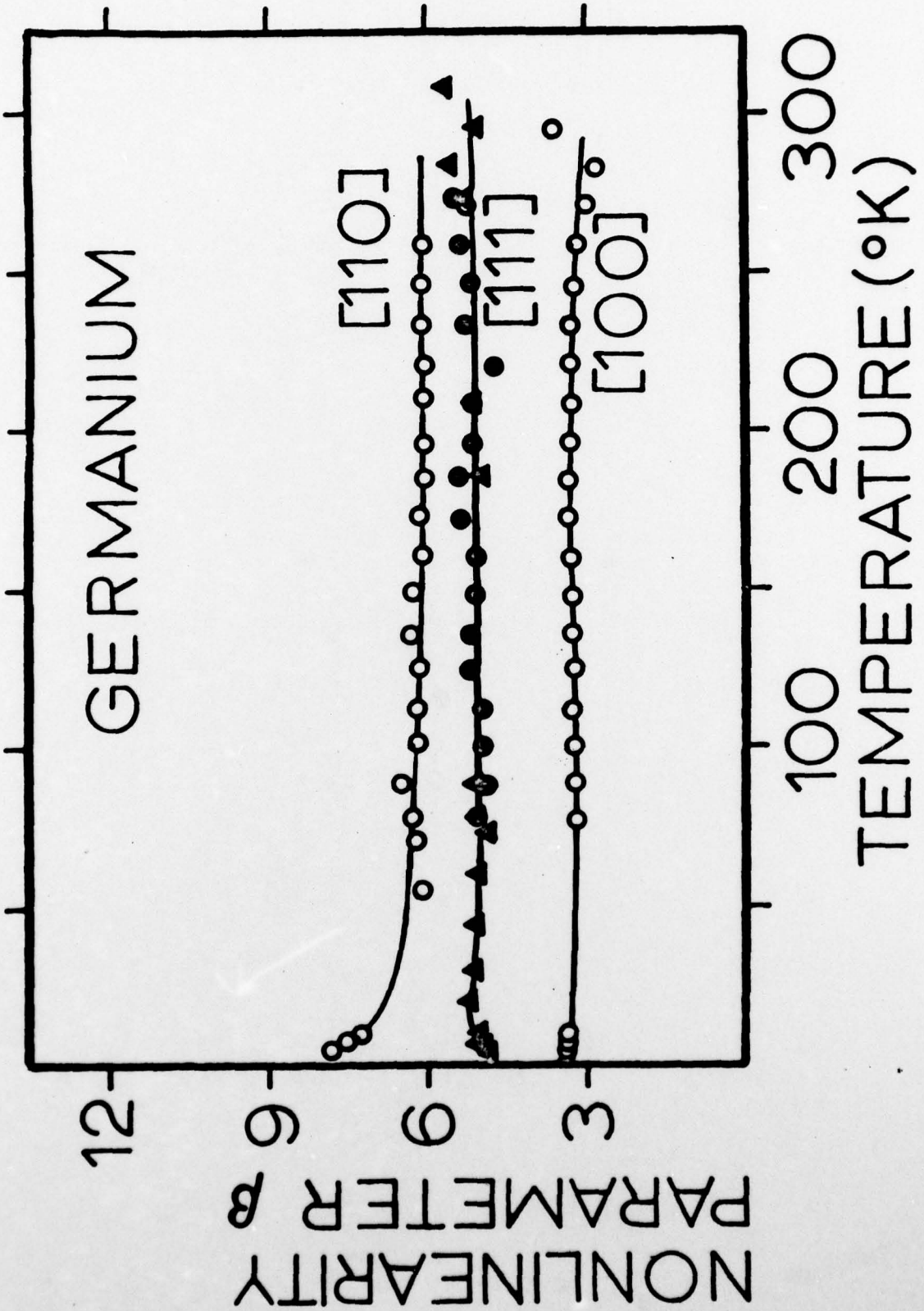

Breazeale, Fig. 1

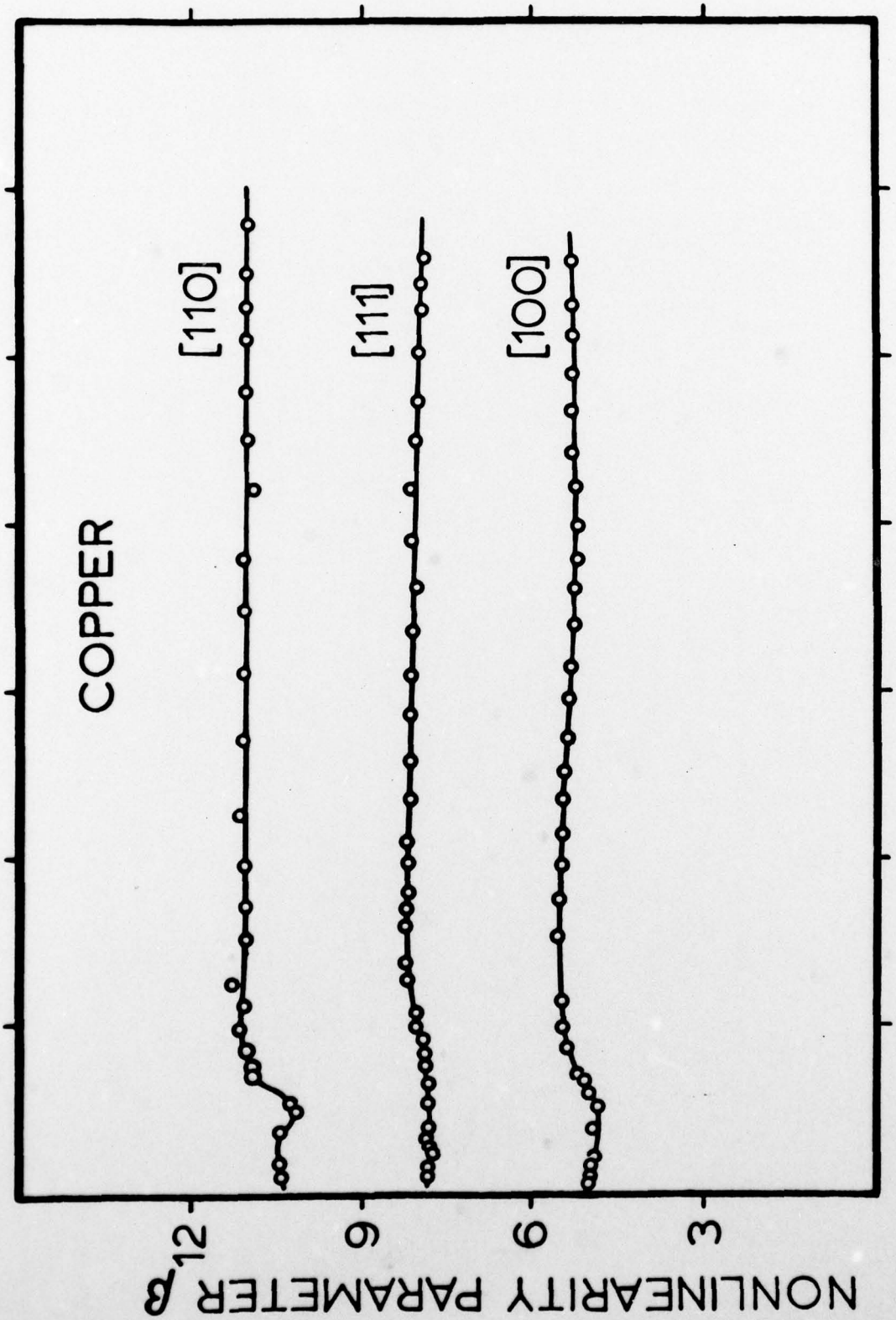

Breazeale, Fig. 2

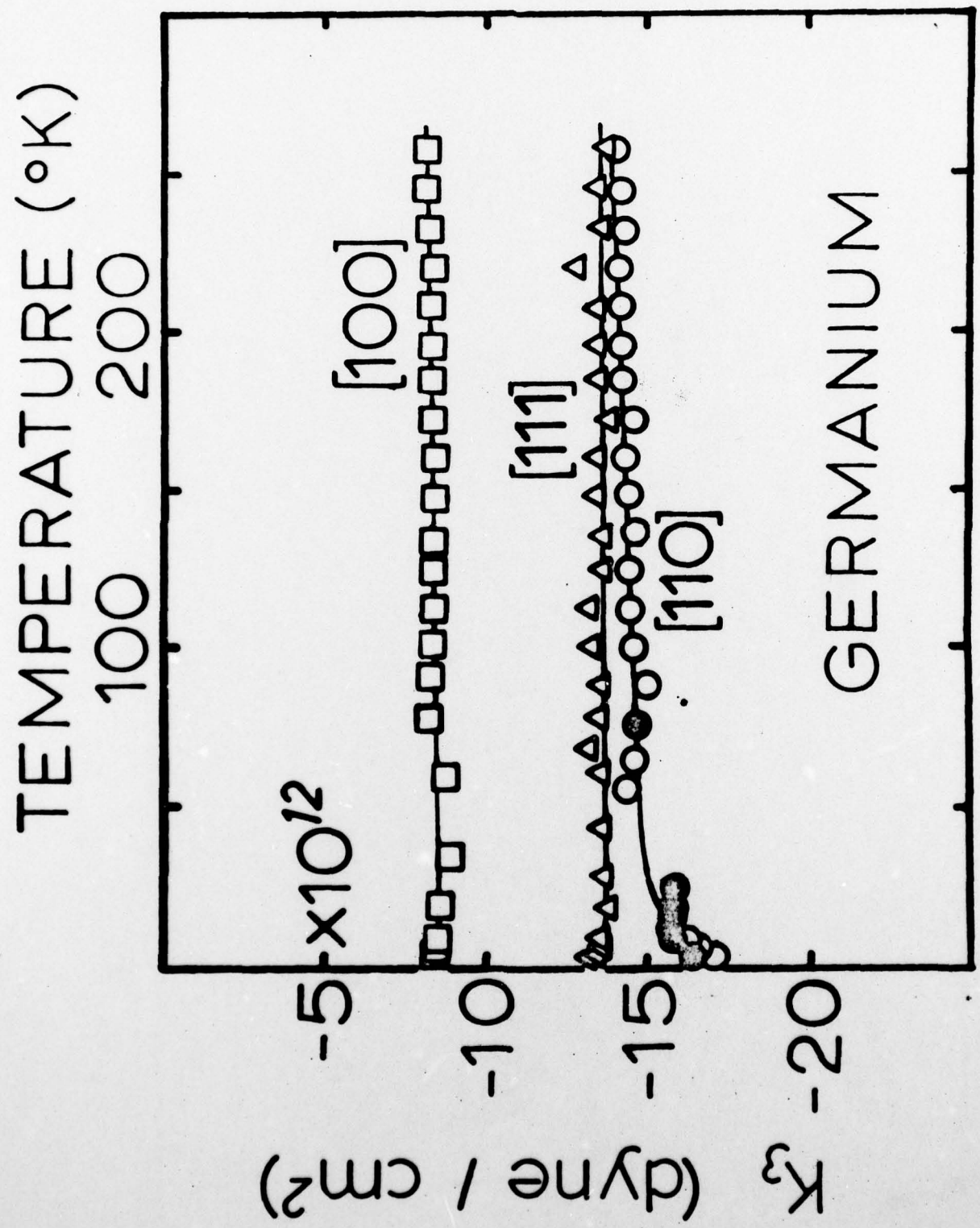

Breazeale, Fig. 3

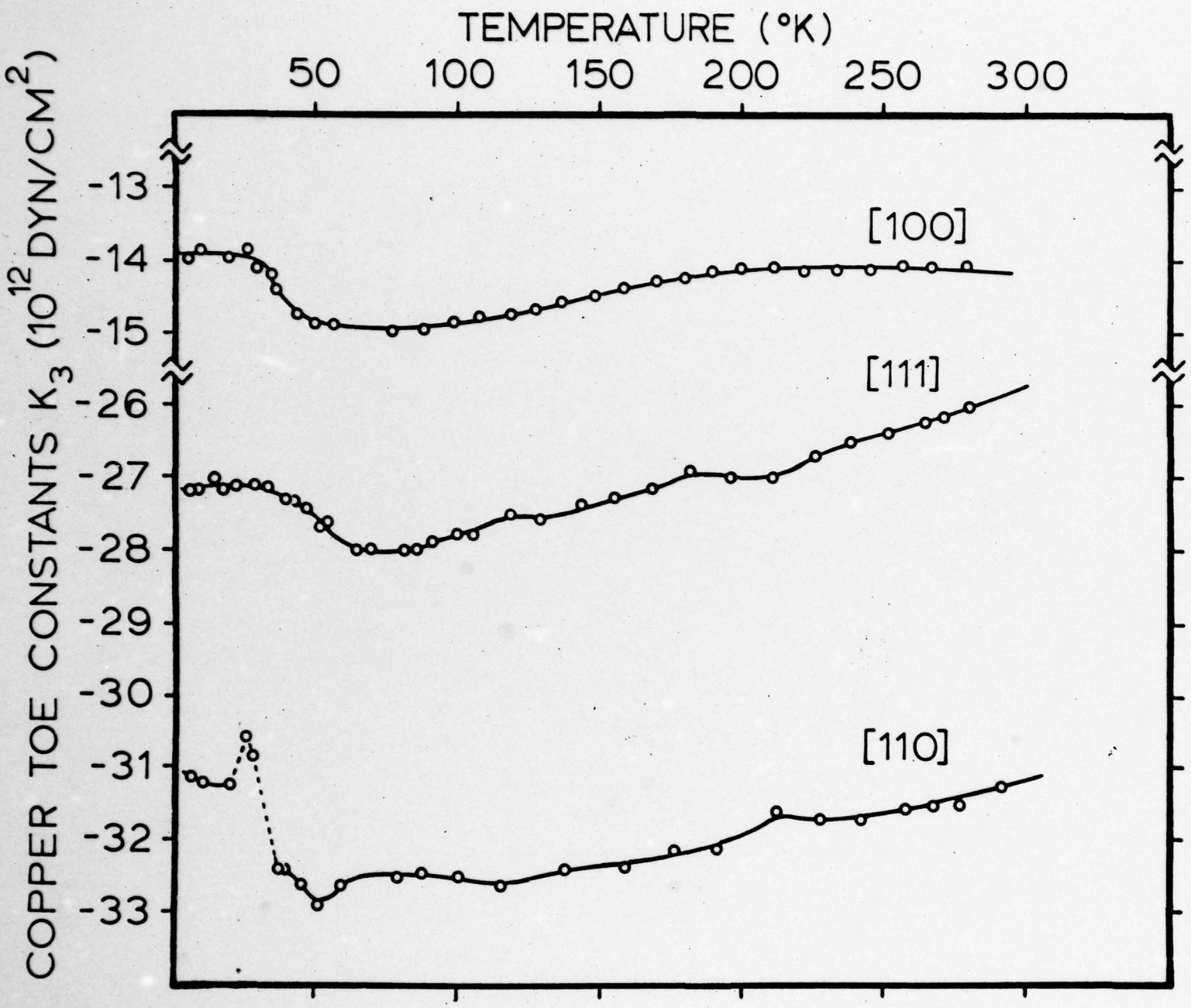

[70]

Breazeale, Fig. 4

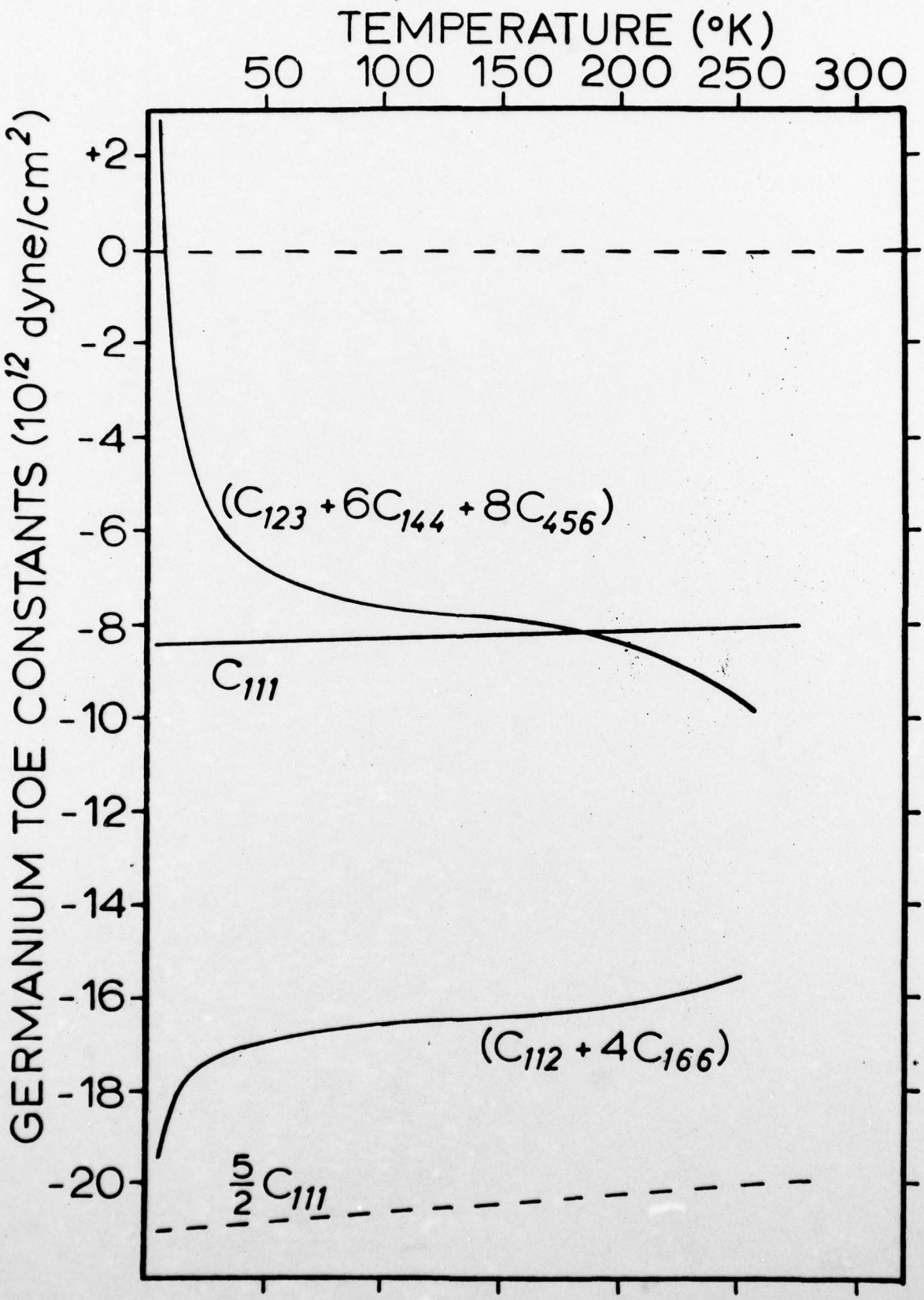

Breazeale, Fig. 5

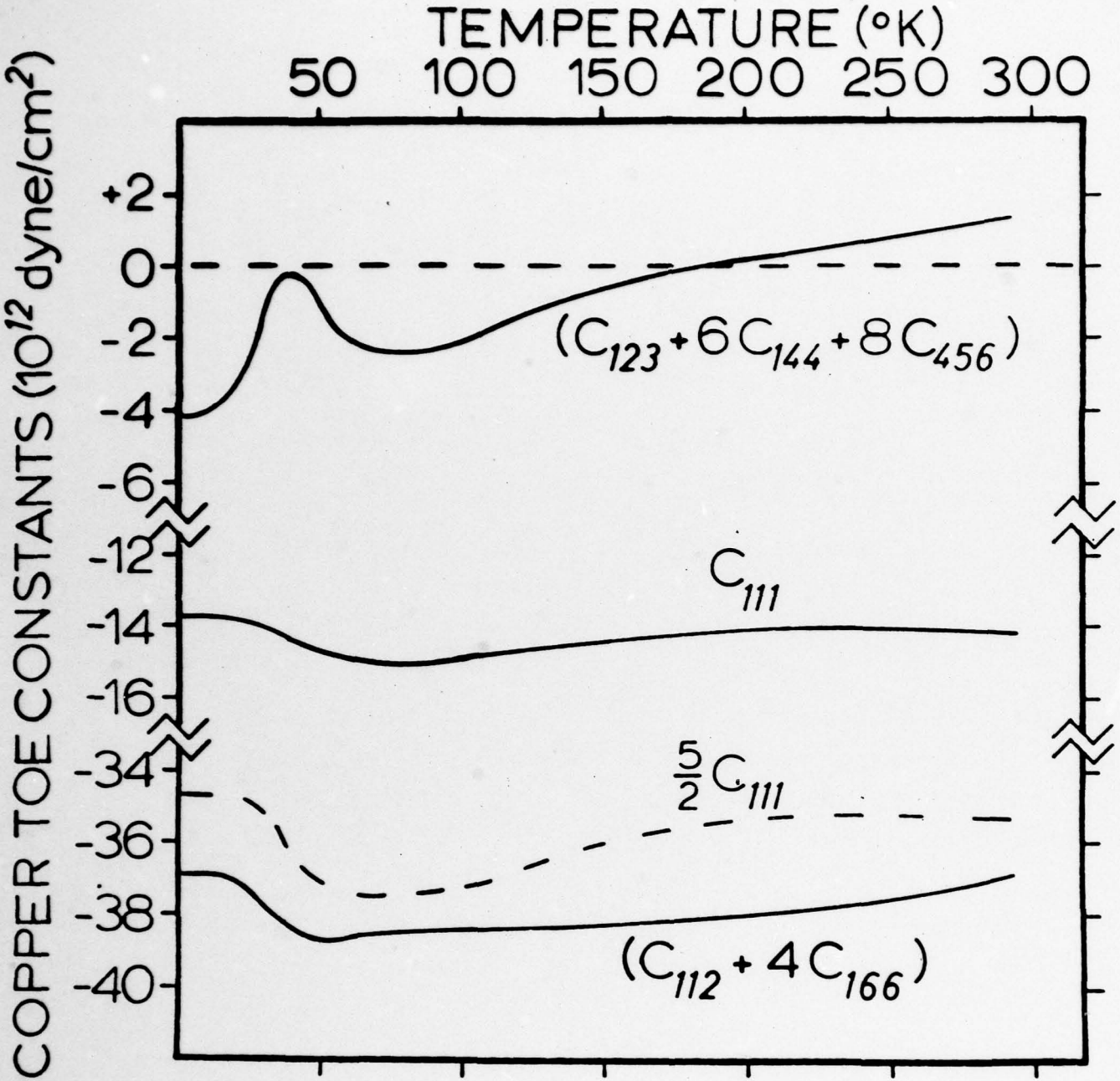

[72]

Breazeale, Fig. 6

June 1978

REPORTS DISTRIBUTION LIST FOR ONR PHYSICS PROGRAM OFFICE
UNCLASSIFIED CONTRACTS

Director Defense Advanced Research Projects Agency Attn: Technical Library 1400 Wilson Blvd. Arlington, Virginia 22209	3 copies
Office of Naval Research Physics Program Office (Code 421) 800 North Quincy Street Arlington, Virginia 22217	3 copies
Office of Naval Research Assistant Chief for Technology (Code 200) 800 North Quincy Street Arlington, Virginia 22217	1 copy
Naval Research Laboratory Department of the Navy Attn: Technical Library Washington, D. C. 20375	3 copies
Office of the Director of Defense Research and Engineering Information Office Library Branch The Pentagon Washington, D. C. 20301	3 copies
U. S. Army Research Office Box 12211 Research Triangle Park North Carolina 27709	2 copies
Defense Documentation Center Cameron Station (TC) Alexandria, Virginia 22314	12 copies
Director, National Bureau of Standards Attn: Technical Library Washington, DC 20234	1 copy
Commanding Officer Office of Naval Research Branch Office 536 South Clark Street Chicago, Illinois 60605	3 copies

Commanding Officer — 3 copies
Office of Naval Research Branch Office
1030 East Green Street
Pasadena, California 91101

San Francisco Area Office — 3 copies
Office of Naval Research
One Hallidie Plaza
Suite 601
San Francisco, California 94102

Commanding Officer — 3 copies
Office of Naval Research Branch Office
666 Summer Street
Boston, Massachusetts 02210

New York Area Office — 1 copy
Office of Naval Research
715 Broadway, 5th Floor
New York, New York 10003

Director — 1 copy
U. S. Army Engineering Research
and Development Laboratories
Attn: Technical Documents Center
Fort Belvoir, Virginia 22060

ODDR&E Advisory Group on Electron Devices — 3 copies
201 Varick Street
New York, New York 10014

Air Force Office of Scientific Research — 1 copy
Department of the Air Force
Bolling AFB, D. C. 22209

Air Force Weapons Laboratory — 1 copy
Technical Library
Kirtland Air Force Base
Albuquerque, New Mexico 87117

Air Force Avionics Laboratory — 1 copy
Air Force Systems Command
Technical Library
Wright-Patterson Air Force Base
Dayton, Ohio 45433

Lawrence Livermore Laboratory — 1 copy
Attn: Dr. W. F. Krupke
University of California
P. O. Box 808
Livermore, California 94550

Harry Diamond Laboratories — 1 copy
Technical Library
2800 Powder Mill Road
Adelphi, Maryland 20783

Naval Air Development Center — 1 copy
Attn: Technical Library
Johnsville
Warminster, Pennsylvania 18974

Naval Weapons Center — 1 copy
Technical Library (Code 753)
China Lake, California 93555

Naval Training Equipment Center — 1 copy
Technical Library
Orlando, Florida 32813

Naval Underwater Systems Center — 1 copy
Technical Library
New London, Connecticut 06320

Commandant of the Marine Corps — 1 copy
Scientific Advisor (Code RD-1)
Washington, DC 20380

Naval Ordnance Station — 1 copy
Technical Library
Indian Head, Maryland 20640

Naval Postgraduate School — 1 copy
Technical Library (Code 0212)
Monterey, California 93940

Naval Missile Center — 1 copy
Technical Library (Code 5632.2)
Point Mugu, California 93010

Naval Ordnance Station — 1 copy
Technical Library
Louisville, Kentucky 40214

Commanding Officer — 1 copy
Naval Ocean Research & Development Activity
Technical Library
NSTL Station, Mississippi 39529

Naval Explosive Ordnance Disposal Facility — 1 copy
Technical Library
Indian Head, Maryland 20640

Naval Ocean Systems Center — 1 copy
Technical Library
San Diego, California 92152

Naval Surface Weapons Center — 1 copy
Technical Library
Dahlgren, Virginia 22448

Naval Surface Weapons Center (White Oak) — 1 copy
Technical Library
Silver Spring, Maryland 20910

Naval Ship Research and Development Center — 1 copy
Central Library (Code L42 and L43)
Bethesda, Maryland 20084

Naval Avionics Facility — 1 copy
Technical Library
Indianapolis, Indiana 46218

Dr. Werner G. Neubauer — 1 copy
Code 8130
Physical Acoustics Branch
Naval Research Laboratory
Washington, D.C. 20375

Dr. Bill D. Cook — 1 copy
Dept. of Mechanical Engineering
University of Houston
Houston, Texas 77004

Dr. Floyd Dunn — 1 copy
Biophysical Research Laboratory
University of Illinois
Urbana, Illinois 61801

Dr. E. F. Carome — 1 copy
Department of Physics
John Carroll University
University Heights
Cleveland, Ohio 44017

Dr. David Blackstock — 1 copy
Applied Research Laboratories
University of Texas at Austin
P.O. Box 8029
Austin, Texas 78712